

2001

Receptor- G Protein Interactions in the Visual System: A Study of Structures and Mechanisms That Couple the Cytoplasmic Surface of Rhodopsin to the Nucleotide-Binding Pocket of Transducin

Ethan P. Marin

Follow this and additional works at: http://digitalcommons.rockefeller.edu/student_theses_and_dissertations

 Part of the [Life Sciences Commons](#)

Recommended Citation

Marin, Ethan P., "Receptor- G Protein Interactions in the Visual System: A Study of Structures and Mechanisms That Couple the Cytoplasmic Surface of Rhodopsin to the Nucleotide-Binding Pocket of Transducin" (2001). *Student Theses and Dissertations*. 349. http://digitalcommons.rockefeller.edu/student_theses_and_dissertations/349

This Thesis is brought to you for free and open access by Digital Commons @ RU. It has been accepted for inclusion in Student Theses and Dissertations by an authorized administrator of Digital Commons @ RU. For more information, please contact mcsweej@mail.rockefeller.edu.



Receptor-G protein Interactions in the Visual System:

A study of structures and mechanisms that couple the cytoplasmic surface of rhodopsin to the nucleotide-binding pocket of transducin

Ethan P. Marin

A thesis presented to the faculty of
THE ROCKEFELLER UNIVERSITY
in partial fulfillment of
the requirements for the degree of
DOCTOR OF PHILOSOPHY

June, 2001

"The great thing is to last and get your work done and see and hear and learn and understand and write when there is something that you know; and not before; and not too damned much after."

-Ernest Hemingway

Acknowledgments

The work described in this thesis would never have been completed without the contribution, both direct and indirect, of many people. Credit is due to my thesis advisor, Dr. Thomas P. Sakmar, who was resolute in his policy of treating students as colleagues-- which meant never telling me what to do. In addition, I am appreciative of the members of my thesis committee for their input on my projects.

I would also like to acknowledge all the members of the Sakmar laboratory with whom I have worked during my stay there, especially the people who helped me get started during my first years in the lab: Steve Lin, Cecille Unson, Tanya Zvyaga, Lenore Snyder, Steve Gravina, May Han, Manija Kazmi and the two students who came before me, Aaron Cypess and Chris Min. Thanks are due also to Carol Valli and Cliff Sonnenbrot, who helped keep the lab running smoothly.

Several people contributed directly to the work in this thesis. Tanya Zvyaga performed the rhodopsin-derived peptide competition experiment described in Chapter 3. The photoregeneration work in Chapter 4 was done in Berlin, in the lab of Dr. K. P. Hofmann, in collaboration with one of his graduate students, Christoph Meyer. I am grateful to Dr. Hofmann and his group for allowing me into their Institute to complete those studies. I am also grateful to the Alexander Mauro Travel Fellowship which supported a portion of my stay in Germany. Dr. Steve Graber (West Virginia University) provided purified recombinant G α_1 , and guidance on expression and purification procedures. Vincent Archambault, a graduate student, performed some of the early experiments with *in vitro* expression of G α_t during a rotation in the Sakmar Lab. Eugene Simuni, a high school student, spent three summers in the lab working on analyzing the interdomain interface of G proteins, and helping with experiments related to that project. Wing-Yee Fu, a technician in the lab, provided tremendous assistance with large-scale preparations of rhodopsin mutants. I am particularly indebted to A. Gopala Krishna, a post-doc in the Sakmar Lab who helped me with many of the experiments described in Chapters 5 and 6, and also performed the studies on peptide binding to transducin subunits in Chapter 3.

Finally, I would like to thank my wife and family for supporting me through this endeavor.

Table of contents

	<i>Page</i>
Abstract.....	1
Chapter 1: Introduction.....	3
The Phototransduction Cascade.....	3
The biochemistry of the phototransduction cascade: an historical overview.....	4
The Central Role of Rhodopsin- G_t Interactions.....	7
Rhodopsin structure and function.....	7
Rhodopsin structure.....	7
Opsin-Chromophore Interactions.....	9
R^* interactions with G_t	11
G_t structure and function.....	13
G_t interactions with R^*	16
The mechanism of R^* catalyzed nucleotide exchange.....	17
Advantages of rhodopsin and transducin as a model system.....	20
Outline of the Thesis.....	22
Chapter 2: Materials and Methods.....	31
Reagents.....	31
Preparation of rhodopsin-derived peptides.....	31
Preparation of G_t -derived peptides.....	31
Preparation of G_t , $G\alpha_t$, $G\beta\gamma_t$, and Rhodopsin from Bovine Retinas....	32
Measurement of Intrinsic Fluorescence of G_t , $G\alpha_t$, and $G\beta\gamma$	34
Site Directed Mutagenesis of Rhodopsin.....	34

Table of Contents (con't)

Fluorescence G_t Activation Assay.....	35
Measurement of [3H]Palmitic Acid Incorporation.....	36
Instrumentation for Measurement of Photoregeneration Traces.....	36
Photoregeneration Experiments.....	37
Numerical Fitting Procedures	37
Site-Directed Mutagenesis of $G\alpha_t$ and $G\alpha_i$	38
<i>In vitro</i> Translation of $G\alpha_t$	39
Trypsin Proteolysis and Analysis.....	40
Control Reactions for Trypsin Proteolysis of $G\alpha_t$	40
Uncatalyzed Activation Time Course of $G\alpha_t$	41
Rhodopsin/ $G\beta\gamma_t$ -Catalyzed Activation Time Course of $G\alpha_t$	41
Data Analysis of Trypsin Proteolysis Patterns.....	41
 Chapter 3: The Amino Terminus of the Fourth Cytoplasmic Loop of Rhodopsin	
Modulates Rhodopsin—Transducin Interaction.....	43
Summary.....	43
Introduction.....	44
Results.....	45
Inhibition of G_t Activation by Synthetic Peptides.....	45
A Synthetic Peptide Derived From C4 of Rhodopsin, rho(310-321), Alters the Fluorescence Emission Wavelength Maximum of $G\alpha_t$ But Not of $G\beta\gamma_t$	45
Preparation of Substitution Mutants in C4 of Rhodopsin.....	46
Activation of G_t by Solubilized Purified Recombinant Pigments.....	48

Table of Contents (con't)

Characterization of Pigment-catalyzed GTP γ S Uptake by G α_t As a	
Function of G $\beta\gamma_t$ Concentration.....	49
Palmitoylation of CTr1, Ctr2, and CTr4.....	50
Amino Acid Sequence Analysis of Vertebrate Opsins and Biogenic Amine	
Family Receptors.....	50
Discussion.....	59
Loop C4 of Rhodopsin Is Involved in the Activation of G $_t$	59
Factors Affecting the Structure of the C4 Loop Region.....	61
The Role of the C4 Loop Involves Modulation of Rhodopsin-G $_t$	
Interactions.....	62
Chapter 4: Mutation of the Fourth Cytoplasmic Loop of Rhodopsin Affects Binding	
of Transducin and Peptides Derived from the Carboxyl-terminal Sequences of	
Transducin α and γ Subunits.....	64
Summary.....	64
Introduction.....	65
Results.....	66
The Effect of G $_t$ and G $_t$ -derived Peptides on the Photoregeneration of	
Rhodopsin.....	66
Specificity of the Effects of α (340-350) and γ (50-71)-far Peptides.....	67
Photoregeneration Assay of Recombinant Rhodopsin and Loop C4	
Mutants.....	69
Discussion.....	80
Photoregeneration is Sensitive to Interactions with G $_t$ and Certain G $_t$ -	
derived Peptides.....	81
The Role of a Conserved Region at the Amino Terminus of Loop C4 of	
Rhodopsin in G $_t$ Binding.....	82

Table of Contents (con't)

Possible Role of $G\gamma_t$ -farnesyl in Docking of G_t to the Active Receptor	84
Chapter 5: The Function of Interdomain Interactions in Controlling Nucleotide	
Exchange Rates in $G\alpha_t$	86
Summary.....	86
Introduction.....	88
Results.....	90
Expression of $G\alpha_t$ <i>in vitro</i> and Trypsin Digestion Assay of Nucleotide	
Binding and Exchange	90
Analysis of Single Amino Acid Replacements in the Interdomain Interface	
of $G\alpha_t$	93
Analysis of Double Amino Acid Replacements.....	94
Analysis of $G\alpha_i$ mutants.....	95
Discussion.....	108
Analysis of Trypsin-Digest Products of <i>in vitro</i> Translated $G\alpha_t$ to	
Evaluate Nucleotide Exchange Kinetics.....	108
Site-Directed Mutation of K273 or K276 Increases Basal Nucleotide	
Exchange Rates	110
Interdomain Interactions in $G\alpha_t$ Do Not Affect Basal or Rhodopsin-	
Catalyzed Nucleotide Exchange Rates	112
The function of residues at the interdomain interface differs among $G\alpha_t$,	
$G\alpha_i$ and $G\alpha_s$	113
Chapter 6: Rapid Activation of Transducin by Mutations on the $\alpha 5$ Helix Distant	
From the Nucleotide-Binding Site: Evidence for a Mechanistic Model of	
Receptor-Catalyzed Nucleotide Exchange by G Proteins.....	115
Summary.....	115

Table of Contents (con't)

[illegible]

List of Figures

<i>Number</i>	<i>Title</i>	<i>page</i>
1-1	The G_t activation cycle	24
1-2	Crystal structures of the G_t heterotrimer and rhodopsin	25
1-3	Primary and secondary structure of rhodopsin	27
1-4	The structure of $G\alpha_t$	28
1-5	Primary and secondary structures of $G\alpha_t$	29
3-1	Schematic representation of bovine rhodopsin	52
3-2	Peptides derived from the second, third, and fourth intracellular loops of rhodopsin inhibit activation of G_t by rhodopsin	53
3-3	Effect of rho(310-321) on the intrinsic fluorescence of $G\alpha_t$ and $G\beta\gamma_t$ subunits	54
3-4	Amino acid sequences of the fourth loop of bovine rhodopsin, human β_2 AR, human m1 MR, and fourth loop mutants of rhodopsin	55
3-5	Rates of G_t activation catalyzed by solubilized, purified recombinant pigments	56
3-6	The relative rates of pigment-catalyzed $GTP\gamma S$ uptake by $G\alpha_t$ as a function of $G\beta\gamma_t$ concentration are similar for both rhodopsin and CTr2	57
3-7	The amino-terminal half of the fourth loop of rhodopsin is more conserved than the carboxyl-terminal half within the family of vertebrate opsins.	58
4-1	Amino acid sequences of recombinant rhodopsins and G_t -derived peptides	73

List of Figures (con't)

4-2	Photoregeneration of rhodopsin in the presence of increasing concentrations of G_t or G_t -derived peptides	74
4-3	Altered peptides do not inhibit photoregeneration	76
4-4	The effect of G_t , $\alpha(340-350)$ and $\gamma(50-71)$ -far on photoregeneration of heterologously expressed rhodopsin and C4 loop mutants	77
4-5	Quantitation of the effects of G_t , $\alpha(340-350)$, and $\gamma(50-71)$ -far on the photoregeneration of recombinant rhodopsin and rhodopsin mutants	79
5-1	Structure of the interdomain interface of GDP-bound $G\alpha_t$	98
5-2	Determination of nucleotide exchange rates by analysis of trypsin digestion patterns	99
5-3	Plots of uncatalyzed and catalyzed nucleotide exchange time courses derived from analysis of trypsin digest patterns of <i>in vitro</i> translated $G\alpha_t$	100
5-4	Time courses of activation of mutants of residues located on the helical domain	101
5-5	Time courses of activation of mutants of residues located on Switch III (a.k.a. Insert 2)	102
5-6	Time courses of activation of mutants of residue 228 located on Switch III (a.k.a. Insert 2)	103
5-7	Time courses of activation of mutants of residues located on the αG region (a.k.a. Insert 3)	104
5-8	Time courses of uncatalyzed activation of double mutants	105
5-9	Uncatalyzed activation of $G\alpha_{i1}$ and mutants of $G\alpha_{i1}$	106
5-10	Structure of the interdomain interface of GDP-bound $G\alpha_{i1}$	107
6-1	Structure of the $\alpha 5$ helix of $G\alpha_t$	125

List of Figures (con't)

6-2	Nucleotide exchange time courses of proline mutants in $\alpha 5$	126
6-3	Truncation and insertion mutants of $G\alpha_t$	127
6-4	Uncatalyzed nucleotide exchange time courses of alanine mutants in $\alpha 5$	128
6-5	Trypsin digest analysis of wild-type, A322S, and the rapidly activating alanine mutants (T325A, V328A and F332A)	129
6-6	Rhodopsin/ $G\beta\gamma_t$ -catalyzed nucleotide exchange time courses of alanine mutants in $\alpha 5$	130
6-7	Nucleotide exchange time courses of mutants of residues near $\alpha 5$ and in the $\beta 6/\alpha 5$ loop	131
6-8	Schematic representation of the phenotypes of proline mutants in $\alpha 5$	132
6-9	Schematic representation of the phenotypes of alanine mutants in $\alpha 5$: a model for R^* -catalyzed G_t activation	133
7-1	Close-up of Helix 8 (H8) of rhodopsin	149

List of Tables

<i>Number</i>	<i>Title</i>	<i>Page</i>
3-I	Biochemical Characterization of Rhodopsin Fourth Loop Mutants	51
4-I	G _t activation and photoregeneration data	72
5-I	Rate constants for basal nucleotide exchange measured for Gα _t and Gα _t mutants.	97
6-I	Rate constants of uncatalyzed nucleotide exchange of Gα _t and Gα _t mutants.	124

Abbreviations

$\alpha 5$	the $\alpha 5$ helix of $G\alpha_t$
AR.....	adrenergic receptor
C1, C2, etc.....	First, second, etc. cytoplasmic loop of rhodopsin
DM.....	n- dodecyl- β -D-maltoside
E1, E2, etc.....	First, second, etc. extracellular loop of rhodopsin
G_t	holo-transducin
$G\alpha_t$	α subunit of transducin
$G\beta\gamma_t$	$\beta\gamma$ heterodimer subunit of transducin
$G\beta_t$	β subunit of transducin
$G\gamma_t$	γ subunit of transducin
GTP γ S	guanosine -3-O-(thio)triphosphate
GPCR.....	G protein coupled receptor
IVT.....	<i>in vitro</i> translated
MII.....	metarhodopsin II
MR.....	muscarinic receptor
R*.....	signaling active state of rhodopsin
Ras.....	Ras p21 ^{ras}
RM.....	reverted metarhodopsin
TM.....	transmembrane

Mutants proteins are designated by the amino acid present in the wild-type protein (using the single letter code) and its position, followed by the amino acid present in the mutant. For example, a mutant in which phenylalanine 332 is replaced by alanine is designated F332A.

Abstract

The intermolecular interaction between the photoreceptor rhodopsin and the heterotrimeric G protein transducin (G_t) initiates the vertebrate phototransduction cascade. This interaction also serves as a model system for the study of the molecular basis of related G protein-coupled receptor mediated signal transduction systems. Photoactivated rhodopsin (R^*) activates G_t by catalyzing the exchange of bound GDP for GTP on its α subunit ($G\alpha_t$). The structure of the R^* - G_t complex and the mechanism of nucleotide exchange are unknown. We studied the function of the fourth cytoplasmic loop (C4) of rhodopsin in interactions with G_t . Chimeric mutants of rhodopsin were characterized in which regions of C4 were replaced with amino acid sequences from the β_2 adrenergic receptor or the m1 muscarinic receptor. Chimeras in which the amino terminus of C4 was altered were defective in catalyzing G_t activation. A spectroscopic photoregeneration assay was used to demonstrate that mutants of the amino terminus of C4 were defective in binding holo- G_t , a peptide derived from the carboxyl terminus of $G\alpha_t$, and in certain circumstances a peptide derived from the carboxyl terminus of $G\gamma_t$. These results suggested that C4 mediated G_t binding and activation and that C4 interacted specifically with the carboxyl termini of $G\alpha_t$ and possibly $G\gamma_t$. We next studied how R^* induces nucleotide exchange by G_t at a distance. We tested the validity of two longstanding hypotheses: 1) that R^* induces opening of the interdomain cleft of $G\alpha_t$, and 2) that R^* communicates with the nucleotide binding pocket via the $\alpha 5$ helix of $G\alpha_t$. We developed an expression and assay system to characterize a large number (>50) of site-directed mutants of $G\alpha_t$ designed to test these hypotheses. The mutants were expressed *in vitro* in rabbit reticulocyte lysate and the kinetics of both basal and R^* -catalyzed nucleotide exchange were determined by quantitative analysis of trypsin digest patterns. Mutations in a series of residues at the interface between the two domains of $G\alpha_t$ had only minor effects on the basal and catalyzed activation rates. In contrast,

Abstract

mutations in a cluster of residues on the buried face of the $\alpha 5$ helix, 0.7-1.5 nm from the nucleotide, greatly (up to 165-fold) accelerated nucleotide exchange. Mutations of residues on the adjacent solvent-exposed surface of $\alpha 5$ disrupted R^* -catalyzed activation, as did substitution of $\alpha 5$ residues with prolines. These results provided evidence that R^* induced nucleotide exchange primarily by perturbing the structure of buried residues on $\alpha 5$ and not by opening the interdomain cleft. Structural analysis and biochemical data were used to propose a mechanistic model for receptor-catalyzed G protein activation.

Chapter 1: Introduction

The Phototransduction Cascade

The phototransduction cascade of the vertebrate rod cell can be defined as the set of regulated molecular interactions responsible for photon detection and subsequent neuronal signaling (Wald, 1968; Stryer, 1988). Extensive investigation by biochemists, biophysicists and physiologists over many decades has yielded a detailed understanding of phototransduction, which has emerged as a model for how cells detect and respond to a wide variety of extracellular stimuli. In this introductory chapter the basic features of phototransduction are discussed and a brief historical review of the key studies that unraveled the central biochemical cascade is presented. Subsequently, the structure and function of two important proteins in the cascade, rhodopsin and transducin, are examined in more detail. Finally, an overview of the thesis research, which examines the molecular mechanism of interactions between rhodopsin and transducin, is provided.

Rod cells are specialized dim-light photosensor cells. They are sensitive enough to detect single photons (Baylor *et al.*, 1979) as a result of high signal amplification and low thermal background noise. They are one of two photoreceptor cell types in the retina, the laminated layer of neural tissue at the back of the vertebrate eye. The second photoreceptor cell type, cone cells, are specialized for bright light and color vision. In addition to the photoreceptors, the neural retina consists of four neuronal cell types (bipolar cells, ganglion cells, horizontal cells, and amacrine cells) as well as glial cells (Cepko *et al.*, 1996). The simplest neuronal signaling pathway in the retina involves transmission from photoreceptors to bipolar cells to ganglion cells, whose axons form the optic nerve which exits the retina and travels to the brain (Sakmar, 2001).

The initial step in rod cell phototransduction takes place in the rod outer segment (ROS). The ROS is filled with stacks of disc-shaped membranes and contains the

molecular machinery of phototransduction. Rhodopsin, the photoreceptor pigment molecule, is an integral membrane protein localized primarily to the disc membranes. Rhodopsin consists of an apoprotein called opsin and a covalently attached chromophore derived from 11-*cis*-retinal (Wald, 1968). Upon absorption of a photon, the 11-*cis*-retinylidene chromophore isomerizes to all-*trans*-retinylidene (ATR) (Wald, 1968). Subsequent biochemical reactions lead to the hyperpolarization of the rod cell. Hyperpolarization alters synaptic transmission between rod cells and adjoining neurons in the retina, initiating a signal that is ultimately transmitted to the brain. The biochemical mechanisms that couple chromophore isomerization (which is the only light dependent step in phototransduction) and rod cell hyperpolarization were elucidated by a series of key experiments in the 1970s and early 1980s.

The Biochemistry of the Phototransduction Cascade: an Historical Overview

In the early 1970s Bitensky and co-workers identified a key intermediate in the phototransduction pathway when they demonstrated that light could regulate the levels of cyclic guanosine monophosphate (cGMP) in photoreceptor cells by activation of a light-dependent cGMP phosphodiesterase (PDE) activity (Miki *et al.*, 1974). Activation of a single molecule of rhodopsin was found to result in the hydrolysis of 10^5 molecules of cGMP (Yee and Liebman, 1978). cGMP was shown to play a crucial role in phototransduction by Miller and Nicol who demonstrated that injection of cGMP into rod cells induced depolarization of the rod cell and increased the latency for hyperpolarization by illumination (Miller and Nicol, 1979; Nicol and Miller, 1978).

Interestingly, the PDE activity demonstrated a requirement for GTP, and appeared to be regulated by a light-sensitive GTPase activity in the ROS (Wheeler and Bitensky, 1977). In 1979, Godchaux and Zimmerman reported the isolation of a protein with GTPase activity that interacted with isolated ROS membranes (Godchaux and Zimmerman, 1979). They showed that the protein could bind GDP or GTP. The activity

was purified and found initially to involve two polypeptide chains. Hermann Kühn expanded on these findings by reporting in 1980 that three proteins of molecular mass 37, 35, and 6 kDa bound to isolated ROS membranes only following exposure to light (Kühn, 1980). The two larger proteins were apparently the same as those observed by Godchaux and Zimmerman. Furthermore, Kühn showed that the three proteins could be eluted specifically from the photolyzed membranes with GTP. These observations allowed for the easy purification of the guanine nucleotide binding protein and its subsequent characterization.

At about the same time, Fung and Stryer reported that photoactivated rhodopsin (R^*) catalyzed nucleotide exchange -- the release of GDP followed by the binding of GTP-- by the guanine nucleotide binding protein (Fung and Stryer, 1980). Significantly, they showed that a single molecule of R^* could catalyze the exchange of several hundred nucleotides.

By 1981, the stage was set for a key paper by Stryer and co-workers that tied together the previous observations (Fung *et al.*, 1981). Using purified preparations of the heterotrimeric guanine nucleotide binding protein, they showed that the nucleotide bound exclusively to the largest polypeptide, which they termed the α subunit. The binding of GTP induced the separation of the α subunit from the two smaller subunits, β and γ . Second, they showed that R^* could stimulate the replacement of GDP with GTP in the absence of PDE. Finally, they demonstrated that GTP-bound α subunit (but not GDP-bound α) could activate PDE in the absence of R^* . Based on these data, Stryer proposed the key steps of the rhodopsin-transducin cycle (Fig. 1-1). Absorption of a photon by rhodopsin causes chromophore isomerization, which leads to conformational changes that create R^* . R^* catalyzes the exchange of GDP for GTP by the α subunit of transducin ($G\alpha_t$). GTP-bound $G\alpha_t$ dissociates from rhodopsin and $G\beta\gamma_t$ and then activates PDE. Activated PDE rapidly hydrolyzes cGMP to GMP, resulting in decreased [cGMP] in the

rod cell. Hydrolysis of bound GTP to GDP by the intrinsic GTPase activity of $G\alpha_t$ returns the protein to the inactive conformation, whereupon it disengages PDE and again binds $G\beta\gamma$. Since the nucleotide binding protein subunit could transduce a signal from activated rhodopsin to PDE, Stryer named it "transducin" (G_t).

The final piece of the cascade-- the connection between decreased intracellular [cGMP] and hyperpolarization of the rod cell-- was discovered in 1985. Fesenko and colleagues demonstrated using isolated patches of ROS plasma membrane that cation channels in the membrane required cGMP to remain open (Fesenko *et al.*, 1985). It had been known previously that a "dark" current, carried primarily by Na^+ ions, flowed into the ROS through plasma membrane cation channels in the absence of light (Yau, 1994). Na^+ ions were simultaneously ejected from the rod cells by pumps in the inner segment. In the dark, the membrane potential of the rod cell is $\sim -35mV$ (Yau, 1994). Thus, following the light-induced decrease in [cGMP], the cation channels closed, blocking the inward cation current and causing rod cell hyperpolarization.

Interestingly, at about the same time as the rod cell biochemistry was elucidated, Gilman, Rodbell and others studying the hormonal regulation of adenylyl cyclase activity were uncovering the importance of a GTP-binding protein in transducing signals from agonist-occupied hormone receptors to the enzyme adenylyl cyclase (Ross and Gilman, 1980). It eventually became clear that the stimulatory GTP binding protein of the hormonal system, G_s , and the GTP-binding protein of the rod cell, G_t , were both members of the same superfamily of guanine nucleotide binding regulatory proteins, or G proteins. The molecular cloning of rhodopsin (Nathans and Hogness, 1983) and of the β_2 adrenergic receptor (Dixon *et al.*, 1986) would reveal that the receptors shared amino acid sequence (and presumably structural) similarity. The close resemblance of the photon and hormone signal transduction systems was a surprising example of the

conservation of a basic mechanism in biology for the execution of similar tasks in different contexts.

The Central Role of Rhodopsin-G_t Interactions

As the experiments described above revealed, G_t plays a central role in the phototransduction cascade. It couples together two separate highly specialized proteins: the photon detector rhodopsin and the efficient second messenger modulator PDE. G_t activation by R* represents a key amplification step in the cascade in that a single R* can catalyze the activation of hundreds of G_t molecules (Heck and Hofmann, 2001; Fung and Stryer, 1980). This amplification is crucial to the sensitivity of the system. In addition, G_t exhibits a low rate of basal (uncatalyzed) nucleotide exchange that contributes to the sensitivity by maintaining low background noise. Finally, G_t provides an important site of regulation in the cascade. The rates of GTP loading and GTP hydrolysis by G_t greatly affect the amplitude and the temporal resolution of the resulting signal.

The molecular mechanisms that underlie the interaction between rhodopsin and transducin have been studied intensively over the past 20 years since Kühn, Bitensky, Zimmerman, Stryer and others worked out their central role as the first intermolecular interaction in the phototransduction cascade (Fig. 1-2) (for recent reviews, see (Bourne, 1997; Sakmar, 1998; Menon *et al.*, 2001)).

Rhodopsin Structure and Function

Rhodopsin Structure

The crystal structure of dark state rhodopsin was recently solved at 2.8 Å resolution (Fig. 1-2) (Palczewski *et al.*, 2000). The structure confirmed many of the topological and structural features that had been predicted by models based on sequence, biochemical and cryoelectron microscopy analyses (e.g., (Baldwin *et al.*, 1997; Shieh *et al.*, 1997). The

primary and secondary structures of rhodopsin are depicted schematically in Fig. 1-3. The tertiary structure reveals seven transmembrane helices (TM), most of which are tilted and kinked, arranged in a bundle surrounding the chromophore. The chromophore is covalently attached to K296 of TM7 via a protonated Schiff base. E113, the experimentally determined counterion to the protonated Schiff base (Sakmar *et al.*, 1989), lies 0.35 nm away. Side chains of amino acid residues from a number of helices, especially TM3, TM6 and TM7 interact closely with the chromophore. There are two solvent exposed regions of rhodopsin, the cytoplasmic and intradiscal surfaces. (The intradiscal surface is often referred to as the extracellular surface in analogy to related receptors which are localized to the plasma membrane.) The extracellular surface consists of three interhelical loops (E1, E2 and E3), as well as the amino terminal tail. The cytoplasmic surface consists of three interhelical loops (C1, C2 and C3) and the carboxyl terminal tail. In addition a "fourth" cytoplasmic loop (C4) is created by the membrane insertion of palmitoyl groups attached to two adjacent cysteines (C322 and C323) in the carboxyl terminus (Ovchinnikov *et al.*, 1988; Moench *et al.*, 1994). The solvent exposed surfaces of rhodopsin were found to have a considerable amount of ordered structure. The extracellular surface is notable for a distorted β sheet consisting of sequence elements from the amino-terminal tail and the E2 loop. The E2 loop forms a "plug" that contacts the chromophore at the base of the helix bundle. The structure of the extracellular surface is supported by a disulfide bond between C110 and C187. The cytoplasmic surface reveals that helices extend from TM3 and TM6 beyond the apparent border of the lipid bilayer. The C2 loop projects outward from the helical bundle in an extended conformation. C3 is partially disordered, which is consistent with the conformational flexibility previously suggested by site directed spin labeling (Altenbach *et al.*, 1996). Unexpectedly, much of C4 is an amphipathic helix (designated helix 8, or H8), which extends outward from the helical bundle along the apparent surface of the membrane. Together with C2, this structure increases the size of the cytoplasmic surface

beyond what would be predicted from the diameter of the transmembrane helical bundle alone.

Opsin-Chromophore Interactions

In the dark state, 11-*cis*-retinal acts pharmacologically as an inverse agonist that keeps rhodopsin in the signaling “off” state (Han *et al.*, 1997). The first step in the phototransduction, the isomerization of the chromophore to a distorted ATR, is accomplished within 200 fsec (Schoenlein *et al.*, 1991), qualifying it as one of the fastest biological events known. Following isomerization, the chromophore-opsin complex thermally relaxes. During this relaxation, photolyzed rhodopsin sequentially assumes a number of spectrally defined transient conformations. These intermediates were originally identified in low temperature trapping experiments, and subsequently a similar set of intermediates have been observed by time resolved spectroscopy of photolyzed rhodopsin samples (Sakmar, 1998). Within milliseconds, an equilibrium between two metastable intermediates, metarhodopsin I (MI) and metarhodopsin II (MII), is reached. This equilibrium is sensitive to environmental conditions including temperature, pH, membrane or detergent composition, and the binding of G_t . A subconformation of MII defined by the spectrally silent uptake of two protons from the aqueous environment, MIIb, is thought to be identical with the signaling active conformation of rhodopsin, R^* (Kibelbek *et al.*, 1991; Arnis and Hofmann, 1993). ATR acts as a pharmacological agonist which favors formation of R^* .

The conformational changes that follow chromophore isomerization are induced in part by steric interactions between the all-*trans* chromophore and the opsin protein (Shieh *et al.*, 1997). A recent study using a retinal derivative with a crosslinking group on the six-membered ring of the retinal mapped significant changes in the ring-protein interactions following photolysis (Borhan *et al.*, 2000). In the dark state, the modified ring crosslinked to W265 of TM6. Following photolysis at room temperature, crosslinks

formed with A169 of TM4. The importance of steric interactions between the chromophore and the TM helices is suggested by the reduction in the formation of R* in artificial pigments created by the regeneration of opsin with retinal analogs that lack either the methyl group attached to C-9 of the polyene chain (Han *et al.*, 1998) or the ring (Nukada *et al.*, 1986).

Extensive research has gone into understanding the conformational and chemical changes of rhodopsin that define the formation of R*. The protonation state of several residues changes. UV-visible spectroscopy revealed that the Schiff base is deprotonated (Fahmy and Sakmar, 1993b), and FTIR studies indicate that the ground state counterion E113 becomes protonated (Jager *et al.*, 1994). In addition, time-resolved spectroscopic measurements with pH-sensitive dyes indicate that two protons are taken up by the protein from the bulk solvent upon R* formation (Arnis and Hofmann, 1993). One of the proton acceptors appears to be E134, part of a highly conserved E/D-R-Y sequence at the cytoplasmic end of TM3 (Arnis *et al.*, 1994). The importance of protonation of E134 in R* formation is also supported by the finding that the E134Q mutant of rhodopsin had increased ability to activate G_t at alkaline pH relative to wild-type rhodopsin (Fahmy and Sakmar, 1993a). The site of the second proton acceptor is unknown. There are also a number of documented conformational changes involved in formation of R*. Obviously, the chromophore is isomerized to the all-*trans* conformation. Additionally, TM3, TM6, and possibly TM7 appear to move apart from one another upon R* formation. This "helix movement" model is supported by a number of observations, including: (1) naturally occurring tryptophan residues on TM3 and TM6 experienced altered microenvironments following MII formation as detected by UV difference spectroscopy (Lin and Sakmar, 1996); (2) site-directed spin labeling studies showed that photoactivation increases the distance between spin labels on the cytoplasmic ends of TM3 and TM6 (Farrens *et al.*, 1996); (3) the formation of disulfide crosslinks between

cysteine residues engineered into the cytoplasmic ends of TM3 and TM6 prevented activation of G_t (Farrens *et al.*, 1996); (4) Zn^{2+} inhibited G_t activation by rhodopsin mutants containing Zn^{2+} binding sites in the form of His residues engineered into the cytoplasmic ends of TM3 and TM6 (Sheikh *et al.*, 1996); and (5) replacement of G121 on TM3 with larger residues caused constitutive activity in the dark whereas substitution of F261 on TM6 with smaller residues suppressed the effects of the G121 mutants (Han *et al.*, 1997; Han *et al.*, 1996).

It is not understood how steric interactions in the chromophore binding pocket may be propagated to the cytoplasmic surface of rhodopsin (Shieh *et al.*, 1997). It has been proposed that structural changes of TM3 and TM6 at the cytoplasmic surface involve rigid body movements of these helices (Farrens *et al.*, 1996), which suggests a possible mechanism. However, the finding that the TM helices are highly kinked and irregular (Palczewski *et al.*, 2000) raises the issue of the extent to which they can move individually as rigid bodies. As would be expected, the structural connection between the chromophore binding pocket and the cytoplasmic surface runs in both directions. Not only is the structure of the chromophore binding pocket communicated to the cytoplasmic surface, but binding of G_t to the cytoplasmic surface of rhodopsin affects the conformation of the chromophore binding pocket (Arnis and Hofmann, 1995; Ernst *et al.*, 2000). This phenomenon is exploited as the basis of a G_t -binding assay described in Chapter 4.

R Interactions With G_t*

A variety of techniques has been used to identify the regions of R^* that interact with G_t . Involvement of the second (C2) and third (C3) intracellular loops of rhodopsin are suggested by site directed mutagenesis (Franke *et al.*, 1992; Franke *et al.*, 1990) and peptide competition studies (König *et al.*, 1989). In particular, the highly conserved R135 in C2 appears to be required for proper activation of G_t (Acharya and Karnik,

1996). In the crystal structure of dark state rhodopsin, R135 interacts with E134. Protonation of E134, which is suggested to occur upon R* formation (see above), could free R135 to assume alternate conformations. The importance of the amino terminus of the fourth loop (C4) is discussed in detail in Chapters 3 and 4. The data regarding regions of R* that interact with G_t fit well with the data relating to the conformational changes that occur at the cytoplasmic surface during formation of R*. TM3 and TM6, which are thought to move upon R* formation, are linked to C2 and C3. These helix movements may expose the otherwise occluded determinants of G_t activation located at the juxtacytoplasmic regions of C2, C3, and C4.

R* activity is reduced by phosphorylation on the carboxyl terminus (Miller *et al.*, 1986). Phosphorylation is catalyzed by rhodopsin kinase, which specifically recognizes MII. Multiply phosphorylated rhodopsin is bound by arrestin with high affinity (Wilden *et al.*, 1986). Thus arrestin sterically interferes with G_t binding. Eventually, R* decays to the apoprotein opsin and free ATR.

G_t structure and function

Crystal structures of a variety of conformations of G_t have been solved to date, including the GTPγS (Noel *et al.*, 1993), the GDP (Fig. 1-4) (Lambright *et al.*, 1994), and the GDP/AlF₄⁻-bound structures of Gα_t (Sondek *et al.*, 1994), as well as the GDP-bound heterotrimer (Fig. 1-2) (Lambright *et al.*, 1996), and free Gβγ_t (Sondek *et al.*, 1996). More recently, the structure of the ternary complex of Gα_t bound to its effector PDE γ and RGS9 was reported (Slep *et al.*, 2001). These structures have provided detailed information on a number of G protein mechanisms, including the nature of the conformational change induced by GTP binding, the mechanism and regulation of GTP hydrolysis, and the nature of interactions between Gα_t and Gβγ_t.

Gα_t, a 350 amino acid protein, consists of two domains (Fig. 1-4): the Ras-like domain, named due to its homology with the structure of the monomeric G protein, p21^{ras} (Ras); and the helical domain, named to reflect its composition of 6 α helices (αA–αF). The nucleotide is bound in a cleft between the domains. The Ras-like domain consists of a central mixed 6-stranded β-sheet (designated β1–β6), surrounded on either side by a total of 6 α-helices (designated α1–α5, plus αG). The majority of the direct contacts to the nucleotide originate from conserved regions of the Ras-like domain, which map to loops emanating from the strands of the central β-sheets. These loops are homologous to canonical nucleotide-binding domains of the monomeric G proteins (Sprang, 1997). The Ras-like domain contains four regions not homologous to Ras, called Inserts 1–4. These are discussed in more detail in Chapter 5. The primary and secondary structures of Gα_t are presented in Fig. 1-5.

The conformational changes that accompany the exchange of GDP for GTP are localized to three regions, denoted Switch I, II, and III. Switch I (S173-T183) and II (F195-T215) are similar to Switch regions described in Ras; Switch III (D227-R238) is unique to the heterotrimeric G proteins (Fig. 1-4). Switch I and II respond directly to the

presence of the γ phosphate of GTP, whereas Switch III appears to move in response to reorganization of the Switch II (Lambright *et al.*, 1994). The conformational changes in Switch II involve a partial rotation of the $\alpha 2$ helix, which leads to the movement of several amino acid side chains from exposed to partially buried positions. These changes serve as the basis of assays of $G\alpha_t$ activation. In particular, the movement of W207 is detected as a large increase in fluorescence emission intensity (Faurobert *et al.*, 1993) (see Chapter 3), and the burial of R204 protects it from cleavage by trypsin (Fung and Nash, 1983) (see Chapter 5).

$G\alpha_t$ -GTP activates PDE, a tetrameric enzyme consisting of α , β , and γ subunits in a 1:1:2 stoichiometry, by removing the inhibitory constraints that the γ subunits exert upon the catalytic α and β subunits. The binding site for PDE γ on $G\alpha_t$ was recently determined by X-ray crystallography, and found to reside between the $\alpha 2$ helix of the Switch II region and the adjacent $\alpha 3$ helix (Slep *et al.*, 2001).

$G\alpha_t$ returns to its inactive GDP-bound state by hydrolyzing the bound GTP to GDP. Rapid turn-off of the cascade is essential for the temporal resolution of the signal (He *et al.*, 1998). GTP hydrolysis is accelerated by the simultaneous binding of the effector, cGMP γ subunit, and a second protein, regulator of G protein signaling 9 (RGS9) (He *et al.*, 1998). $G\alpha_t$ (GDP) recombines with $G\beta\gamma_t$, and can then be activated anew by R^* .

$G\beta_t$ is a 340 amino acid protein, constructed from an amino terminal α helix, followed by a β propeller structure (Sondek *et al.*, 1996). The β propeller consists of seven “blades” of 4 β sheets each. Each blade is roughly related to the others by rotational symmetry (Fig. 1-2). At the sequence level, $G\beta_t$ is notable for 7 WD40 domains, sequence repeats of roughly 40 amino acids that frequently end with Trp-Asp (WD in the single letter code). Each WD40 repeat corresponds to the fourth strand of one propeller blade, and the first three strands of an adjacent blade. $G\beta_t$ is a member of a

large family of proteins containing WD40 repeats, which perform a variety of functions; all are thought to fold into β propeller structures (Neer *et al.*, 1994b; Garcia-Higuera *et al.*, 1996). $G\beta_t$ is also a member of a larger family of proteins which fold into β propeller structures, many of which do not share significant sequence homology.

$G\gamma_t$ is the shortest transducin subunit, consisting of only 74 amino acids. It contains an amino terminal α helix, which interacts with the amino terminus of $G\beta_t$ in a coiled-coil conformation (Fig. 1-2). Interestingly, a study conducted prior to the determination of the structure showed that peptides derived from the helical regions of $G\beta_t$ and $G\gamma_t$ do not associate with each other in solution (Marin and Neubig, 1995). The remainder of $G\gamma_t$ wraps around $G\beta_t$ in an extended conformation. $G\beta_t$ and $G\gamma_t$ can be dissociated from one another only under denaturing conditions, and physiologically they function as a single entity.

The structure of the G_t heterotrimer (Lambright *et al.*, 1996) reveals two distinct sites of interaction between $G\alpha_t$ and $G\beta\gamma_t$: between the amino-terminal helix of $G\alpha_t$ and the side of the $G\beta_t$ propeller, and between the Switch I / Switch II region of $G\alpha_t$ and the top of the $G\beta_t$ propeller structure (Fig. 1-2). Direct contacts between $G\alpha_t$ and $G\gamma_t$ are not observed in the structure, although interactions between lipids attached to each subunit (see below) have been proposed. The structure of free $G\beta\gamma_t$ compared with $G\beta\gamma_t$ in the heterotrimer reveals that $G\beta\gamma_t$ is virtually unchanged by the binding of $G\alpha_t$ (Sondek *et al.*, 1996). However, the structure of $G\alpha_t$ is altered in the conformationally flexible Switch I/II binding region, which makes contacts with $G\beta_t$ (Lambright *et al.*, 1996). The structure of the amino terminal helix of $G\alpha_t$ is also likely altered by the binding of $G\beta\gamma_t$.

A number of important post-translational modifications of G_t have been described. $G\alpha_t$ is heterogeneously acylated, primarily with saturated C12 and C14 lipids, at its amino terminal glycine (Kokame *et al.*, 1992). This modification is thought to be

important for interactions with $G\beta\gamma_t$ (Kokame *et al.*, 1992), and possibly with membranes and rhodopsin (Min, 1996). Recently, a report describing the phosphorylation of $G\alpha_t$ at Y142 by the tyrosine kinase Src in rod outer segments has been published (Bell *et al.*, 2000). The significance of this modification is not yet understood. $G\gamma_t$ is modified in a three step process that includes farnesylation of a cysteine in the carboxyl-terminal CAAX motif, followed by cleavage of the three carboxyl terminal amino acids, and carboxymethylation of the free carboxyl terminus (Wedegaertner *et al.*, 1995). Farnesylation has been found to be important for interactions with $G\alpha_t$ (Matsuda *et al.*, 1998) as well as with rhodopsin (Scheer and Gierschik, 1995; Kisselev *et al.*, 1994). There is evidence that rhodopsin can discriminate between farnesyl (C15) and geranylgeranyl (C20) lipids (Kisselev *et al.*, 1995a), suggesting the existence of a specific prenyl binding site on rhodopsin.

*G_t Interactions With R^**

A variety of biochemical and biophysical techniques have been used to identify sites on G_t that interact with membranes and with R^* . The involvement of the carboxyl terminal 11 amino acids of $G\alpha_t$ (a.a. 340-350) in interactions with R^* is suggested by many studies, including: (1) the finding that Pertussis toxin catalyzes the ADP-ribosylation of C347, which uncouples G_t from rhodopsin; (2) a peptide corresponding to amino acids 340-350 can uncouple rhodopsin from G_t and can itself bind to rhodopsin and mimic the effects of G_t (Hamm *et al.*, 1988); (3) site directed mutagenesis (Garcia *et al.*, 1995; Osawa and Weiss, 1995); and (4) the demonstration in related G proteins that specificity of coupling to particular receptors resides in the carboxyl terminus (Conklin *et al.*, 1993). In addition, peptide and site-directed mutagenesis studies have suggested the involvement of the $\alpha 4/\beta 6$ loop of $G\alpha_t$, which lies adjacent to the carboxyl terminus, in interacting with R^* (Hamm *et al.*, 1988; Natochin *et al.*, 1999). Experimental evidence suggests that $G\beta\gamma_t$ is also in direct contact with rhodopsin (Phillips and Cerione, 1992;

Kelleher and Johnson, 1988). The specific contacts between $G\beta\gamma_t$ and R^* involve the carboxyl terminus of $G\gamma_t$, as suggested by studies with peptides derived from that region (Kisselev *et al.*, 1994; Kisselev *et al.*, 1995a) and possibly the seventh propeller blade of $G\beta\gamma_t$ (Taylor *et al.*, 1996).

All of the structures of G_t thought to participate in interactions with rhodopsin or the membrane cluster to a common face on the structure of G_t , and identify a putative rhodopsin interacting surface (Lambright *et al.*, 1996; Bohm *et al.*, 1997) (Fig. 1-2). However, in the crystal structure of the heterotrimer, neither the carboxyl terminus of $G\alpha_t$ nor that of $G\gamma_t$ is included. Thus the structure of the specific rhodopsin-interacting regions is unclear. A partial remedy has been provided by an NMR study of a peptide derived from the carboxyl terminus of $G\alpha_t$ in its rhodopsin bound conformation; these data suggest that it forms a helical extension of the $\alpha 5$ helix of $G\alpha_t$ (Kisselev *et al.*, 1998) (Fig. 6-1).

The Mechanism of R^* -Catalyzed Nucleotide Exchange

The photoisomerization of 11-*cis*-retinal to ATR leads to local structural alterations in the chromophore binding pocket of rhodopsin. These structural changes are propagated to the cytoplasmic surface of rhodopsin, and following binding of G_t , on to the nucleotide binding pocket of $G\alpha_t$ where GDP is released. In this way, the chromophore binding pocket of rhodopsin is allosterically coupled to the nucleotide binding pocket of $G\alpha_t$ approximately 5 nm away (Fig. 1-2). This conformational coupling transfers information that the chromophore of rhodopsin has absorbed a photon an equal distance.

Several key observations characterize the process of R^* -catalyzed nucleotide exchange. In the absence of a catalyst, the rate limiting step in nucleotide exchange is release of GDP from $G\alpha_t$ to form empty-pocket G_t , $G\alpha_t(e)\beta\gamma_t$. $G\alpha_t(e)$ is by itself very unstable. R^* catalyzes nucleotide exchange by inducing GDP release and stabilizing the

reaction intermediate, $G\alpha_t(e)\beta\gamma_t$. The empty pocket G_t can be dissociated from R^* by either GDP or GTP; R^* and nucleotide binding are mutually exclusive. GTP binding is nearly irreversible since conformational changes in the Switch II region destroy the $G\beta\gamma_t$ binding site and induce dissociation of $G\alpha_t(\text{GTP})$ from $G\beta\gamma_t$ and R^* . R^* interacts specifically with heterotrimeric G_t ; $G\beta\gamma_t$ appears to be absolutely required for efficient R^* -catalyzed nucleotide exchange on $G\alpha_t$ (Fung, 1983). It is unclear whether $G\beta\gamma_t$ plays a mechanistic role in the catalysis process (Iiri *et al.*, 1998) or whether it merely facilitates binding between rhodopsin and $G\alpha_t$ (Phillips *et al.*, 1992). Binding of G_t to R^* and dissociation of GDP appear to be distinct steps; rhodopsin mutants have been described which bind G_t but do not induce GDP release (Franke *et al.*, 1990; Ernst *et al.*, 1995).

The molecular mechanism by which R^* induces GDP release from G_t is the least understood step in the G_t signaling cycle. Despite a great deal of data regarding structures of G_t and rhodopsin that interact with each other, little is known about the detailed structure of the complex (Liu *et al.*, 1995). The structure of R^* is not known, and the conformational changes, if any, that occur in R^* and G_t -GDP upon complex formation are not known. Very few sites of point-to-point contacts between R^* and G protein have been reliably identified (Acharya *et al.*, 1997), and those that have been found do not greatly constrain possible geometric alignments of the two proteins in the complex. Crystallographic analysis of the R^* - $G_t(e)$ complex may prove difficult due to the instability of R^* . The alignment of the interacting surfaces in the structures of rhodopsin and G_t produces a hypothetical low resolution model of the complex (Bourne, 1997) (Fig. 1-2). These analyses, while lacking details, do suggest clearly that the cytoplasmic loops of rhodopsin, which are roughly 1.5 nm long (at most) are too short to contact directly the nucleotide-binding pocket of $G\alpha_t$, which is at least 2.5 nm from the

rhodopsin-binding surface of G_t . Consequently, R^* must act “at-a-distance” to induce nucleotide exchange in $G\alpha_t$ (Iiri *et al.*, 1998).

Advantages of Rhodopsin and Transducin as a Model System

Rhodopsin and G_t offer a number of distinct advantages as a model system for the study of the molecular basis of signal transduction. First, both rhodopsin and G_t are available in large quantities from a natural source, the retina. Milligram quantities of both proteins can be purified from bovine retinas using established techniques (Kühn, 1980). Rhodopsin and G_t purified from bovine retinas are integral to the studies presented in this thesis, particularly the fluorescence G_t -activation assays presented in Chapter 3, the G_t -binding photoregeneration assays in Chapter 4, and the rhodopsin-catalyzed nucleotide exchange assays described in Chapters 5 and 6.

Second, rhodopsin is suited to spectroscopic and biophysical studies since it absorbs visible light ($\lambda_{\max} = 500\text{nm}$, $\epsilon = 47,500 \text{ M}^{-1}\text{cm}^{-1}$). The λ_{\max} is sensitive to the environment of the chromophore, which is determined by the conformation of the surrounding protein. In particular, the λ_{\max} shifts dramatically from 480 nm to 380 nm upon deprotonation of the Schiff base, which occurs during the transition from MI to MII. Therefore, visible spectroscopy is a powerful monitor of rhodopsin conformation. A spectroscopic assay is used in Chapter 4 to probe rhodopsin conformations. $G\alpha_t$ conformation is effectively assayed by both fluorescence spectroscopy (Chapter 3) and trypsin proteolysis (Chapters 5 and 6), both of which rely on changes in conformations of residues in the Switch II region (see above).

Third, synthetic genes have been developed for both rhodopsin (Ferretti *et al.*, 1986) and $G\alpha_t$ (Sakmar and Khorana, 1988) allowing for facile preparation of site-directed mutants. Robust methods for the heterologous expression and purification of recombinant rhodopsin (Sakmar *et al.*, 1989) allow for the study of site directed mutants in Chapters 3 and 4. Although G_t is difficult to express heterologously, *in vitro*

expression methods have been developed for the characterization of recombinant samples, as described in Chapters 5 and 6.

Finally, rhodopsin and G_t are each members of large families of related proteins. Rhodopsin is a prototypical member of the superfamily of seven transmembrane G protein coupled receptors (GPCRs). Members of this family, of which there are hundreds, have evolved for the detection of a tremendous array of external stimuli, from hormones, to neurotransmitters, ions, odorants, and tastants. Likewise, as the pioneering work of Rodbell and Gilman suggested, $G\alpha_t$, $G\beta_t$ and $G\gamma_t$ are members of families containing at least 20, 6, and 12 subtypes, respectively (Hamm, 1998). These proteins are widely expressed and transduce signals between a wide variety of GPCRs and effectors. Two well-studied subtypes of the α family are $G\alpha_i$ and $G\alpha_s$, which cause the inhibition and stimulation of adenylyl cyclase activity, respectively. Membership in large families provides two advantages to the study of rhodopsin and G_t as a signal transduction model. First, comparison and contrast between the sequences, structures, and functions of these closely related proteins provides insight into their molecular mechanisms. Chimeric proteins constructed from different subtypes have proven to be powerful tools to localize domains responsible for specific functions in both GPCRs (Liu *et al.*, 1995; Eason and Liggett, 1996) and in G proteins (Skiba *et al.*, 1996; Remmers *et al.*, 1999). Chimeric constructs between rhodopsin and two related receptors, the β_2 adrenergic receptor, and the m2 muscarinic receptor, are used in Chapters 3 and 4 to identify regions of rhodopsin specifically involved in G_t interactions. Second, the molecular mechanisms by which rhodopsin binds and activates G_t likely apply to interactions between the huge variety of GPCRs and G proteins which mediate numerous important functions.

Outline of the Thesis

In this thesis the role of several structures thought to be involved in the coupling of the chromophore binding pocket of rhodopsin to the nucleotide binding pocket of G_t are evaluated. The work begins at the cytoplasmic surface of R^* . In Chapter 3, the role of the fourth cytoplasmic loop of rhodopsin (C4) in interactions with G_t is evaluated using peptides, site-directed mutagenesis, and fluorescence G_t -activation assays. In Chapter 4 a highly sensitive spectroscopic assay is used to measure the specific binding of G_t and peptides derived from the carboxyl termini of $G\alpha_t$ and $G\gamma_t$ to the cytoplasmic surface of a subset of the mutants in C4. This assay exploits the chromophore as a monitor of the conformation of rhodopsin. Together, the results in Chapters 3 and 4 provide evidence for the involvement of the amino terminus of C4 in rhodopsin- G_t interaction, and suggest a specific point-to-point interaction between C4 and the carboxyl terminus of $G\alpha_t$. The work in Chapters 3 and 4 on C4 of rhodopsin was completed and published (Marin *et al.*, 2000; Ernst *et al.*, 2000) before the determination of the crystal structure of rhodopsin (Palczewski *et al.*, 2000). The structure does not alter any of the key conclusions reached in those chapters; however, in Chapter 7 those experiments are re-addressed in light of the new structural information.

In Chapter 5, the development of a sensitive and accurate method of assaying the rates of both uncatalyzed and R^* -catalyzed nucleotide exchange of $G\alpha_t$ and recombinant $G\alpha_t$ mutants expressed *in vitro* is described. These methods are used to examine a long-standing hypothesis regarding the mechanism of nucleotide exchange that suggests the involvement of interdomain interactions between the Ras-like and the helical domains of $G\alpha_t$. The data demonstrate that contrary to what would be predicted by the hypothesis, disruption of interdomain interactions by site-directed mutations does not affect either basal or R^* -catalyzed nucleotide exchange rates. In Chapter 6, similar methods are used

to test a specific hypothesis regarding the mechanism by which C4-mediated R* interactions with the carboxyl terminus of $G\alpha_t$ could affect the nucleotide binding pocket “at-a-distance”. This hypothesis suggests a key role for the $\alpha 5$ helix of $G\alpha_t$. The $\alpha 5$ helix connects the carboxyl-terminus to the $\beta 6/\alpha 5$ loop, which lies adjacent to the nucleotide. The results identify a cluster of residues on the $\alpha 5$ helix, which when mutated, dramatically accelerate nucleotide exchange. A mechanistic model for R*-catalyzed nucleotide exchange is presented based on these data. Finally, in Chapter 7, a discussion of the thesis research as a whole is presented.

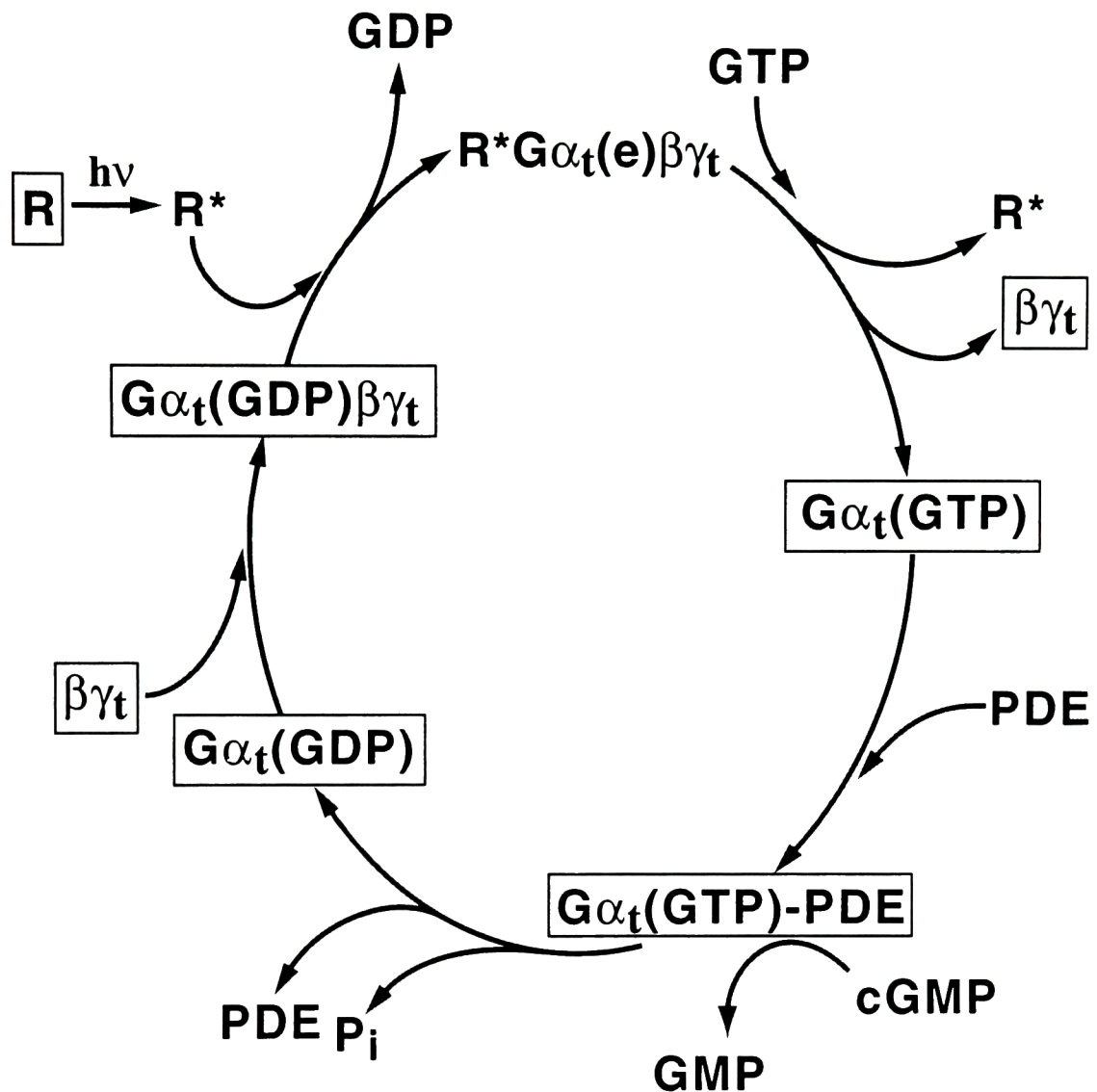
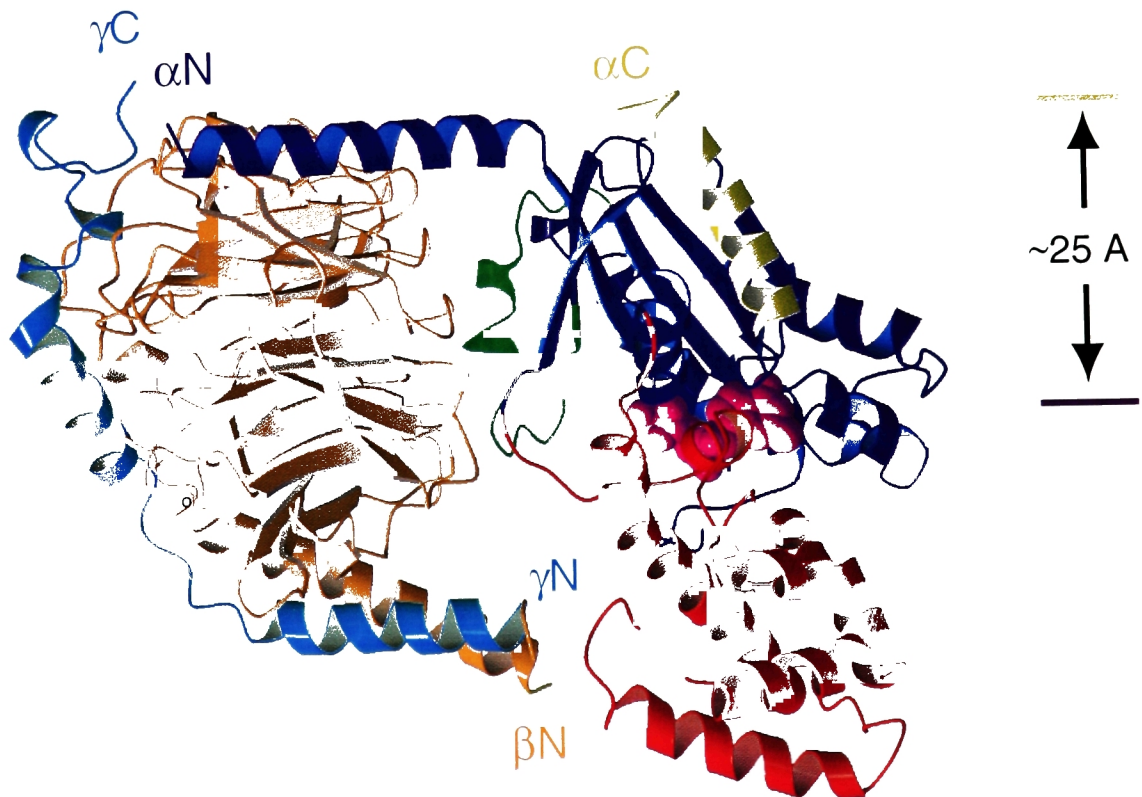
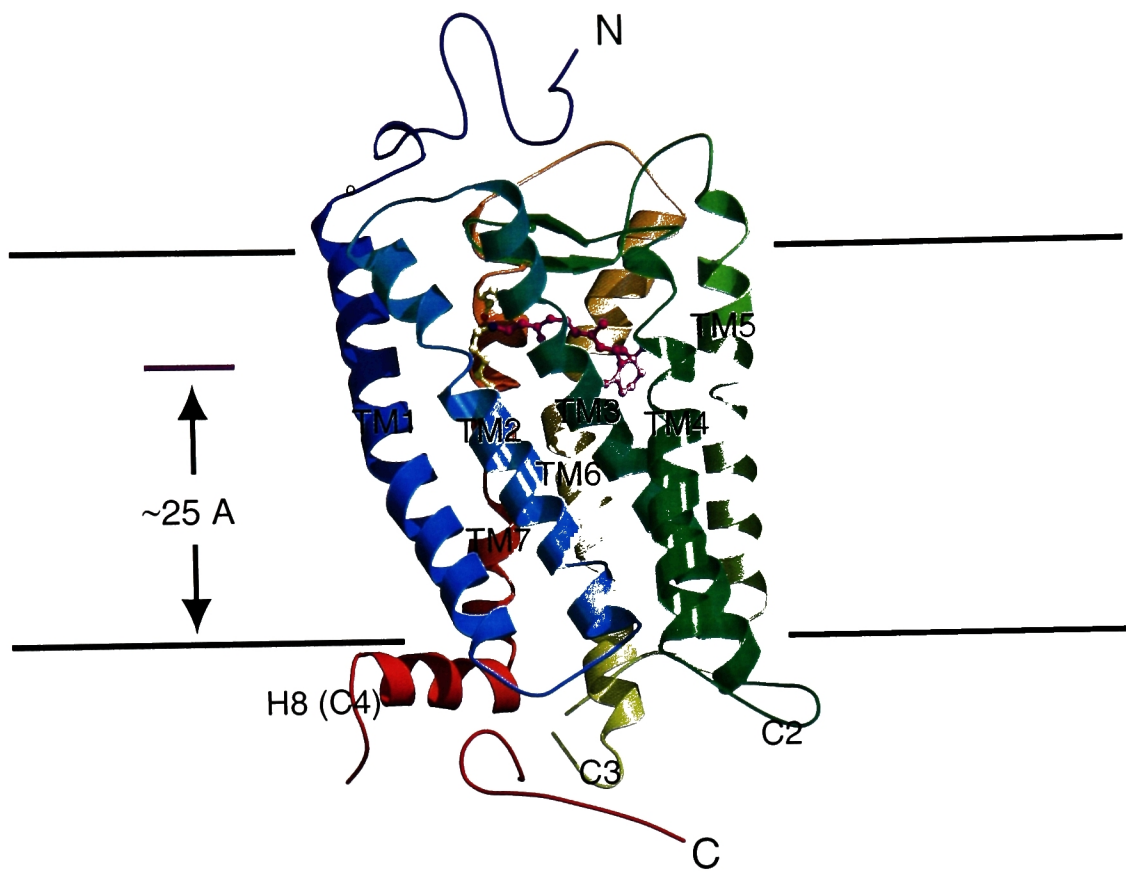


FIG. 1-1. The G_t activation cycle. Rhodopsin (R) is activated by light, and forms R*. R* binds inactive, GDP-bound G_t heterotrimer (Gα_t(GDP)βγ_t). GDP is released, and a complex between R* and empty pocket G_t (Gα_t(e)βγ_t) is formed. Subsequently, GTP binds and activates Gα_t. Gα_t(GTP) then dissociates from R* and from βγ_t, and interacts with its effector, PDE. Activated PDE catalyzes the hydrolysis of cGMP to GMP. GTP is hydrolyzed by an intrinsic GTPase activity of Gα_t, leading to re-formation of the inactive, GDP bound heterotrimer. Those protein molecules for which crystal structures have been determined are boxed.

FIG. 1-2. Crystal structures of the G_t heterotrimer and rhodopsin. *Top*, The crystal structure of dark state rhodopsin (PDB code 1f88) is shown with the cytoplasmic surface at the bottom, and the extracellular surface facing up. The chromophore, 11-*cis*-retinal, is magenta. The transmembrane helices are labeled TM1-TM7. The second (C2), third (C3) and fourth (C4) cytoplasmic loops are labeled; helix 8 (H8) is part of C4. Unordered segments of the cytoplasmic surface are not shown. The approximate position of the disc membrane surfaces are indicated by black lines. *Bottom*, The structure of GDP bound G_t (PDB code 1got) is shown with the presumed rhodopsin-interacting surface facing up. The Ras-like domain of $G\alpha_t$ is blue, the helical domain of $G\alpha_t$ is red, GDP is magenta, the $\alpha 5$ helix of the Ras-like domain is yellow, and the Switch II region of the Ras-like domain is green. $G\beta_t$ is orange, and $G\gamma_t$ is cyan. The carboxyl-terminal 7 residues of $G\alpha_t$, and 5 residues of $G\gamma_t$, are not present in the structure. The amino and carboxyl termini of $G\alpha_t$ and $G\gamma_t$, and the amino terminus of $G\beta_t$ are labeled. Structures thought to interact with rhodopsin and/or the membrane, including the amino and carboxyl termini of $G\alpha_t$ and the carboxyl terminus of $G\gamma_t$ cluster on a common surface of G_t . The relative orientation of the cytoplasmic surface of rhodopsin and the rhodopsin-binding surface of G_t is arbitrary. Upon formation of the R^*-G_t complex, the chromophore binding pocket becomes allosterically coupled to the nucleotide binding pocket of $G\alpha_t$, approximately 50 Å away (see text). The structure of the complex is unknown.



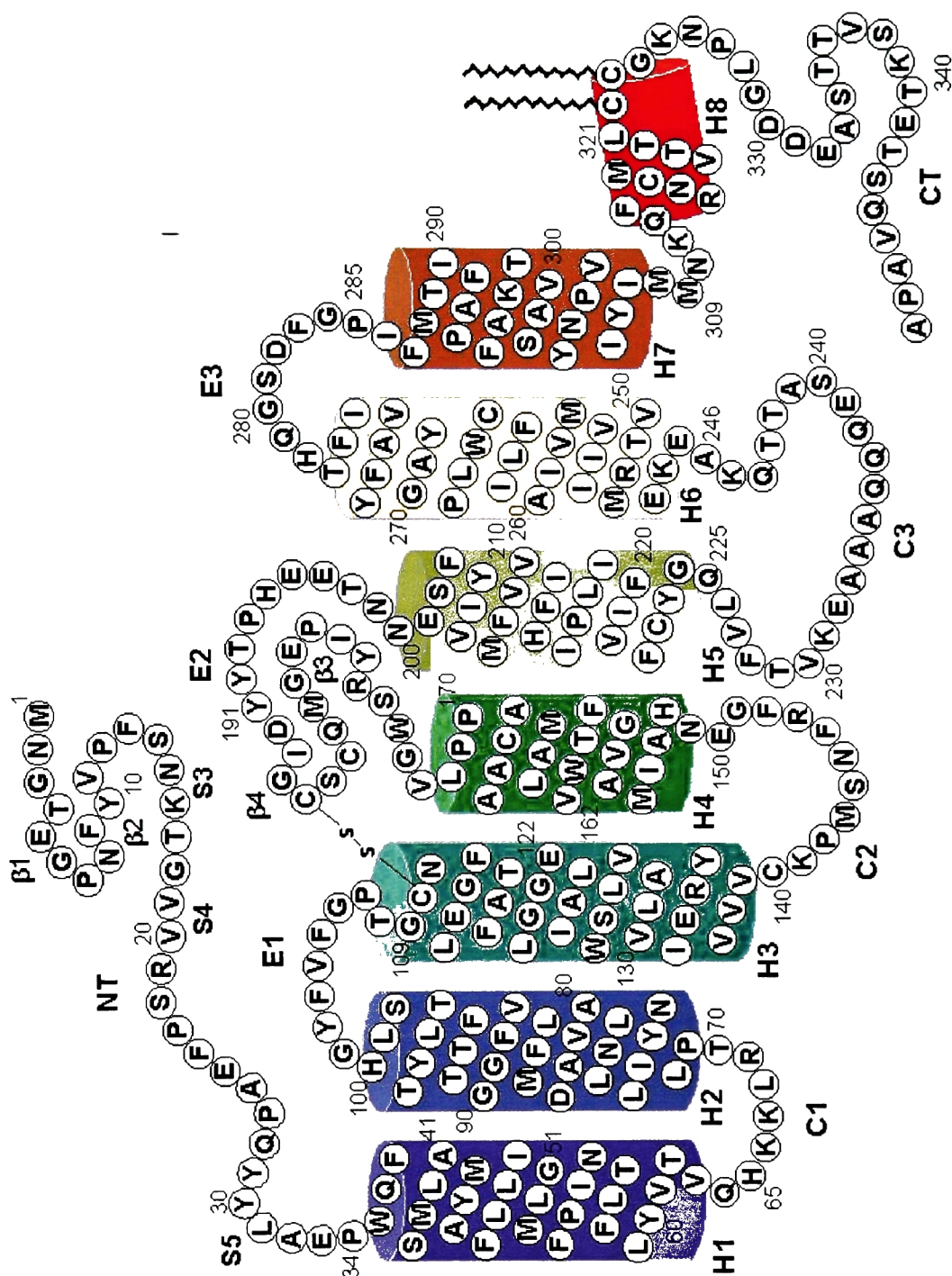


FIG. 1-3. Primary and secondary structure of rhodopsin. This figure is adapted from Menon et. al. (2001). The seven transmembrane helices are indicated by colored cylinders; the membrane associated H8 is shown as a red cylinder.

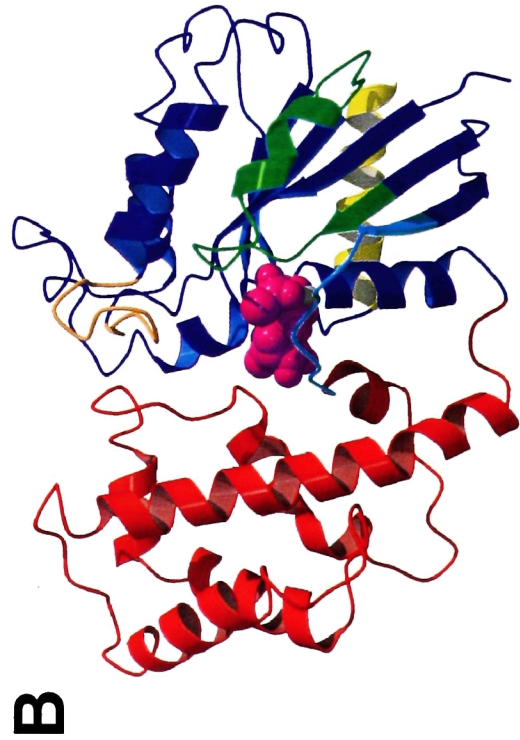
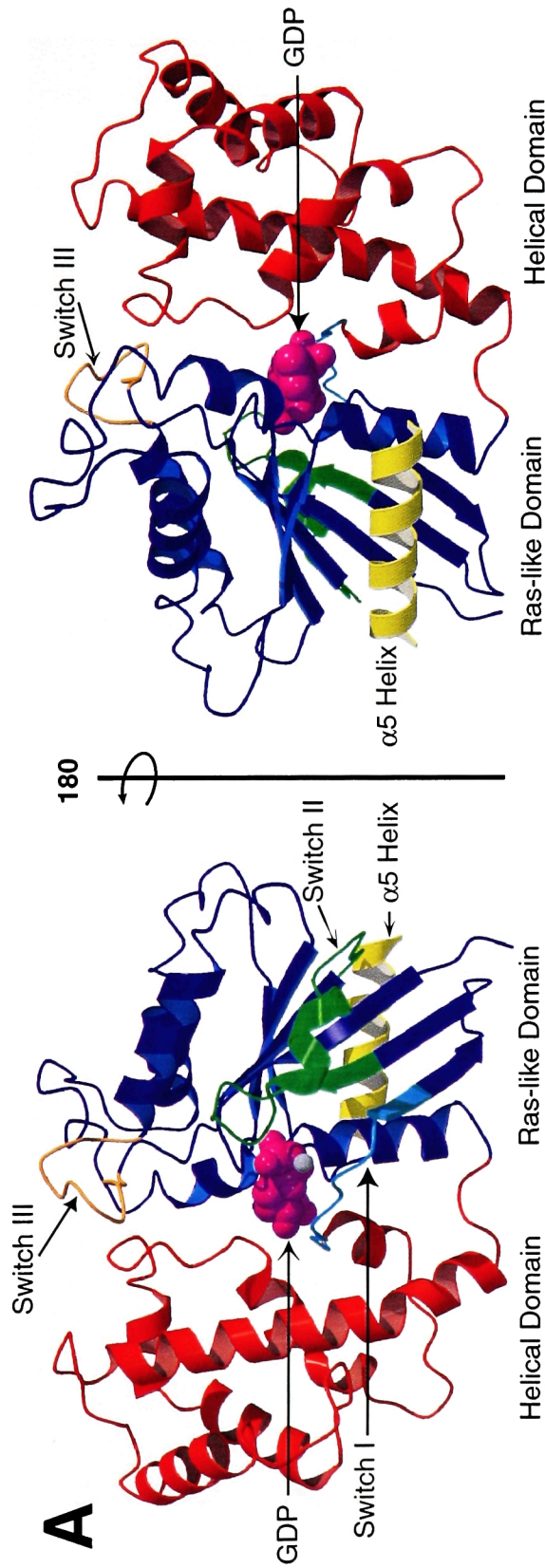
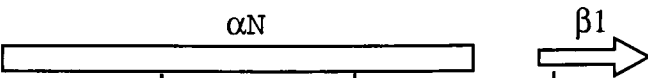


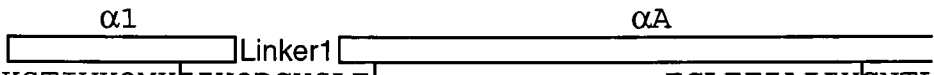
FIG. 1-4. The structure of $G\alpha_t$. **A**, GDP-bound $G\alpha_t$ (PDB code 1tag). The structure includes residues 27-340. The ras-like domain is blue, the helical domain is red, the nucleotide is magenta, and the $\alpha 5$ helix of the ras-like domain is yellow. The Switch I region is cyan, the Switch II region is green, and the Switch III region is orange. **B**, The structure of GTP-bound $G\alpha_t$ (PDB code 1tnd). The structure includes residues 26-342. The coloring is the same as in panel A. Note the GTP-induced conformational changes in the Switch regions relative to the GDP-bound structure in panel A.

FIG. 1-5. Primary and secondary structures of $G\alpha_t$. The aligned sequences of $G\alpha_t$, $G\alpha_s$, and $G\alpha_i$ are presented. Tick marks are placed after every 10th residue in the $G\alpha_t$ sequence. Secondary structure elements, deduced from the structure of GDP-bound $G\alpha_t$, are presented above the sequence. Certain regions, such as the Switch regions and the Insert (I) regions (see Chapter 5) are presented below the sequence. The helical domain consists of helices $\alpha A - \alpha F$; the rest of the molecule contributes to the Ras-like domain. The linker regions which connect the Ras-like and helical domains are indicated above the sequence. Residues mutated in Chapters 5 are colored blue, and those mutated in Chapter 6 are colored red. This figure is adapted from Lambright, et. al., 1994.

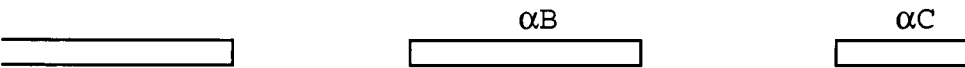
Chapter 1: Introduction



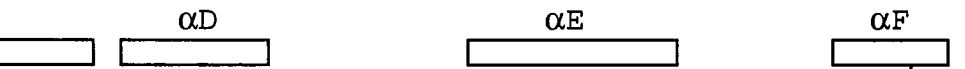
$G\alpha_t$ (1) MGA-GAS-----AEE-----KHSRELEKKLKEDA EK DARTV K L L L L GAGE
 $G\alpha_s$ (1) MGCLGNSKTEDQRNEEKAQREANKKIEKQLQKDKQVYRATHR L L L L L GAGE
 $G\alpha_i$ (1) MGC-TLS-----AEDKAAVERSKMIDRN L REDGEKAAREVK L L L L L GAGE




$G\alpha_t$ (40) S G K S T I V K Q M K I I H Q D G Y S L E ----- E C L E F I A I I Y G N T L
 $G\alpha_s$ (51) S G K S T I V K Q M R I L H V N G F N G E G G E E D P Q A A R S N S D G E K A T K V Q D I K N N L K
 $G\alpha_i$ (44) S G K S T I V K Q M K I I H E A G Y S E E ----- E C K Q Y K A V V Y S N T I




$G\alpha_t$ (75) Q S I L A I V R A M T T L N I Q Y G D S A R Q D D A R - K L M H M A D T I E E G T M P K E M S D I I
 $G\alpha_s$ (101) E A I E T I V A A M S N L V P P V E L A N P E N Q F R V D Y I L S V M N V P D F D F P P E F Y E H A
 $G\alpha_i$ (79) Q S I I A I I R A M G R L K I D F G D S A R A D D A R - Q L F V L A G A A E E G F M T A E L A G V I



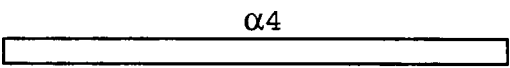
$G\alpha_t$ (124) Q R L W K D S G I Q A C F D R A S E Y Q L N D S A G Y Y L S D L E R L V T P G Y V P T E Q D V L R S
 $G\alpha_s$ (151) K A L W E D E G V R A C Y E R S N E Y Q L I D C A Q Y F L D K I D V I K Q D D Y V P S D Q D L L R C
 $G\alpha_i$ (128) K R L W K D S G V Q A C F N R S R E Y Q L N D S A A Y Y L N D L D R I A Q P N Y I P T Q Q D V L R T




$G\alpha_t$ (174) R V K T T G I I E T Q F S F K D L N F R M F D V G G Q R S E R K K W I H C F E G V T C I I F I A A L
 $G\alpha_s$ (201) R V L T S G I F E T K F Q V D K V N F H M F D V G G Q R D E R R K W I Q C F N D V T A I I F V V A S
 $G\alpha_i$ (178) R V K T T G I V E T H F T F K D L H F K M F D V G G Q R S E R K K W I H C F E G V T A I I F C V A L
 -Switch I- Switch II-



$G\alpha_t$ (224) S A Y D M V I V E D D E V N R M H E S L H L F N S I C N H R Y F A T T S I V L F L N K K D V F S E K
 $G\alpha_s$ (251) S S Y N M V I R E D N Q T N R L Q E A L N L F K S I W N N R W L R T I S V I L F L N K Q D L L A E K
 $G\alpha_i$ (228) S D Y D L V L A E D E M N R M H E S M K L F D S I C N N K W F T D T S I I L F L N K K D L F E E K
 -Switch III-
 12



$G\alpha_t$ (274) I - - K K A H L S I C F P D Y N G P N T Y E D A - - - - - G N Y I K V Q F L E L N M
 $G\alpha_s$ (301) V L A G K S K I E D Y F P E F A R Y T T P E D A T P E P G E D P R V T R A K Y F I R D E F L R I S T
 $G\alpha_i$ (278) I - - K K S P L T I C Y P E Y A G S N T Y E E A - - - - - A A Y I Q C Q F E D L N K
 -Switch IV-
 13



$G\alpha_t$ (309) R R D V K E - - I Y S H M T C A T D T Q N V K F V F D A V T D I I I K E N L K D C G L F
 $G\alpha_s$ (351) A S G D G R H Y C Y P H F T C A V D T E N I R R V F N D C R D I I Q R M H L R Q Y E L L
 $G\alpha_i$ (313) R K D T K E - - I Y T H F T C A T D T K N V Q F V F D A V T D V I I K N N L K D C G L F
 -Switch V-
 14

Chapter 2:

Materials and Methods

Reagents

Buffers and salts were from Sigma or Boehringer Mannheim. Nucleotides and protease inhibitors were from Roche. The TnT Quick Coupled Transcription/Translation kit (rabbit reticulocyte lysate) for *in vitro* expression of G α_t was purchased from Promega. [³⁵S]Methionine was purchased from New England Nuclear. TPCCK-treated trypsin was from Worthington Biochemicals. Synthetic oligonucleotides were synthesized on an Applied Biosystems 392 DNA/RNA Synthesizer, or were purchased from Genelink, Inc. DNA sequencing was carried out using BigDye Terminator Cycle sequencing in the DNA sequencing core facility at the Rockefeller University.

Preparation of Rhodopsin-derived Peptides

Peptides used in Chapter 3 were synthesized at the Rockefeller University Protein/DNA Technology Center and HHMI Biopolymer Facility by solid phase technique using Fmoc chemistry. All peptides were prepared with free amino termini, and were amidated at the carboxyl termini. The peptides were purified by HPLC and characterized by mass spectrometry. The names and amino acid sequences of the peptides used in Chapter 3 are the following: rho(132-144), AIERYVVVCKPMS; rho(240-252), SATTQKAEKEVTR; rho(310-321), NKQFRNCMVTTTL; rho(313-321), FRNCMVTTTL; rho(310-321)*scr*, TLTVNMKCQNFR; rho(310-321)*SPD*, SPDFRNCMVTTTL.

Preparation of G α_t -Derived Peptides

The synthetic peptides used in Chapter 4 are listed in Fig. 4-1B. Peptides were synthesized by Dr. P. Henklein, Humboldt University, Berlin, using the Fmoc strategy with HBTU activation (Fastmoc 0.1 mmol small-scale cycles) on an ABI Model 433A

peptide synthesizer. Farnesylation of $G\gamma_t$ -derived peptides was carried out by dissolving pure peptide (60 mg) in 5 ml of a solution of 50% (v/v) 1-propanol containing 35 mmol sodium carbonate. The resulting solution was saturated with nitrogen and 0.6 ml of a freshly prepared 10% (v/v) farnesyl bromide solution in 1-propanol was slowly added under vigorous stirring while pH was adjusted to >9. The solution was flushed with nitrogen again and incubated for 24-48 hrs with shaking. The farnesyl peptides were purified by reverse phase HPLC.

Preparation of G_t , $G\alpha_t$, $G\beta\gamma_t$, and Rhodopsin from Bovine Retinas

G_t was prepared from frozen bovine retinas (Lawson, Inc., Lincoln, NE) using standard techniques (Kühn, 1980; Fung *et al.*, 1981). In a typical preparation, 200 retinas were thawed and combined with 120 ml of 30% sucrose solution in isotonic buffer (70 mM potassium phosphate, pH 6.8, 1 mM magnesium acetate, 1 mM DTT, 0.1 mM PMSF, and 1 μ g/ml E-64). All subsequent steps were performed in a cold room under ambient light. The rod outer segments were released by vortexing the solution for 1 min. The resulting solution was centrifuged for 6 min at 5000 rpm in a Sorvall SS-34 rotor. The supernatant was collected. Each pellet was resuspended in 15 ml of 30% sucrose solution, and centrifuged again. The supernatants were pooled and diluted with an equal volume of isotonic buffer, and then centrifuged in a Sorvall SS-34 rotor for 10 min at 10,000 rpm. The supernatants were discarded, and the pellets were resuspended in 100 ml of 15% sucrose solution in isotonic buffer by passing the pellets through a 23 gauge needle 3 times. The resuspended pellets were distributed into 8 centrifuge tubes, and underlayered with 10 ml of 0.64 M sucrose in isotonic buffer. The samples were centrifuged for 10 min at 10,000 rpm, and the supernatants were discarded. The pellets were resuspended in 0.64 M sucrose solution by passage through a 23 gauge needle. The solution was overlaid onto a discontinuous sucrose gradient consisting of 9 ml each of 1.2 M, 1.0 M, and 0.78 M sucrose. The tubes were centrifuged a Beckman SW-28 rotor

for 30 min at 25,000 rpm in a Beckman ultracentrifuge with the acceleration and deceleration set to 6. The rod out segments (ROS) formed a band at the interface of the 0.78 M and 1 M sucrose solutions; the band was collected using a syringe. The collected ROS were diluted to a total volume of 200 ml using isotonic buffer. The ROS was pelleted by centrifugation for 20 min at 28,000 rpm in a Beckman Ti- 45 rotor. The pellets were resuspended in 200 ml isotonic buffer by passage through a syringe, and pelleted and resuspended twice more. The pellets were resuspended in 200 ml hypotonic buffer (5 mM Tris, pH 7.5, 5 mM magnesium acetate, 1 mM DTT, 0.1 mM PMSF, and 1 μ g/ml E-64). The resulting suspension was photolyzed for 10 min using a Dolan-Jenner lamp equipped with a >495 nm filter and a fiber optic attachment. The ROS were pelleted as before, and resuspended in hypotonic buffer a total of three times. Transducin was eluted from the ROS by resuspending the membrane pellet in 100 ml hypotonic buffer supplemented with 0.1 mM GTP. The membranes were pelleted, and the supernatant collected. The membranes were extracted with GTP a total of three times. The eluted transducin was further purified and concentrated by hexyl agarose chromatography. The GTP extracts (300 ml) were loaded onto a 10 ml hexyl agarose column overnight at a flow rate of <0.3 ml/min. The column was washed with 50 ml of hypotonic buffer, followed by 50 ml of hypotonic buffer with 75 mM NaCl. Transducin was eluted with hypotonic buffer with 300 mM NaCl. The eluted transducin, generally 3-10 ml, was dialyzed overnight into storage buffer (10 mM NaHEPES, pH 7.5, 2 mM MgCl_2 , 1 mM DTT, 5 μ M GDP, and 50% glycerol). Typical yields were from 1-8 mg.

Specific activities of G_t samples were determined by spectrofluorometric titration, as described previously (Fahmy and Sakmar, 1993a). G_t used in the photoregeneration studies was purified as described (Heck and Hofmann, 1993). $G\beta\gamma_t$ and $G\alpha_t$ were isolated from holo- G_t essentially according to published methods (Shichi *et al.*, 1984) using a Hitachi LC-organizer HPLC system with 1 ml Hi-Trap Blue Sepharose column

(Amersham Pharmacia Biotech). The proteins were eluted from the column by applying a 0-2 M NaCl gradient. Protein concentrations were determined using the Bio-Rad protein assay reagent according to manufacturer's instructions. The subunits were stored at -20°C in a 50% glycerol buffer until use. Urea-washed disc membranes, the gift of Dr. K. C. Min, were prepared as described elsewhere (Min *et al.*, 2000). The membranes were solubilized in 1% (w/v) n-dodecyl β -d-maltoside (DM), and insoluble material was removed by centrifugation. The resulting solubilized rhodopsin, used in Chapters 5 and 6, displayed a A_{280}/A_{500} spectral ratio of <1.8 and a concentration of $\sim 8\ \mu\text{M}$.

Measurement of Intrinsic Fluorescence of G_t , $G\alpha_t$, and $G\beta\gamma_t$

Fluorescence measurements were done on a Spex Fluorolog 3-11 $\tau 3$ spectrofluorometer equipped with a 450 W Xenon arc lamp. All fluorescence experiments were performed in 10 mM Tris-HCl buffer (pH 7.2) containing 100 mM NaCl, 2 mM MgCl_2 , 1 mM DTT, 5 μM GDP and 0.01% (w/v) dodecyl maltoside (DM). Spectra were recorded at $10\ ^{\circ}\text{C}$ in a 4 mm x 4 mm quartz cuvette. Protein fluorescence was obtained by exciting at 295 nm and monitoring emission from 315 to 450 nm. The excitation and emission slit bandpass were 1.5 and 5 nm, respectively. Titration experiments were typically performed by adding 10 μl aliquots of the peptide from a stock solution of 250 μM to a protein solution of 200 nM.

Site Directed Mutagenesis of Rhodopsin

Site directed mutagenesis was achieved primarily by using restriction fragment replacement (Lo *et al.*, 1984) in a synthetic rhodopsin gene (Ferretti *et al.*, 1986) cloned into a eukaryotic expression vector (Franke *et al.*, 1988). Mutants CTr1 and CTr3 were constructed by substituting the *BspE* I-*Sal* I restriction fragment with a synthetic duplex containing the desired codon alterations; mutant CTr2 involved a similar substitution of the *Apa* I-*Sal* I fragment. Mutants CTr4 and the K311 point mutations involved

substitution of an *Apa* I-*Bsp*E I fragment. The mutant CysXV (C322S/C323S) was constructed by substituting the *Xho* I-*Bst*E II fragment of the rhodopsin gene into CysXIII (C140S/C316S/C322S/C323S). CysXIII was prepared by substituting the *Bsp*E I-*Sal* I fragment of a C140S mutant (Karnik *et al.*, 1988) with a synthetic fragment that contained the appropriate codon alterations for C316S, C322S, and C323S. The combination mutant CTr4/CysXV was prepared by cloning the *Xho* I-*Bst*E II fragment of CTr4 into a *Xho* I-*Bst*E II digested CysXV vector. Cell culture, transfection, and immunoaffinity purification procedures have been described elsewhere (Sakmar *et al.*, 1989; Min *et al.*, 1993; Han *et al.*, 1996). For samples used in photoregeneration studies, the samples were concentrated ~10-fold using Centricon-30 filtration devices (Amicon) following purification. Membranes from transfected cells were prepared prior to regeneration with 11-*cis*-retinal using sucrose density gradient centrifugation, as described previously (Han and Sakmar, 2000).

Fluorescence G_t Activation Assay

The assay was performed essentially as described (Fahmy and Sakmar, 1993a). A Spex Fluorolog instrument was used with a 150 W xenon arc lamp. A solution of 250 nM G_t was prepared in fluorescence buffer (100 mM NaCl/10 mM Tris, pH 6.9/2 mM MgCl₂/1 mM DTT/0.01% DM). 1.5 ml of solution was placed in a semi-micro cuvette, and loaded into the thermostatted cuvette holder equipped with a magnetic stirrer at 10°C. The cuvette was continually illuminated with a HeNe laser and a fiber optic attachment. Protein fluorescence was excited at 300 nm with 2 nm bandpass, and emission intensity was collected at 345 nm with a 12 nm bandpass. At 100 s, 50 µl of rhodopsin or rhodopsin mutant was injected into the cuvette using a Hamilton syringe to a final concentration of 1 nM. At 200 s, the activation reaction was initiated by injecting a 50 µl solution of GTPγS to a final concentration of 5 µM. Activation of G_t was observed as an increase in the intensity of tryptophan fluorescence emission that results from

conformational changes in W207 that occur upon binding GTP. Peptide competition assays were performed with 200 nM G_t and 1 nM of purified COS cell-expressed rhodopsin from which 1D4 peptide introduced in the purification procedure was removed by gel filtration on a G-50 Nick column (Pharmacia Biotech). The appropriate concentration of peptide was added from a 15 mM stock solution and pre-incubated with G_t for 30 min before the start of the assay.

Measurement of [3H]Palmitic Acid Incorporation

Opsin was metabolically labeled with [3H]palmitic acid (New England Nuclear, Boston, MA) essentially as described previously (Karnik *et al.*, 1993). Briefly, 48 h post-transfection, COS cells were grown for 8 h in serum-free media. The cells were then incubated for 30 min in 1% serum, followed by 2 h in 1% serum supplemented with 100 μ Ci/ml [3H]palmitic acid (43 Ci/mmol). Cells were washed with phosphate-buffered saline, harvested, and solubilized in 0.1% (w/v) DM solution. The detergent extracts were incubated overnight with resin conjugated with 1D4 monoclonal antibody as used in the standard rhodopsin purification procedure (Oprian *et al.*, 1987). The resin was washed extensively, as monitored by the decreasing tritium counts present in successive washes. Opsin was eluted from the resin by incubation with wash buffer containing the 1D4 peptide. The relative amounts of [3H]palmitic acid incorporated into the eluted samples were analyzed by scintillation counting.

Instrumentation for Measurement of Photoregeneration Traces

Time-resolved absorption traces of rhodopsin samples were recorded on a custom-built single-wavelength absorption photometer in the laboratory of Dr. K. P. Hofmann, Humboldt University, Berlin. Light from a 150-W halogen light source passes through a Jobin-Yvon HR460 monochromator (focal length 460 mm, 1200 lines/mm, slit width set to 1 mm) tuned to 543 nm, and from there through the cuvette (4-mm optical pathlength)

and a bandpass interference filter onto a large surface PIN photodetector. The output is nulled and amplified twice, filtered with a 500 μ s electronic low-pass filter and recorded using a modified Nicolet 2090-IIIa digital oscilloscope.

Photoregeneration Experiments

The rhodopsin photoregeneration assay was performed as reported (Arnis and Hofmann, 1995) with adaptation for recombinant pigments as follows. All samples contained 2 μ M pigment in a volume of 0.26 ml of 200 mM Na_2HPO_4 (pH 8.0), 10 mM NaCl, and approximately 0.03% (w/v) dodecyl maltoside (DM). Due to the concentration procedure required for recombinant samples, the final DM concentration was not precisely known, but was estimated not to exceed 0.035% (w/v). After equilibrating the sample cuvette to 13 °C, the sample was illuminated for 30 s with a green HeNe laser (543.5 nm, 5 mW, Melles Griot) to cause quantitative formation of MII. Absorption at 543 nm was recorded continuously. After 50 ms, a flash of blue light (412 ± 7 nm, ca. 20 μ s duration) was applied to the sample and formation of photo-regenerated pigment was measured at 543 nm for an additional 200 ms. Discharge of the flashlamp affected the sensitive electronics of the detector, causing a brief artifactual negative deflection. Four records induced by four separate flashes were collected from each sample with 30 s intervals between the recordings. Starting with the initial illumination, each experiment took approximately 140 s. The four records were averaged to produce experimental data traces as presented in Fig. 4-2. The experimental photoregeneration signal traces are depicted as absorbance changes at 543 nm *versus* time (*i.e.*, a rising signal indicates a proportional increase of absorbance due to reprotonation of the Schiff base).

Numerical Fitting Procedures and Determination of Initial Slope Values of Photoregeneration Traces

The photoregeneration signal comprises a fast phase, which is not resolved, and a slow phase, which is monitored for 200 ms (see Fig. 4-2). Data points obtained 4.5–7.0

ms after the blue flash were averaged and used as an estimate for the amplitude of the fast phase. The relative amplitude of the fast phase of the photoregeneration of the recombinant pigments was the same as that of rhodopsin. The initial slope of the slow phase of a photoregeneration trace was determined from the numerical fit of a simple exponential-rise function offset by the amplitude of the fast phase. Values for *relative slope* are presented (Table 4-I) to demonstrate the effect of G_t or G_t -derived peptides on the initial slope of the photoregeneration signal. *Relative slope* is defined as the ratio of the initial slope of the slow phase of the photoregeneration trace in the presence of G_t or G_t -derived peptides *versus* the initial slope in their absence. A relative slope of 1.0 indicates no effect, whereas a slope of <1.0 indicates inhibition of photoregeneration. The relative slope for an experiment with rhodopsin and G_t (3 μ M) was typically about 0.7.

Site-Directed Mutagenesis of $G\alpha_t$ and $G\alpha_i$

The parent for all $G\alpha_t$ constructs was pGEM2sT α , the synthetic bovine $G\alpha_t$ gene cloned into the pGEM2 plasmid under control of a SP6 promoter. Point mutations and the 25-amino-acid deletion from the carboxyl terminus were prepared using the QuickChange method (Stratagene). For each mutant, two complementary primers were designed that coded for the desired mutation as well as 10-15 bases of complementary sequence on either side of the mutation site. Most amino acid substitutions could be accomplished with two or less nucleotide changes. The total length of each primer was 20-30 bases. The mutagenesis reaction (50 μ L final) consisted of 5ng of template plasmid, 1 μ L of cloned Pfu polymerase (2.5 units/ μ L)(Stratagene), 5 μ L of 10x Pfu buffer (Stratagene), 250 nM of each primer, 800 μ M of dNTP mix. The reactions were thermocycled in a GeneAmp 9600 (Perkin Elmer Cetus) thermocycler with the following program: 3 min at 95°; 14 cycles of 30 s at 95°, 1 min at 55°, 8 min at 68°; and then 10 min at 72°. Amplification of the mutated plasmid was verified by running 1 μ L of the

reaction on a 1% agarose gel. The parental plasmid was selectively digested using 1 μL of the restriction enzyme DpnI (New England Biolabs) per reaction for 1.5 h at 37°. Since DpnI digests only methylated DNA the wild type template plasmid was restricted. The DpnI-treated mutant plasmid was transformed into chemically competent bacteria (subcloning efficiency DH-5 α (Gibco) or OneShot TOP10 (Invitrogen)). Generally the ratio of recombinant transformants from QuickChange reactions done with primers compared with control reactions run without primers was >50:1. All constructs were verified by automated DNA sequencing of the entire coding region of G α_t .

The insertion mutants $\alpha 5$ ala3, $\alpha 5$ ala4, and CT ala4 as well as the deletion mutants CT del10 and CT del5 (Fig. 6-3) were prepared using cassette mutagenesis. DNA duplexes corresponding to the *BstEII/XbaI* fragment of the synthetic G α_t gene were synthesized to encode the appropriate mutation. The duplexes were ligated into *BstEII/XbaI* digested pGEM2sT α . The pGEM2sT α was prepared from a *dam* bacterial strain to prevent methylation of a GATC sequence that partially overlaps the *XbaI* restriction site.

The parent for all G α_{i1} constructs was pGEM2G α_{i1} , the G α_{i1} gene cloned into the pGEM2 plasmid under control of a SP6 promoter. To improve expression, a 217 bp segment of the 5' untranslated region was removed by QuickChange mutagenesis.

In vitro Transcription and Translation of G α_t

Recombinant G α_t subunits were prepared using the TNT Quick Coupled rabbit reticulocyte lysate transcription/translation kit (Promega). For each translation, 20 μL of lysate mix was combined with 4 μL of DNA (0.5 μg total) and 1 μL of $\sim 9 \mu\text{M}$ [^{35}S]methionine (New England Nuclear) at a specific activity of approximately $\sim 1250 \text{ Ci/mmol}$. The reactions were incubated at 30°C for 90 min. Subsequent manipulations were performed on ice or at 4°C. The translated products were passed over BioSpin 6 gel

filtration spin columns (BioRad) twice consecutively to remove excess nucleotides. The volume of each reaction was then adjusted to 100 μ l in a buffer of 5 mM Tris, pH 7.5, 150 mM NaCl, 2 mM $MgCl_2$, 1 mM DTT, 0.01% (w/v) DM. If the reaction was to be studied in a rhodopsin catalyzed assay, $G\beta\gamma_t$ was added to a final concentration of 30 nM. Every experiment was performed on freshly translated material.

Trypsin Proteolysis and Analysis

The digestion procedure was adapted from Garcia *et al.*, 1995. Aliquots (8 μ l) of the *in vitro* expressed protein were withdrawn and mixed with 1.5 μ l of digest buffer (5% Lubrol, 2 mM GDP, 1 mg/mL TPCK trypsin) or digest control buffer (5% Lubrol, 2 mM GDP). The reactions were incubated on ice for 30 min (or 5 min for $G\alpha_{i1}$ samples). Digestion was terminated by the addition of 2.5 μ l of 10 mg/ml aprotinin/10 μ M phenyl methyl sulfonyl fluoride (PMSF), followed by 6 μ l of 3x SDS sample buffer (New England Biolabs). Samples were occasionally stored at -20° for up to 48 hrs. Subsequently, the samples were boiled for 3 min and the protein fragments were resolved by polyacrylamide gel electrophoresis on 15% pre-cast Tris-HCl minigels (BioRad). Following electrophoresis, the gels were fixed for >30 min in 50% MeOH/ 10% acetic acid and then soaked for 5 min in 7% methanol/ 7% acetic acid/ 2% glycerol. The gels were vacuum-dried onto filter paper (Whatman) and then exposed to a storage phosphor screen (Molecular Dynamics) for 1 to 7 days.

Control Reactions for Trypsin Proteolysis of $G\alpha_t$

Control reactions were performed on each sample of expressed $G\alpha_t$ in order to check the quantity and apparent molecular weight of the expressed protein, as well as the digest patterns following incubation with GDP and GDP/AlF_4^- . 30 μ l of each sample was combined with GDP to a final concentration of 100 μ M. One 8 μ L aliquot was removed and digested ("GDP"); another 8 μ l aliquot was removed and mock digested with digest

control buffer ("not digested"). The remaining 14 μ l was combined with a final concentration of 0.17 mM AlCl_3 and 10 mM NaF added from separate 30x stock solutions. Following a 10 min incubation at room temperature, a 8 μ l aliquot was removed and digested (" +GDP/ AlF_4^- ").

Uncatalyzed Activation Time Course of $G\alpha_t$

Samples (70 μ l each) of *in vitro* translated $G\alpha_t$ were quickly warmed to room temperature in a water bath and GTP γ S was added to a final concentration of 100 μ M. Aliquots were withdrawn at 1, 2, 3, 4, and 6 h following GTP γ S addition, and digested. In mutants that activated slowly, the activity of the protein following 6 h incubation at room temperature was investigated by addition of rhodopsin and $G\beta\gamma_t$ (30 nM each, final concentration) and incubation under room light for 20 min. A final 8 μ l aliquot was then removed and digested. For certain mutants which activated very quickly, aliquots were taken at 10, 20, 30, 60, 90, and 120 min, and the rhodopsin/ $G\beta\gamma_t$ mix was not added.

Rhodopsin/ $G\beta\gamma_t$ -Catalyzed Activation Time Course of $G\alpha_t$

Samples (70 μ l each) were quickly warmed to room temperature in a water bath. A mixture of rhodopsin and GTP γ S (4 μ l) was added to the sample yielding a final concentration of 30 nM rhodopsin and 14 μ M GTP γ S. The rhodopsin was first photolyzed by illumination for 15 s with a fiber optic cable connected to a Dolan Jenner lamp equipped with a >495 nm long-pass filter. The samples were incubated at room temperature under the illumination. Aliquots were withdrawn and digested at 1, 2, 3, 5, 10, and 20 min following addition of the rhodopsin/ GTP γ S mix.

Data Analysis of Trypsin Proteolysis Patterns

Following exposure to the dried gels, the phosphor storage screens were scanned using a Molecular Dynamics Storm Imager machine (Molecular Dynamics) at 200 micron resolution. The resulting images of the gels were analyzed using ImageQuant software

(Molecular Dynamics). Lines were drawn down the center of each lane on the gel, perpendicular to the bands in the lane. The intensity of each pixel along the line was determined as the average of 5-10 pixels on either side of the line. In this way, most of the width of each lane was considered. Any defect in the gel was avoided by careful placement of the lines. The intensity of each pixel was plotted as a function of position along the line. The result was a graph of intensity as a function of distance down the lane; where the bands on the gel correspond to peaks on the graph. The baseline of the graph was set so as to exclude nonspecific background intensity. The areas of the ~23- and ~34-kDa peaks were then calculated and recorded in an Excel spreadsheet. The fraction of $G\alpha_t$ activated in a given lane was determined by the formula: (area of ~34-kDa peak) / ((1.4 * area of ~23-kDa peak) + (area of ~34-kDa peak)). The area of the ~23-kDa peak was multiplied by 1.4 to normalize for the smaller number of methionines in the smaller fragment relative to those in the ~34-kDa fragment. This coefficient was adjusted (to 1.3) for analysis of M228 mutations. Activation kinetics were analyzed by plotting the fraction of $G\alpha_t$ activated as a function of time. In uncatalyzed assays, the data were fit to a single exponential rise to a maximum equation of the form: percent activated = $c + 100(1 - \exp(-kt))$. The apparent rate constants derived from the fits are presented in Table 5-I and 6-I.

For experiments conducted with $G\alpha_i$, the intensity of the GDP-dependent band could not be determined reliably due to nonspecific background intensities in the region of the gel where the GDP band migrated. This background was present even in undigested samples of $G\alpha_i$. Since the ratio of the GTP dependent band to the sum of the GTP and GDP bands could not be determined, the intensity of the GTP band was expressed as a fraction of the total intensity in each lane. Activation time courses are plotted as the change in this intensity over time. For fully activated $G\alpha_i$, the GTP band accounted for roughly 35% of the intensity in each lane.

Chapter 3:

The Amino Terminus of the Fourth Cytoplasmic Loop of Rhodopsin Modulates Rhodopsin—Transducin Interaction*

Summary

Rhodopsin is a seven-transmembrane helix receptor that binds and catalytically activates the heterotrimeric G protein transducin (G_t). This interaction involves the cytoplasmic surface of rhodopsin, which comprises four putative loops and the carboxyl-terminal tail. The fourth loop connects the carboxyl end of transmembrane helix 7 with C322 and C323, which are both modified by membrane-inserted palmitoyl groups. Published data on the roles of the fourth loop in the binding and activation of G_t are contradictory. Here, we attempt to reconcile these conflicts and define a role for the fourth loop in rhodopsin— G_t interactions. Fluorescence experiments demonstrated that a synthetic peptide corresponding to the fourth loop of rhodopsin inhibited the activation of G_t by rhodopsin and interacted directly with the α subunit of G_t . A series of rhodopsin mutants was prepared in which portions of the fourth loop were replaced with analogous sequences from the β_2 adrenergic receptor or the m1 muscarinic receptor. Chimeric receptors in which residues 310-312 were replaced could not efficiently activate G_t . The defect in G_t interaction in the fourth loop mutants was not affected by preventing palmitoylation of C322 and C323. We suggest that the amino terminus of the fourth loop interacts directly with G_t , particularly with $G\alpha_t$, and with other regions of the intracellular surface of rhodopsin to support G_t binding.

*Material in this chapter has been published previously in: Marin, E. P., Krishna, A. G., Zvyaga, T. A., Isele, J., Siebert, F., and Sakmar, T. P. (2000) The amino terminus of the fourth cytoplasmic loop of rhodopsin modulates rhodopsin-transducin interaction. *J. Biol. Chem.* **275**:1930-1936.

Introduction

Considerable evidence has implicated C2 and C3 of rhodopsin as participating in the complex with G_t (König *et al.*, 1989; Franke *et al.*, 1990; Franke *et al.*, 1992; Borjigin and Nathans, 1994). However, the literature addressing the role of C4 (Fig. 3-1) in interactions with G_t is contradictory. Studies have shown that peptides derived from C4 can disrupt the stabilization of MII by G_t (König *et al.*, 1989), interfere with rhodopsin stimulated GTPase activity of G_t (Takemoto *et al.*, 1986), and bind directly to a fluorescently labeled $G\beta\gamma_t$ and prevent $G\beta\gamma_t$ - rhodopsin interactions (Phillips and Cerione, 1992). In contrast, truncation of rhodopsin following N315, in the middle of C4, does not impair G_t activation (Weiss *et al.*, 1994). Since truncation at the beginning of C4 precluded proper expression and/or processing of rhodopsin, a follow-up study examined a series of single and double mutations in the amino-terminal half of C4, from N310 through N315. None of the mutations was found to disrupt G_t activation, leading to the conclusion that C4 is not required for productive interactions with G_t (Osawa and Weiss, 1994).

In this Chapter, we have carefully re-examined and defined the role of the C4 loop in rhodopsin— G_t interactions. We used fluorescence spectroscopy to demonstrate that a synthetic peptide corresponding to C4 of bovine rhodopsin, rho(310-321), binds to G_t and free $G\alpha_t$. Furthermore, we demonstrate the potent inhibition of rhodopsin-catalyzed G_t activation by rho(310-321). We also prepared and characterized a series of site-directed mutants of bovine rhodopsin with alterations of the C4 loop. These data show that when either the entire C4 loop or a tripeptide (N310-K311-Q312) at the amino terminus of the loop is replaced with the analogous sequence of the β_2 adrenergic receptor (β_2 AR), the G_t -activating function of rhodopsin is diminished. Neither replacement of the carboxyl-terminal half of the loop, nor removal of the palmitoylation

sites disrupt G_t activation. We conclude that the C4 loop is involved in mediating interactions between rhodopsin and G_t .

Results

Inhibition of G_t Activation by Synthetic Peptides Corresponding to Cytoplasmic Loops of Rhodopsin

Peptides derived from the C2, C3, and C4 loops of rhodopsin have been shown to disrupt the ability of G_t to stabilize MII as measured by an extra-MII assay (König *et al.*, 1989). An experiment done by a post-doc in the Sakmar lab, Tatanya Zvyaga, examined whether similar peptides could also disrupt the activation of G_t by catalytic amounts of solubilized rhodopsin in a fluorescence activation assay. In Fig. 3-2, a dose-dependent decrease in the rate of G_t activation is observed in the presence of synthetic peptides derived from the amino terminus of C2 (rho(132-144)), the carboxyl terminus of C3 (rho(240-252)), and C4 (rho(310-321)). The effective concentration at 50% inhibition (IC_{50}) for all peptides was in the 0.1-0.3 mM range; all peptides inhibited activation completely at concentrations ≤ 1 mM. A C1-derived peptide, rho(61-75), only modestly inhibited G_t activation at 1 mM (not shown).

A Synthetic Peptide Derived From C4 of Rhodopsin, rho(310-321), Alters the Fluorescence Emission Wavelength Maximum of $G\alpha_t$ But Not of $G\beta\gamma_t$

In an effort to characterize the interactions of C4 with G_t , a postdoc in the Sakmar Lab, A. Gopala Krishna, studied the intrinsic fluorescence emission spectra of $G\alpha_t$ and $G\beta\gamma_t$ in the presence of increasing concentrations of rho(310-321). A significant red shift (7.8 ± 0.3 nm, $n=4$) in the λ_{max} of tryptophan emission of $G\alpha_t$ was observed in the presence of 45 μ M peptide (Fig. 3-3A). The shift was accompanied by a modest (~10%) increase in intensity. These spectral changes are indicative of a change in the molecular environment of at least one of the two tryptophans of $G\alpha_t$ caused by the binding of the

peptide. The extent of the red shift was dependent on the concentration of peptide (Fig. 3-3A, inset). In contrast, the λ_{\max} of tryptophan fluorescence emission of $G\beta\gamma_t$ was only minimally (1.0 ± 0.3 nm, $n=4$) affected by the peptide (Fig. 3-3B). These data suggest that the peptide does not bind to free $G\beta\gamma_t$, but they do not rule out binding in a manner that does not alter the molecular environment of enough of its 8 intrinsic tryptophans to allow for spectroscopic detection. The emission spectrum of holo- G_t was red shifted by approximately 4 nm in the presence of the peptide (data not shown), which is consistent with interaction with $G\alpha_t$ but not $G\beta\gamma_t$ in the context of the heterotrimer. The effects of three additional peptides on the λ_{\max} of $G\alpha_t$ emission were examined. The peptides, which were derivatives of rho(310-321), were: (a) rho(313-321), in which residues 310, 311, and 312 were not present; (b) rho(310-321)*scr* in which the order of the amino acids was scrambled; and (c) rho(310-321)*SPD* in which the first three positions of the peptide were changed from NKQ to SPD. The sequence of rho(310-321)*SPD* is derived from the rhodopsin mutant CTr4 (Fig. 3-4). The peptides rho(313-321) and rho(310-321)*scr* did not affect the λ_{\max} of $G\alpha_t$ emission, whereas rho(310-321)*SPD* caused a ~4-nm red shift, with no change in fluorescence intensity (data not shown). As an additional control, the λ_{\max} of the emission spectrum of bovine serum albumin was shown to be insensitive to the presence of rho(310-321) (data not shown).

Preparation of Substitution Mutants in C4 of Rhodopsin

Three rhodopsin mutants were prepared in which portions of C4 were replaced with sequences from analogous segments of the β_2 AR or the m1 muscarinic receptor (m1 MR) (Fig. 3-4). These two receptors were chosen because they have fourth loops of similar lengths to that of rhodopsin and at least one cysteine homologous to C322 or C323 of rhodopsin. The β_2 AR has been shown to be palmitoylated (O'Dowd *et al.*, 1989), while this modification in the m1 MR is inferred to be very likely because of the

presence of a Cys residue at the required location. Furthermore, these receptors bind G protein types not related to G_t , which is a member of the $G_{i/o}$ class. The m1 MR couples to G_q , and the β_2 AR couples to G_s .

In mutants CTr1 and CTr2, portions of C4 are replaced with sequence derived from the β_2 AR (Fig. 3-4). CTr1 involves replacement of the carboxyl-terminal half of the loop, while the entire fourth loop is replaced in CTr2. Only a carboxyl-terminal replacement was constructed with the m1 MR (CTr3), since the amino-terminal halves of the C4 loops of rhodopsin and m1 MR are nearly identical. The chimeric C4 mutant approach offers several advantages. For example, since the replacements are relatively long, and the substituted sequence is derived from receptors that couple to G_s or G_q , the sensitivity of observing a relevant disruption in G protein coupling is high. Additionally, since the fourth loops of the β_2 AR, m1 MR and rhodopsin are of comparable length, the expression, folding, and palmitoylation of the chimeric fourth loop mutants should not be disrupted. Therefore, the confidence of attributing a loss-of-function phenotype to a specific defect in G_t coupling is high.

The analysis of CTr1, CTr2, and CTr3 described below pointed toward the involvement of the amino-terminal part of C4 in G_t interactions. To further examine this region, mutant CTr4 was constructed in which only those positions that differ between CTr1 and CTr2 (*i.e.*, 310, 311, and 312) were replaced (Fig. 3-4). In addition, a series of point mutations in which K311 was replaced by residues with a variety of physicochemical properties were constructed: K311P, K311S, K311R, K311W. Position 311 lies in the center of a proposed helical extension of TM 7 (Altenbach *et al.*, 1999; Yeagle *et al.*, 1996; Altenbach *et al.*, 1999). These mutants were designed specifically to test and control for the possible role of a helix-altering proline in the 311 position in mutant CTr2. Two additional mutants were constructed to assess the role of palmitoylation in the function of C4. In CysXV (C322S/C323S) the sites of

palmitoylation were removed, and in CTr4/CysXV, the CTr4 and CysXV replacements were combined. The mutant CysXV has been previously described and characterized in a detergent solubilized G_t activation assay (Karnik *et al.*, 1993). The mutant CTr4/CysXV was used to test whether the effects of preventing palmitoylation were different in the background of a mutated C4 as compared with rhodopsin.

The mutants were transiently expressed in COS cells and regenerated with 11-*cis*-retinal to yield pigments. The mutant pigments were either purified in DM detergent or isolated in cell membrane preparations. UV-visible spectra taken on purified samples in the dark showed that each mutant pigment had a λ_{\max} value of 500 nm, identical to that of rhodopsin prepared under that same conditions (Table 3-I). Upon illumination, mutants CTr1, CTr2 and CTr3 formed MII-like pigments with λ_{\max} values of 380 nm. Acid denaturation of the photolyzed pigments revealed that the Schiff base bonds of the mutants were at least as stable as that of rhodopsin (data not shown).

Activation of G_t by Solubilized Purified Recombinant Pigments

The ability of the C4 loop substitution mutants to activate purified bovine G_t was measured in a kinetic fluorescence assay. The activation of G_t was observed as an increase in the intrinsic tryptophan fluorescence of $G\alpha_t$ upon binding of GTP γ S (Fahmy and Sakmar, 1993a). The initial rate of GTP γ S uptake by G_t catalyzed by each mutant was normalized to that of rhodopsin (Fig. 3-5). Mutants CTr1 and CTr3, in which the carboxyl-terminal half of the loop was replaced, displayed similar initial rates to that of rhodopsin. However, CTr2, in which the entire loop was replaced, displayed a reduced initial rate. The CTr4 mutant, in which only a tripeptide in the amino-terminal part of the loop was replaced with β_2 AR sequence, was also deficient in activating G_t . The level of activity was comparable to that of CTr2. None of the K311 point mutants was defective

in G_t activation. The non-palmitoylated CysXV mutant exhibited similar activity to that of rhodopsin in the detergent assay. When assayed in membranes, CysXV was slightly hyperactive (data not shown). The activity of the combination mutant CTr4/CysXV was similar to that of CTr4.

Characterization of Pigment-catalyzed GTP γ S Uptake by $G\alpha_t$ As a Function of $G\beta\gamma_t$ Concentration

Efficient activation of $G\alpha_t$ is known to require the presence of $G\beta\gamma_t$ (Fung, 1983). A previous study of a peptide derived from the C4 loop of rhodopsin suggested that this region binds to $G\beta\gamma_t$ (Phillips and Cerione, 1992). Therefore, the reduced activation of G_t by the mutant CTr2 might be a result of disruption of the $G\beta\gamma_t$ binding site on rhodopsin. To test this hypothesis, the rate of G_t activation by solubilized, COS-cell expressed rhodopsin (1 nM) or CTr2 (3 nM) was measured as a function of the concentration of $G\beta\gamma_t$. Higher concentrations of CTr2 were necessary in this experiment due to its reduced activity. Fig. 3-6 shows the change in fluorescence over time due to rhodopsin- or CTr2-catalyzed GTP γ S uptake by $G\alpha_t$ in the presence of different concentrations of $G\beta\gamma_t$. The intrinsic tryptophans of $G\beta\gamma_t$ affected only the background level of fluorescence, which is normalized in Fig. 3-6. If the defect in CTr2 were solely attributable to decreased binding of $G\beta\gamma_t$, then the concentration of $G\beta\gamma_t$ at which half-maximal activity was observed would likely be significantly higher for CTr2 than for rhodopsin. Additionally, one might expect the relative defect in activation rate of CTr2 to be reduced at high concentrations of $G\beta\gamma_t$. The data do not reveal a significant difference between rhodopsin and CTr2 in the effect of $G\beta\gamma_t$ concentration on $G\alpha_t$ activation, nor does the activity of CTr2 approach that of rhodopsin even at a 2:1 ($G\beta\gamma_t$: $G\alpha_t$) stoichiometric excess (Fig. 3-6).

Palmitoylation of CTr1, Ctr2, and CTr4

We investigated whether replacing portions of the fourth loop with β_2 AR sequence disrupted palmitoylation of mutants CTr1, CTr2, and CTr4. The incorporation of [3 H]palmitic acid present in the cell media during transfection into CTr1, CTr2, CTr4, and rhodopsin was comparable (Table 3-I). The levels of incorporation were several fold higher than the incorporation associated with CysXV, which has been reported not to be palmitoylated (Karnik *et al.*, 1993).

Amino Acid Sequence Analysis of Vertebrate Opsins and Biogenic Amine Family Receptors

The sequence alignments and analyses available in the G Protein Coupled Receptor Database (GPCRDB) at <http://swift.embl-heidelberg.de/7tm/> were used to examine the conservation of C4 residues in GPCRs (Horn *et al.*, 1998). Amongst the 86 vertebrate opsins in the database, the residues in the amino-terminal half of C4 were found to be nearly 100% conserved (Fig. 3-7). In contrast, the carboxyl-terminal half of the loop is only ~65% conserved.

Table 3-I: Biochemical Characterization of Rhodopsin Fourth Loop Mutants

Sample	λ_{max} , Abs (nm)	Transducin activation rate ^a	Incorporation of [³ H]Palmitic Acid ^b
Rho	500	100	1.00
CTr1	500	121±11.2 (5)	1.14±0.20 (4)
CTr2	500	20±5.5 (5)	1.34±0.47 (4)
CTr3	500	82±9.6 (4)	
CTr4	500	25±6.2 (3)	1.10±0.20 (4)
CysXV	500	97±15 (4)	0.24±0.10 (4)
CTr4/ CysXV	500	38.8±5.5 (3)	
K311P	500	85±6.7 (8)	
K311S	500	87±0.9 (3)	
K311R	500	123±13.5 (3)	
K311W	500	74±11.7 (3)	

^aActivation rates are normalized to that of rhodopsin and are presented as mean±S.E.M. (n).

^bThe level of incorporation of [³H]palmitic acid for each sample is normalized to that of rhodopsin, after subtraction of nonspecific counts associated with samples prepared from mock transfected cells. Values are presented as mean±S.E.M. (n).

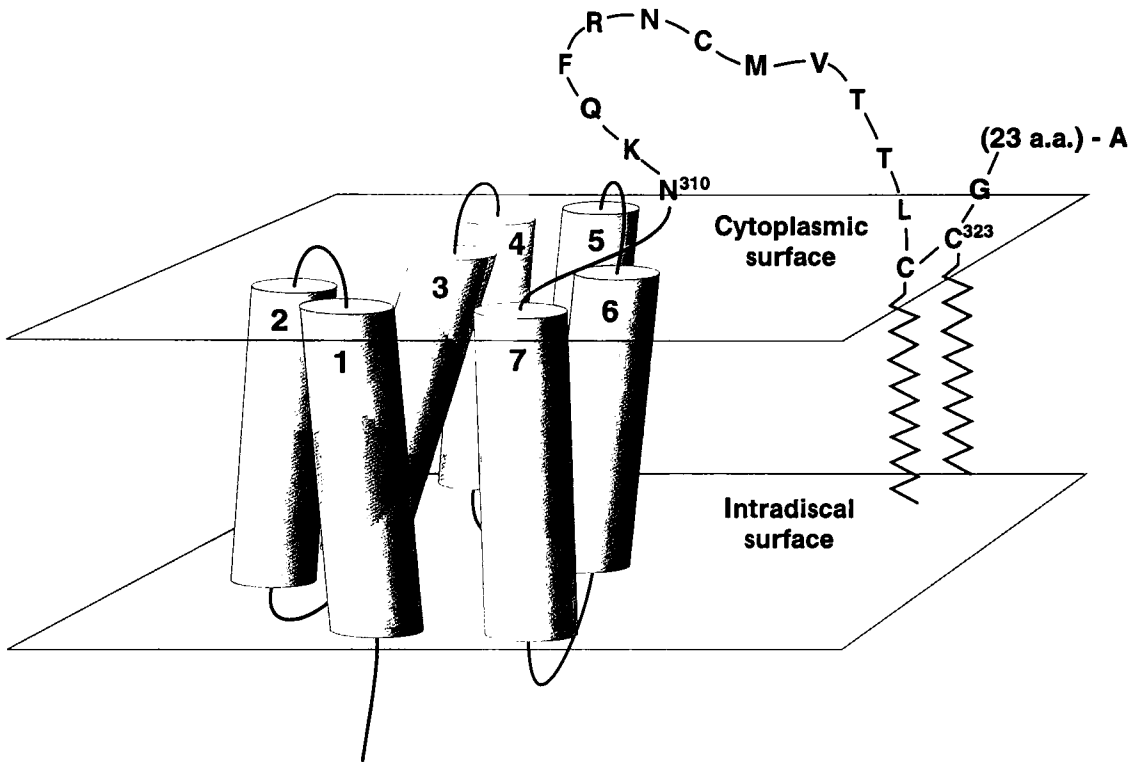


FIG. 3-1. Schematic representation of bovine rhodopsin. Seven putative TM helices are depicted as for previous models of GPCRs. The amino terminus and intradiscal surface are toward the bottom, and the carboxyl terminus and cytoplasmic surface is toward the top of the figure. The intradiscal and cytoplasmic loops are not drawn to scale. The loop C4 is defined as the 12 amino acids beginning with N310, at the membrane border of the TM helix 7, and ending with C322 and C323. Both of these cysteines are palmitoylated (Papac *et al.*, 1992; Ovchinnikov *et al.*, 1988), and the palmitoyl groups are inserted into the membrane (Moench *et al.*, 1994).

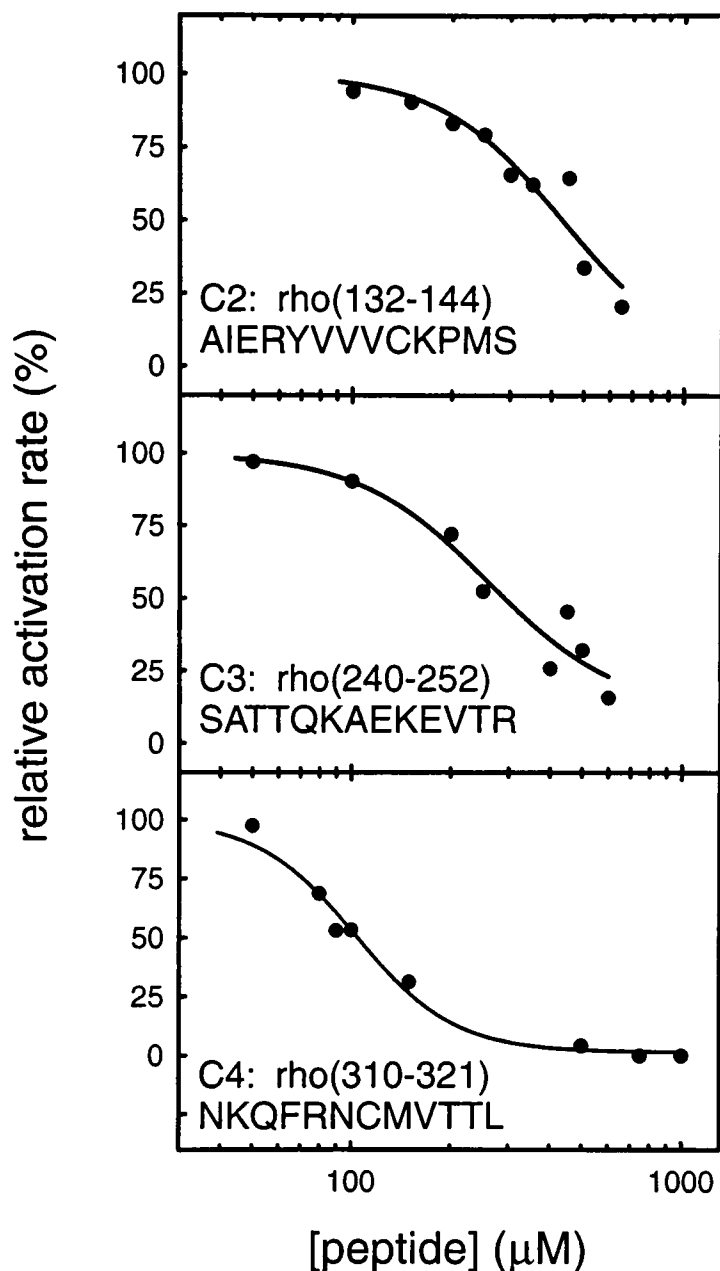


FIG. 3-2. Peptides derived from the second, third, and fourth intracellular loops of rhodopsin inhibit activation of G_t by rhodopsin. Each panel shows the relative initial rate of G_t activation as a function of peptide concentration. Activation rates were determined using a fluorescence assay of G_t activation (Fahmy and Sakmar, 1993). The peptide used in each experiment is described in the lower left hand corner of the corresponding panel. All three peptides completely inhibited activation of G_t , with IC_{50} values in the 0.1-0.3 mM range. A peptide derived from the first intracellular loop only moderately inhibited G_t activation at a concentration of 1 mM (not shown). Each panel represents data from a single set of experiments, which was repeated at least twice with similar results.

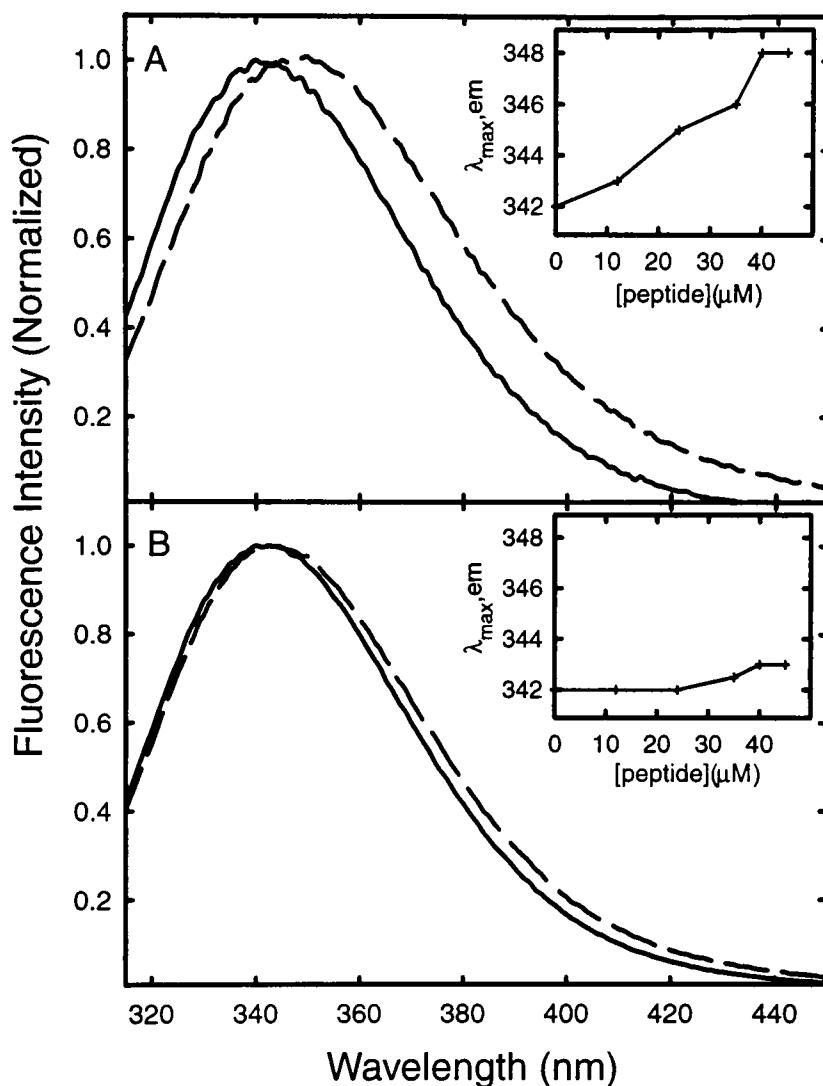


FIG. 3-3. Effect of rho(310-321) on the intrinsic fluorescence of G α_t and G $\beta\gamma_t$ subunits. Fluorescence emission spectra were collected using an excitation wavelength of 295 nm. **A**, Fluorescence emission spectra of G α_t (200 nM) before (solid line) and after (dashed line) incubation with the rhodopsin C4 peptide, rho(310-321) (45 μ M). The inset shows the fluorescence emission λ_{max} of G α_t as a function of rho(310-321) concentration. The mean maximum $\Delta\lambda_{\text{max}} \pm \text{S.E.M.}$ was 7.8 ± 0.3 nm ($n=4$). **B**, Fluorescence emission spectra of G $\beta\gamma_t$ (200 nM) before (solid line) and after (dashed line) incubation with rho(310-321) (45 μ M). Inset shows the fluorescence emission λ_{max} of G $\beta\gamma$ as a function of rho(310-321) concentration. The mean maximum $\Delta\lambda_{\text{max}} \pm \text{S.E.M.}$ was 1.0 ± 0.3 nm ($n=4$). Data shown are representative of at least four independent and reproducible experiments.

Receptor	Source of mutation	Amino Acid Position (Rhodopsin Numbering)													
		310	311	312	313	314	315	316	317	318	319	320	321	322	323
Rho		N	K	Q	F	R	N	C	M	V	T	T	L	C	C
β_2 AR		S	P	D	F	R	I	A	F	Q	E	L	L	C	L
m1 MR		N	K	A	F	R	D	T	F	R	L	L	L	L	C
CTr1	β_2 AR	N	K	Q	F	R	I	A	F	Q	E	L	L	C	C
CTr2	β_2 AR	S	P	D	F	R	I	A	F	Q	E	L	L	C	C
CTr3	m1 MR	N	K	Q	F	R	D	T	F	R	L	L	L	C	C
CTr4	β_2 AR	S	P	D	F	R	N	C	M	V	T	T	L	C	C
CysXV	β_2 AR	N	K	Q	F	R	N	C	M	V	T	T	L	S	S
CTr4/CysXV		S	P	D	F	R	N	C	M	V	T	T	L	S	S
K311P		N	P	Q	F	R	N	C	M	V	T	T	L	C	C
K311R		N	R	Q	F	R	N	C	M	V	T	T	L	C	C
K311S		N	S	Q	F	R	N	C	M	V	T	T	L	C	C
K311W		N	W	Q	F	R	N	C	M	V	T	T	L	C	C

FIG. 3-4. Amino acid sequences of the fourth loop of bovine rhodopsin, human β_2 AR, human m1 MR, and fourth loop mutants of rhodopsin. The amino acid sequence of each position in the fourth loop is shown using the standard single letter amino acid code. The numbering of the positions is from bovine rhodopsin. Regions that were replaced or altered in the creation of mutants are highlighted in gray.

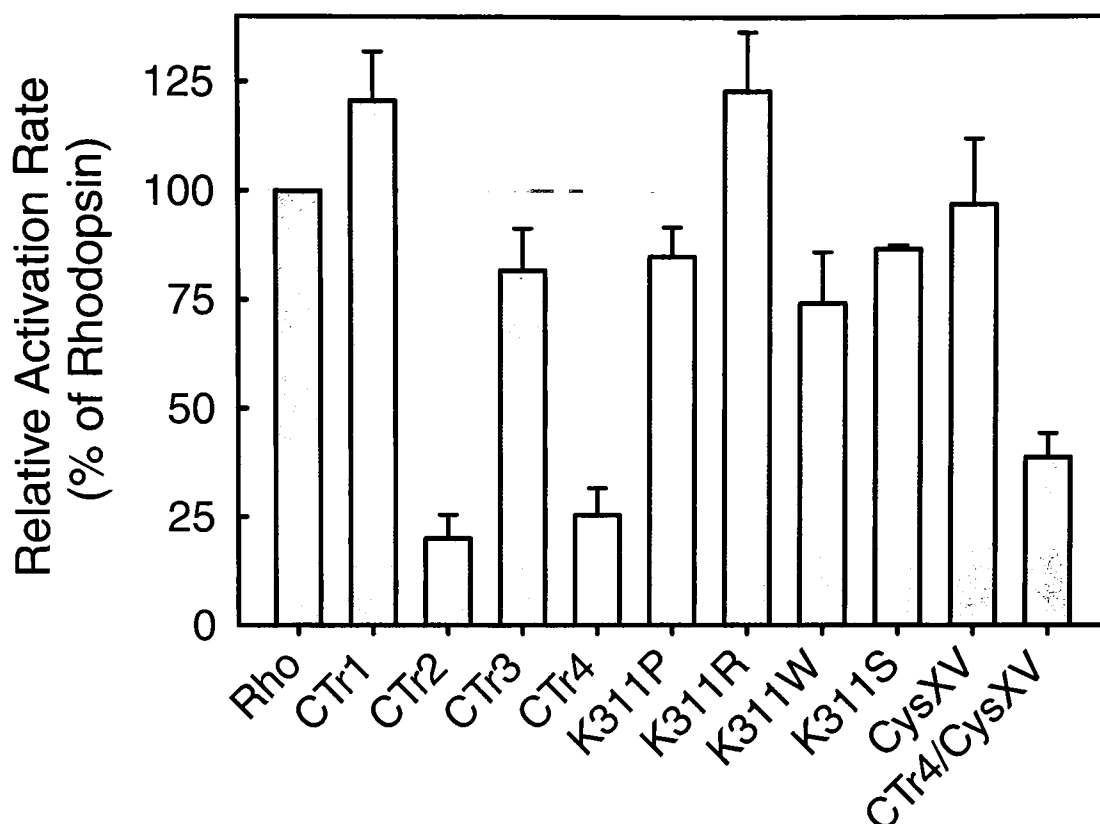


FIG. 3-5. Rates of G_t activation catalyzed by solubilized, purified recombinant pigments. Samples of rhodopsin and C4 rhodopsin mutants were expressed in COS cells, solubilized in DM, and purified by an immunoaffinity procedure as described in Chapter 2. The rates of G_t activation catalyzed by each sample were determined by linear regression through the first 30-60 s of data collected in a fluorescence activation assay (Fahmy and Sakmar, 1993). Each assay contained 1 nM rhodopsin or mutant, 250 nM G_t , and 5 μ M GTP γ S in a volume of 1.5 ml. The bars represent the mean rate, normalized to that of rhodopsin. Error bars depict the standard error of the mean. The data are presented numerically in Table 3-I. Those mutants in which residues 310, 311, and 312 of rhodopsin are replaced with the analogous sequence of the β_2 AR, (i.e., CTr2, CTr4, and CTr4/CysXV) are deficient in G_t activation.

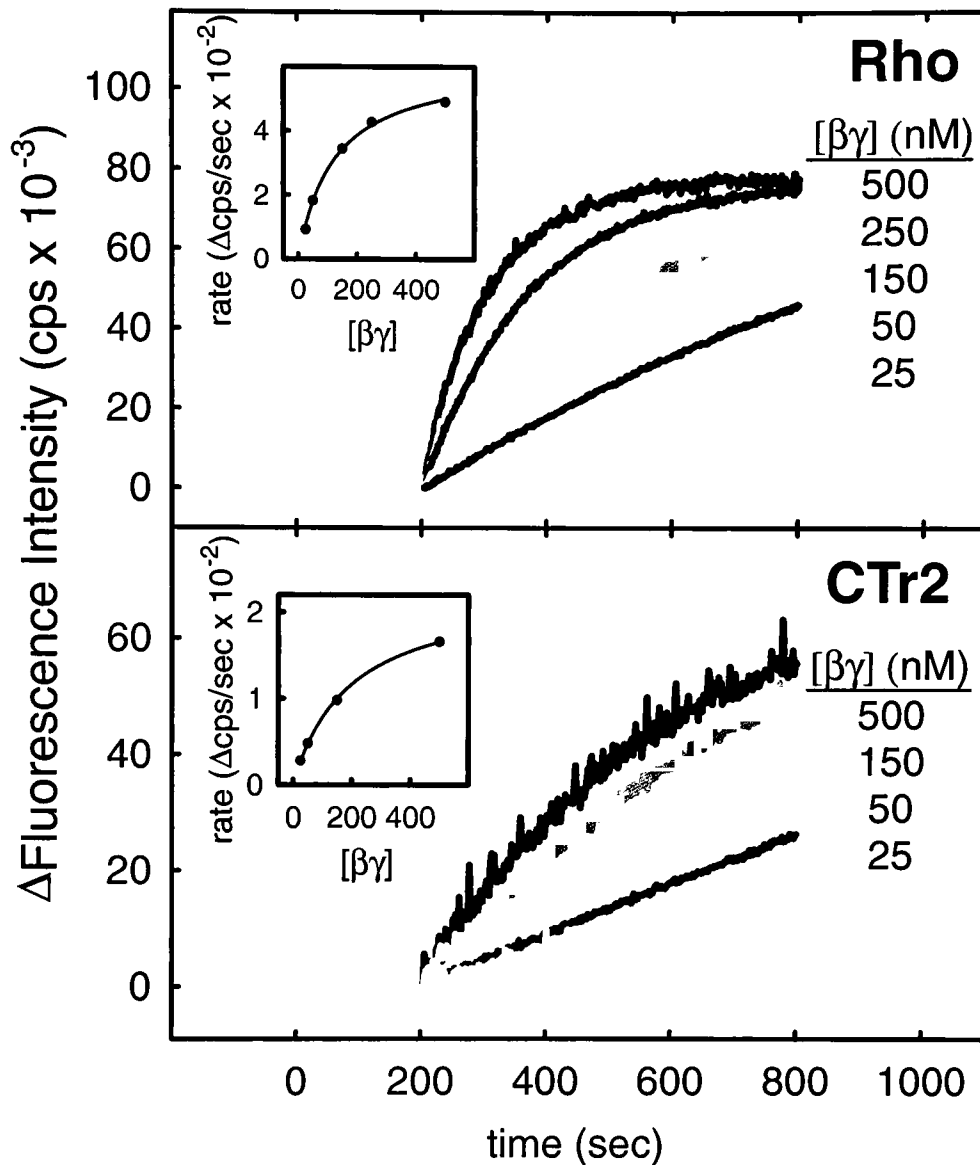


FIG. 3-6. The relative rates of pigment-catalyzed GTPγS uptake by Gα_t as a function of Gβγ_t concentration are similar for both rhodopsin and CTr2. The rate of G_t activation by solubilized, COS-cell expressed pigment was measured as a function of the concentration of Gβγ_t. The top panel shows fluorescence activation traces of 250 nM Gα_t in the presence of 25 - 500 nM Gβγ_t, and catalyzed by 1 nM rhodopsin. Each trace depicts the change in fluorescence emission intensity following the addition of GTPγS at 200 s. The background fluorescence emission is normalized to zero. The concentration of Gβγ_t in each trace is indicated in the column at right, in the same order that the traces are displayed. The inset is a plot of activation rate, determined from the initial slopes of the activation traces, versus concentration of Gβγ_t. The data are fit with a two-parameter hyperbolic function. The bottom panel is identical to the top, except that the experiments were conducted with 3 nM CTr2. The data are from a single experiment that was repeated twice with similar results. The similarity of the Gβγ_t concentration dependency for Rho and CTr2 argues against the hypothesis that the defect in CTr2 is attributable solely to disruption of the Gβγ_t binding site (see text for further discussion).

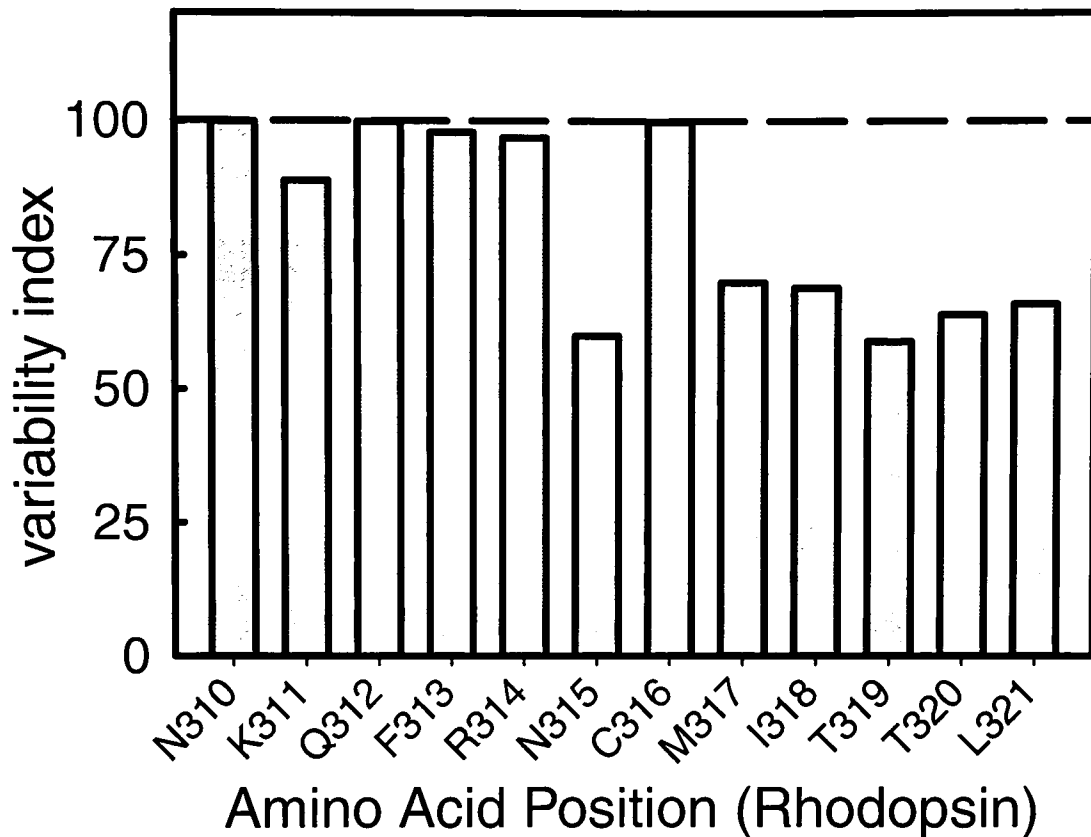


FIG. 3-7. The amino-terminal half of the fourth loop of rhodopsin is more conserved than the carboxyl-terminal half within the family of vertebrate opsins. The conservation of each position within loop C4 of rhodopsin was analyzed in 86 vertebrate opsin sequences. The alignments and the determination of the variability at each position were obtained from the G Protein Coupled Receptor Database (GPCRDB) at <http://swift.embl-heidelberg.de/7tm/> (Horn et al., 1998). The labels on the x-axis indicate the consensus amino acid at each position, using bovine rhodopsin numbering. A variability index of 100 means 100% conservation; the lower the number, the greater the variety of residues found at that particular position. The residues in the amino-terminal half of the loop are nearly 100% conserved, whereas those at the carboxyl-terminal half are only ~65% conserved. This pattern of conservation corresponds to the importance of the amino-terminal half of the loop in G_t activation.

Discussion

Significant efforts have been directed toward elucidating the regions of rhodopsin involved in binding and activating G_t (for reviews, see (Helmreich and Hofmann, 1996))(Wess, 1997; Bourne, 1997). A variety of experiments using peptide competition, mutagenesis, and antibody-based approaches have defined the importance of the intracellular surface, and in particular, loops C2 and C3 in mediating interactions with G_t . Published reports regarding the role of loop C4 are contradictory. Studies based on peptides derived from C4 have suggested the importance of this region (König *et al.*, 1989; Takemoto *et al.*, 1986), but a combination of site-directed mutagenesis and truncation of C4 appeared to rule out an important function for the region in G_t activation (Osawa and Weiss, 1994; Weiss *et al.*, 1994). Our data demonstrate and characterize the importance of the amino-terminal part of the fourth loop, and suggest the role it plays in rhodopsin- G_t interactions.

Loop C4 of Rhodopsin Is Involved in the Activation of G_t

Several different experimental approaches in this report corroborate the importance of the fourth loop of rhodopsin in interactions with G_t . A peptide derived from C4, rho(310-321), can inhibit the catalysis of G_t activation by rhodopsin. Previously, an identical peptide has been reported to inhibit the binding of G_t to rhodopsin as measured by an extra-MII assay (König *et al.*, 1989). Our results extend and confirm this observation by demonstrating that the peptide is active at similar concentrations in the fluorescence activation assay (Fig. 3-2). Significantly, the potency of rho(310-321) was comparable to that of peptides derived from very well characterized G protein-interacting regions, including the highly conserved Glu-Arg-Tyr sequence in the C2-derived

rho(132-144) peptide. Additionally, rho(310-321) induces a red shift in the fluorescence emission spectrum of $G\alpha_t$ (Fig. 3-3), which is evidence that the peptide can bind directly to the $G\alpha_t$ subunit. The relevance of studies with the isolated C4-derived peptide to the function of C4 in the intact receptor is supported by the report that a rho(306-348) peptide assumed a defined structure in solution (Yeagle *et al.*, 1996).

The results of the mutagenesis data strongly support and clarify the involvement of the fourth loop in G_t activation. In particular, the data localize the important region to the amino terminus of C4, as shown by the striking decrease in the rate of G_t activation by the mutants in which residues 310-312 are replaced with β_2 AR sequence (Fig. 3-5). Osawa and Weiss (Osawa and Weiss, 1994) argued against involvement of this region based on the wild-type phenotype of N310A, K311A, and Q312A point mutants. However, a recent report (Cai *et al.*, 1999) corroborates our findings by identifying a mutation in the amino terminus of C4 (N310C) that can disrupt G_t activation. The precise role of N310 in G_t coupling appears complex.

Sequence analysis also supports the importance of the amino terminus of the C4 loop in receptor function. The amino terminus of C4 is nearly 100% conserved within the vertebrate opsins, whereas the carboxyl-terminal half of the loop is only ~65% conserved (Fig. 3-7). Furthermore, the asparagine in position 310 is very highly conserved within the large biogenic amine family of receptors, with the exception of the non- α_2 ARs, where it nearly always is a serine. This latter observation suggests that the amino-terminal part of the fourth loop may be important in GPCRs other than opsins. Indeed, mutagenesis experiments in this region of the fourth loop identified it as critical for receptor-G protein interactions in the β_2 AR (O'Dowd *et al.*, 1988; Liggett *et al.*, 1991).

Several reports have suggested that accessibility to regions in the fourth loop are specifically modulated by photoactivation of rhodopsin, an observation consistent with

the regulated involvement of C4 in G_t activation. The cytoplasmic end of TM helix 7 has been shown to become more accessible following light activation of rhodopsin (Abdulaev and Ridge, 1998), and spin labels attached to positions 316 (Resek *et al.*, 1993) and 313 (Altenbach *et al.*, 1999) in the middle of C4 undergo increased mobility after photolysis. Additionally, a spin label at C316 was reported to move apart from a label at position 65, at the amino terminus of the TM helix 1, upon MII formation (Yang *et al.*, 1996).

Factors Affecting the Structure of the C4 Loop Region

We examined several factors that potentially affect the structure of C4, including the palmitoylation of C322 and C323, the integrity of a proposed helical extension of TM7, and the presence of a membrane environment. The palmitoylation of C322 and C323 does not appear to affect the function of the amino-terminal part of the loop. Both CTr4 and CTr2 are palmitoylated (Table 3-I) despite alterations in amino acids in the vicinity of the acylation site. However, the non-palmitoylated combination mutant CTr4/CysXV is essentially indistinguishable from CTr4 in detergent assays. In membranes, CysXV is slightly more active than rhodopsin, and CTr4/CysXV is slightly more active than CTr4 (not shown). Both observations corroborate previous reports that a nonpalmitoylated mutant was similar to rhodopsin in detergent solution (Karnik *et al.*, 1993), and that chemical depalmitoylation increased activity of rhodopsin when assayed in rod outer segment membranes (Morrison *et al.*, 1991). Given that residues 310-312 are located adjacent to the membrane border of the TM helix 7, it seems plausible that their structure is unaffected by the membrane anchoring of C322 and C323. The same reasoning might explain why truncation of rhodopsin following N315 does not diminish G_t activation (Weiss *et al.*, 1994). Furthermore, C4 may form a loop in the absence of palmitoylation, as suggested by the NMR structure of a fourth loop peptide (Yeagle *et al.*, 1996). The

mechanism of hyperactivity of non-palmitoylated rhodopsin that has been observed in membranes appears to be unrelated to the function of the amino terminus of C4.

The TM helix 7 is likely to extend beyond the membrane border, based on experimental (Yeagle *et al.*, 1996; Altenbach *et al.*, 1999) and theoretical (Ben-Tal *et al.*, 1996) grounds. The TM2 (Farahbakhsh *et al.*, 1995), TM4, and TM5 (Altenbach *et al.*, 1996) helices have all been reported to extend into the aqueous phase. The proline in position 311 of CTr2 and CTr4 might disrupt a helical extension of TM helix 7, leading to the observed phenotype. But the K311P point mutation does not resemble the 310-312 mutation of CTr4 in G_t activation assays, indicating that perturbation of the proposed helical extension does not impair G protein activation.

The Role of the C4 Loop Involves Modulation of Rhodopsin- G_t Interactions

We propose that the role of C4 is to modulate, in conjunction with other structures, the binding site for G_t . We favor this interpretation rather than those in which C4 serves as the sole binding site or participates mechanistically in the catalysis of nucleotide exchange because: (a) residual G_t activation was observed with the CTr2 and CTr4 mutants, (b) point mutations at the 311 position did not affect activation, (c) the amino-terminal C4 sequence of rhodopsin is highly, but not absolutely, conserved in other opsins and in certain other GPCRs (Fig. 3-7), and (d) the substitution of β_2 AR sequence into C4 does not allow rhodopsin to activate G_s (data not shown). The modulatory functions of C4 appear to be mediated both by contacts with G_t and by allosteric interactions with other regions of the receptor.

Specific interaction between C4 and G_t is indicated most directly by the rho(310-321)- $G\alpha_t$ interaction observed by fluorescence emission spectroscopy (Fig. 3-3). Direct contacts are also suggested by the inhibition of rhodopsin-catalyzed G_t activation in the

presence of rho(310-321), an observation plausibly explained by binding of the peptide to the G protein, and occupancy of a receptor contact site (Fig. 3-2). Which part of the heterotrimer is binding to the C4 loop? A C4 derived peptide, rho(310-324), has been reported to bind $G\beta\gamma_t$ (Phillips and Cerione, 1992). However, the similarity of the activation rate versus $G\beta\gamma_t$ concentration profiles for rhodopsin and CTr2, and the failure of high concentrations of $G\beta\gamma_t$ to fully rescue CTr2 activity (Fig. 3-6), argue against the fourth loop as acting solely as a $G\beta\gamma_t$ binding site. Furthermore, the direct binding of rho(310-321) to $G\alpha_t$ (Fig. 3-3) demonstrates that C4 is involved with $G\alpha_t$ binding in addition to, or even instead of, $G\beta\gamma_t$ binding. Perhaps C4 binds $G\alpha_t$ directly, and allosterically regulates other regions of the receptor involved in $G\beta\gamma_t$ binding.

The data in this report demonstrate a conclusive role for the amino terminus of C4 of rhodopsin in G_t interactions. We suggest that this interacts directly with G_t , particularly with $G\alpha_t$, and with other regions of the intracellular surface to support G_t binding. In the following chapter, we study a subset of mutant receptors described here using a biophysical assay that detects binding of G_t or peptides derived from G_t subunit sequences.

Chapter 4:

Mutation of the Fourth Cytoplasmic Loop of Rhodopsin Affects Binding of Transducin and Peptides Derived from the Carboxyl-terminal Sequences of Transducin α and γ Subunits[#]

Summary

The role of the putative fourth cytoplasmic loop of rhodopsin in the binding and catalytic activation of the heterotrimeric G protein, transducin (G_t), is not well defined. We developed a novel assay to measure the ability of G_t , or G_t -derived peptides, to inhibit the photoregeneration of rhodopsin from its active metarhodopsin II state. We show that a peptide corresponding to residues 340-350 of the α subunit of G_t , or a cysteinyl-thioetherfarnesyl peptide corresponding to residues 50-71 of the γ subunit of G_t , are able to interact with metarhodopsin II and inhibit its photoconversion to rhodopsin. Alteration of the amino acid sequence of either peptide, or removal of the farnesyl group from the γ -derived peptide, prevents inhibition. Mutation of the amino-terminal region of the fourth cytoplasmic loop of rhodopsin affects interaction with G_t (Marin *et al.*, 2000). Here, we provide evidence that this segment of rhodopsin interacts with the carboxyl-terminal peptide of the α subunit of G_t . We propose that the amino-terminal region of the fourth cytoplasmic loop of rhodopsin is part of the binding site for the carboxyl terminus of the α subunit of G_t and plays a role in the regulation of $\beta\gamma$ subunit binding.

[#] Material in this chapter has been published previously in: Ernst, O. P.*, Meyer, C. K.*, Marin, E. P.*, Henklein, P., Fu, W.-Y., Sakmar, T. P., and Hofmann, K. P. (2000) Mutation of the fourth cytoplasmic loop of rhodopsin affects binding of transducin and peptides derived from the carboxyl-terminal sequences of transducin alpha and gamma subunits. *J. Biol. Chem.* **275**:1937-1943.
(*authors contributing equally)

Introduction

A variety of experimental approaches, including proteolysis, chemical modification, peptide competition and site-directed mutagenesis in combination with biochemical and biophysical assays, have been employed to map the sites of rhodopsin responsible for the binding and activation of G_t . The salient results have indicated that loops C2 and C3 are involved in G_t binding and activation (Franke *et al.*, 1990; Franke *et al.*, 1992). In addition, recent studies indicate a role for the loop C4 in G_t activation (Marin *et al.*, 2000; Cai *et al.*, 1999; Altenbach *et al.*, 1999). Despite these studies and the availability of a high-resolution crystal structure for the G_t holoprotein (Lambright *et al.*, 1996), there is little information concerning: 1) the key functional intramolecular interactions on the cytoplasmic surface of rhodopsin that form and regulate the catalytic site for G_t , 2) G_t subunit specificity for binding to particular cytoplasmic regions of rhodopsin, 3) the molecular mechanism of rhodopsin-catalyzed nucleotide release by G_t .

In Chapter 3, a region was identified at the amino terminus of loop C4 of rhodopsin that most likely interacts with the α subunit of G_t , $G\alpha_t$. Here, we studied the interaction of site-directed mutants of rhodopsin with G_t and peptides derived from the carboxyl-terminal sequences of $G\alpha_t$ and $G\gamma_t$ (Ernst *et al.*, 1999; Kisselev *et al.*, 1999; Arnis and Hofmann, 1995). We used a novel assay in which the all-*trans*-retinal in metarhodopsin II (MII) is photoconverted to the *cis* configuration using blue light. The flash-induced photoregeneration of rhodopsin from MII can be followed spectroscopically with millisecond time resolution (Arnis and Hofmann, 1995). Since stabilization of R^* by G_t or G_t -derived peptides inhibits the rate of photoregeneration, the assay can be used to monitor the interaction of R^* with G_t (Ernst *et al.*, 1999; Kisselev *et al.*, 1999). We show that peptide $\alpha(340-350)$, corresponding to the carboxyl-terminal undecapeptide of $G\alpha_t$, and peptide $\gamma(50-71)$ -far, corresponding to the carboxyl-terminal cysteinyl-

thioetherfarnesyl peptide of $G\gamma_t$, stabilized R^* . Alteration of the amino acid sequence of either peptide, or removal of the farnesyl group of the $G\gamma_t$ -derived peptide prevented stabilization of R^* . G_t failed to stabilize mutant rhodopsins with alterations of the amino terminus of loop C4 near the TM helix 7 border. The $G\alpha_t$ -derived peptide also failed to stabilize these mutants, suggesting that loop C4 comprises part of a binding site for the carboxyl-terminal tail of $G\alpha_t$.

Results

The Effect of G_t and G_t -derived Peptides on the Photoregeneration of Bovine Retinal Rhodopsin

A “photoregeneration” assay was employed that measures the kinetics of photoconversion of MII to rhodopsin (Arnis and Hofmann, 1995). The assay takes advantage of the conformational coupling of the cytoplasmic surface of the active state of rhodopsin, R^* , to the chromophore-binding pocket in the membrane-embedded domain of the receptor. The slow phase of the photoconversion kinetics essentially monitors the reprotonation of the retinylidene Schiff base as a function of time after a sample of R^* is subjected to a blue flash. Photoconversion of R^* ($\lambda_{\max} = 380$ nm) to rhodopsin ($\lambda_{\max} = 500$ nm) is inhibited if R^* is bound to G_t or certain G_t -derived peptides. R^* that is not bound in a stabilizing complex with G_t or G_t -derived peptides is more readily photoconverted.

The effect of G_t on the photoconversion of R^* was studied first (Fig. 4-2A). The change in absorbance at 543 nm is plotted as a function of time. The blue flash is applied to the sample at 50 ms. Superimposed upon an initial rapid change in amplitude, the slow phase of the trace represents the back conversion of R^* to rhodopsin. The experiment was repeated with identical rhodopsin samples in the presence of increasing concentrations of G_t (0, 0.5, 1.0, 2.0, 3.0, 5.0 μ M). The traces are superimposed to show

a clear dose-dependent inhibition of the photoregeneration reaction by G_t . The experimental traces were fit to an exponential function in order to calculate values for initial slopes. The calculated fits are shown as dashed lines in Fig. 4-2. The initial slopes of the photoregeneration traces are plotted as a function of G_t concentration in the inset. A satisfactory hyperbolic fit yielded an effective concentration at 50% inhibition (IC_{50}) value of $2.56 \pm 2.0 \mu M$. This value effectively represents a binding constant for the interaction between R^* and G_t under the conditions of the assay.

The effects of two peptides corresponding to the carboxyl-terminal regions of $G\alpha_t$ and $G\gamma_t$ on the photoconversion of R^* was studied next (Fig. 4-2, B and C). The amino acid sequences of $\alpha(340-350)$ and $\gamma(50-71)$ -far are presented in Fig. 4-1B. The $\gamma(50-71)$ -far peptide carries the post-translational isoprenylation that is characteristic of $G\gamma_t$. Fig. 4-2B shows six superimposed photoregeneration traces obtained from identical rhodopsin samples in the presence of increasing concentrations of $\alpha(340-350)$ (0 to $1000 \mu M$). The traces show a clear dose-dependent inhibition of the photoregeneration of R^* by $\alpha(340-350)$. The initial slopes of the photoregeneration traces are plotted as a function of $\alpha(340-350)$ concentration in the inset to Fig. 4-2B. A satisfactory hyperbolic fit yielded an IC_{50} value of $49.5 \pm 6.0 \mu M$ for the interaction between R^* and $\alpha(340-350)$.

Fig. 4-2C shows six superimposed photoregeneration traces obtained from identical rhodopsin samples in the presence of increasing concentrations of $\gamma(50-71)$ -far (0 to $1000 \mu M$). The traces show a clear dose-dependent inhibition of the photoregeneration of R^* by $\gamma(50-71)$ -far. Plotting the initial slopes of the photoregeneration traces as a function of $\gamma(50-71)$ -far concentration (inset to Fig. 4-2C) permitted a satisfactory hyperbolic fit that yielded an IC_{50} value of $285 \pm 74 \mu M$ for the interaction between R^* and $\gamma(50-71)$ -far.

Specificity of the Effects of $\alpha(340-350)$ and $\gamma(50-71)$ -far Peptides

The specificity of the effect of the G_t -derived peptides was studied by performing control experiments with altered peptides. The peptides are shown in Fig. 4-1B. One control peptide, $\alpha(340-350)$ K341R/L349A, was studied to evaluate the specificity of the carboxyl-terminal sequence of $G\alpha_t$ in R^* interaction. This peptide failed to show peptide- R^* interaction (Nishimura *et al.*, 1998; Fahmy, 1998) and the substitution of Leu³⁴⁹ by alanine in $G\alpha_t$ was reported to abolish coupling to active rhodopsin (Osawa and Weiss, 1995; Garcia *et al.*, 1995). As shown in Fig. 4-3, the $\alpha(340-350)$ K341R/L349A peptide failed to inhibit the photoregeneration of R^* . Similarly, the requirements for length, primary structure and farnesylation of the $G\gamma_t$ -derived peptide were tested. Peptides $\gamma(60-71)$ -far and $\gamma(50-71)$ -far both inhibited photoregeneration similarly (Fig. 4-3). Positions 64 and 67 in $G\gamma_t$ have been reported to be critical for interaction with MII, as observed with the altered peptide $\gamma(60-71)$ -far F64T/L67S (Kisselev *et al.*, 1995b). The $\gamma(60-71)$ -far F64A/L67A peptide did not inhibit photoregeneration (Fig. 4-3). In addition, the $\gamma(60-71)$ peptide, which lacked cysteinyl farnesylation, did not inhibit photoregeneration (Fig. 4-3). This finding is consistent with earlier results showing that lack of farnesylation prevented MII stabilization by $G\gamma_t$ derived peptides (Kisselev *et al.*, 1994; Kisselev *et al.*, 1995a). In other control experiments, the 1D4 peptide, corresponding to the carboxyl-terminal 18 amino acids of rhodopsin, did not affect photoregeneration, nor did it affect the inhibition of photoregeneration by G_t and the G_t -derived peptides (data not shown).

It has been reported that detergent concentration has an influence on the activation rate of G_t by R^* (Franke *et al.*, 1992; Han *et al.*, 1998). The effect of varying concentrations of DM on the photoregeneration kinetics of rhodopsin and on the inhibition of photoregeneration by G_t (3 μ M), $\alpha(340-350)$ (200 μ M) or $\gamma(50-71)$ -far (500 μ M) was studied. Varying DM concentrations from 0.01% to 0.10% (w/v) had no effect on the photoregeneration kinetics of rhodopsin, and no effect on the inhibition of

photoregeneration by $\alpha(340-350)$ (data not shown). However, the inhibition of photoregeneration by G_t and $\gamma(50-71)$ -far was reduced by increasing DM concentrations from 0.01% to 0.10% (data not shown). This effect mirrors the reduction in the rate of G_t activation by R^* in the presence of increasing [DM], as previously reported (Franke *et al.*, 1992; Han *et al.*, 1998). The final DM concentration under the standard conditions of the photoregeneration assay using heterologously-expressed and purified mutant pigments is estimated to be 0.01-0.035%, a range in which detergent effects were found to be modest. Furthermore, the final DM concentration in assays of each of the recombinant samples is virtually identical.

Photoregeneration Assay of Recombinant Rhodopsin and Loop C4 Mutants

Photoregeneration assays were carried out on wild-type recombinant rhodopsin and four mutant rhodopsins (Fig. 4-1A). Representative photoregeneration traces are presented in Fig. 4-4. In each panel, the change in absorbance at 543 nm is plotted as a function of time. The blue flash is applied to the sample at 50 ms. Superimposed upon an initial rapid change in amplitude, the slow phase of the trace represents the back conversion of R^* to rhodopsin. The black trace shows the result with pigment alone. The red trace shows the result with pigment in the presence of G_t (3.0 μ M), $\alpha(340-350)$ (200 μ M) or $\gamma(50-71)$ -far (500 μ M) as indicated. The behavior of COS-cell expressed rhodopsin was similar to that of bovine rhodopsin in the photoregeneration assay. Fig. 4-4 shows typical experimental traces obtained with purified recombinant rhodopsin in the presence of G_t , $\alpha(340-350)$ and $\gamma(50-71)$ -far. Typical traces obtained with bovine rhodopsin are presented in Fig. 4-2. These results confirm that the photoregeneration assay can be employed to study recombinant pigments prepared in relatively small quantities in a heterologous expression system.

Four mutant pigments with alterations of the amino acid sequence of the C4 loop were prepared (Fig. 4-1A). Mutants CTr1, CTr2 and CTr4 are essentially chimeric

receptors in which parts of the C4 loop of rhodopsin are replaced by sequences from the β_2 adrenergic receptor (β_2 AR). Mutant CysXV (C322S/C323S) was designed to evaluate the effect of receptor palmitoylation on the photoregeneration kinetics. The mutant opsin genes were expressed in COS cells, treated with 11-*cis*-retinal and purified in DM detergent solution. The levels of palmitoylation of the expressed mutant pigments CTr2 and CTr4 were similar to that of the wild-type receptor expressed in parallel; CysXV was not palmitoylated (Table 3-I) (Karnik *et al.*, 1993; Karnik *et al.*, 1993). The ability of each of the mutant pigments to activate G_t was evaluated using a fluorescence G_t activation assay (Table 4-I). Mutant pigments CTr2 and CTr4 were significantly defective in their ability to activate G_t .

In the absence of G_t or G_t -derived peptides, the photoregeneration kinetics of rhodopsin and the four C4 mutants were essentially identical (Fig. 4-4, black traces). This result suggests that the C4 loop mutations do not affect the photoregeneration reaction. The effects of G_t or G_t -derived peptides on the photoregeneration of the mutant pigments are shown in Fig. 4-4 (red traces). The effects can be conveniently evaluated by comparing *relative slopes* (Fig. 4-5A). The *relative slope* is defined as the initial slope of the slow phase of the photoregeneration trace in the presence of G_t , $\alpha(340-350)$ or $\gamma(50-71)$ -far divided by the initial slope of the trace in the absence of G_t or G_t -derived peptide. The *relative slope* provides a quantitative measure of the effect of G_t or a G_t -derived peptide on the slow phase of the photoregeneration kinetics. A *relative slope* of 1.0 indicates no inhibition of photoregeneration, and *relative slopes* of <1.0 indicate a progressive inhibition of photoregeneration. Average values for *relative slopes* are presented in Table 4-I.

Photoregeneration of mutant CTr1 was inhibited by G_t and the G_t -derived peptides. The degrees of inhibition were identical to those seen with wild-type rhodopsin. The behavior of mutants CTr2 and CTr4 was different from that of rhodopsin. G_t and the

peptide $\alpha(340-350)$ did not inhibit photoregeneration of CTr2. This result is best appreciated in Fig. 4-5A, where the relative slopes for CTr2 in the presence of G_t and $\alpha(340-350)$ are ~ 1.0 . However, the $\gamma(50-71)$ -far peptide was able to inhibit photoregeneration of CTr2 to the same extent observed with rhodopsin. The photoregeneration of mutant CTr4 was not affected by G_t , $\alpha(340-350)$ or $\gamma(50-71)$ -far. This result is best seen in Fig. 4-5A, where the *relative slopes* for CTr4 in the presence of G_t and the G_t -derived peptides are ~ 1.0 . Photoregeneration of mutant CysXV was inhibited by G_t and the G_t -derived peptides. However, the inhibition by peptide $\gamma(50-71)$ -far was relatively more pronounced for CysXV than for rhodopsin.

Each of the peptides and G_t inhibit the photoregeneration of rhodopsin to different degrees. Therefore, the ability of each peptide and G_t to affect a particular mutant cannot be compared directly using *relative slopes*. However, by normalizing the *relative slope* of a mutant to that of rhodopsin, such a comparison can be made. This expression, termed the *normalized inhibition*, is obtained from the following equation: $(1 - \text{mean relative slope})_{\text{mutant}} / (1 - \text{mean relative slope})_{\text{rhodopsin}}$. The *normalized inhibition* for rhodopsin is defined to be 1.0. A value of zero indicates no inhibition of the photoregeneration of the mutant pigment by a particular ligand. Data are plotted in Fig. 4-5B and listed in Table 4-I. Mutant CTr1 is similar to rhodopsin with respect to inhibition of photoregeneration by G_t , $\alpha(340-350)$ and $\gamma(50-71)$ -far. Mutant CTr2 shows essentially normal interaction with $\gamma(50-71)$ -far, but fails to be affected by G_t and $\alpha(340-350)$. Mutant CTr4 is unaffected by G_t and both G_t -derived peptides. The photoregeneration of mutant CysXV is inhibited by $\alpha(340-350)$ and G_t normally, but displays an enhanced sensitivity to $\gamma(50-71)$ -far.

Table 4-1: G_t activation and photoregeneration data

		G_t or G_t -derived Peptides								
SAMPLE	Activation of G_t^*	3 μ M G_t			200 μ M $\alpha(340-350)$			500 μ M $\gamma(50-71)$ -far		
		n^b	relative slope ^c	normalized inhibition ^d	n^b	relative slope ^c	normalized inhibition ^d	n^b	relative slope ^c	normalized inhibition ^d
WT-Rho	100	2	0.67 \pm 0.05	1.00 \pm 0.15	2	0.26 \pm 0.01	1.00 \pm 0.01	2	0.59 \pm 0.03	1.00 \pm 0.08
CTr1	121 \pm 11	2	0.73 \pm 0.06	0.82 \pm 0.16	2	0.22 \pm 0.05	1.06 \pm 0.05	2	0.53 \pm 0.11	1.14 \pm 0.20
CTr2	20 \pm 5.5	2	0.98 \pm 0.02	0.06 \pm 0.04	3	0.89 \pm 0.09	0.15 \pm 0.13	3	0.62 \pm 0.01	0.93 \pm 0.05
CTr4	25 \pm 6.2	2	1.03 \pm 0.04	-0.08 \pm 0.09	2	0.96 \pm 0.13	0.06 \pm 0.12	2	0.95 \pm 0.07	0.13 \pm 0.11
CYS XV	97 \pm 15	2	0.61 \pm 0.12	1.19 \pm 0.30	2	0.24 \pm 0.06	1.03 \pm 0.06	4	0.41 \pm 0.06	1.42 \pm 0.10

^a Previously reported (Table 3-I) (Marin *et al.*, 2000)

^b The number given for n refers to the number of independent samples studied. Each kinetic trace (Fig. 4) resulted from four separate photoregeneration experiments per sample.

^c The relative slope is defined as the initial slope of the slow phase of the photoregeneration trace in the presence of G_t , $\alpha(340-350)$ or $\gamma(50-71)$ -far divided by the initial slope of the trace in the absence of G_t or G_t -derived peptide. The initial slope of the slow phase of the photoregeneration trace was determined from the numerical fit of a simple exponential-rise function offset by the amplitude of the fast phase. The data are presented as mean \pm S. E. M.

^d The normalized inhibition is defined as: $(1 - \text{mean relative slope})_{\text{mutant}} / (1 - \text{mean relative slope})_{\text{rhodopsin}}$. The propagated S. E. M. values are also presented.

A

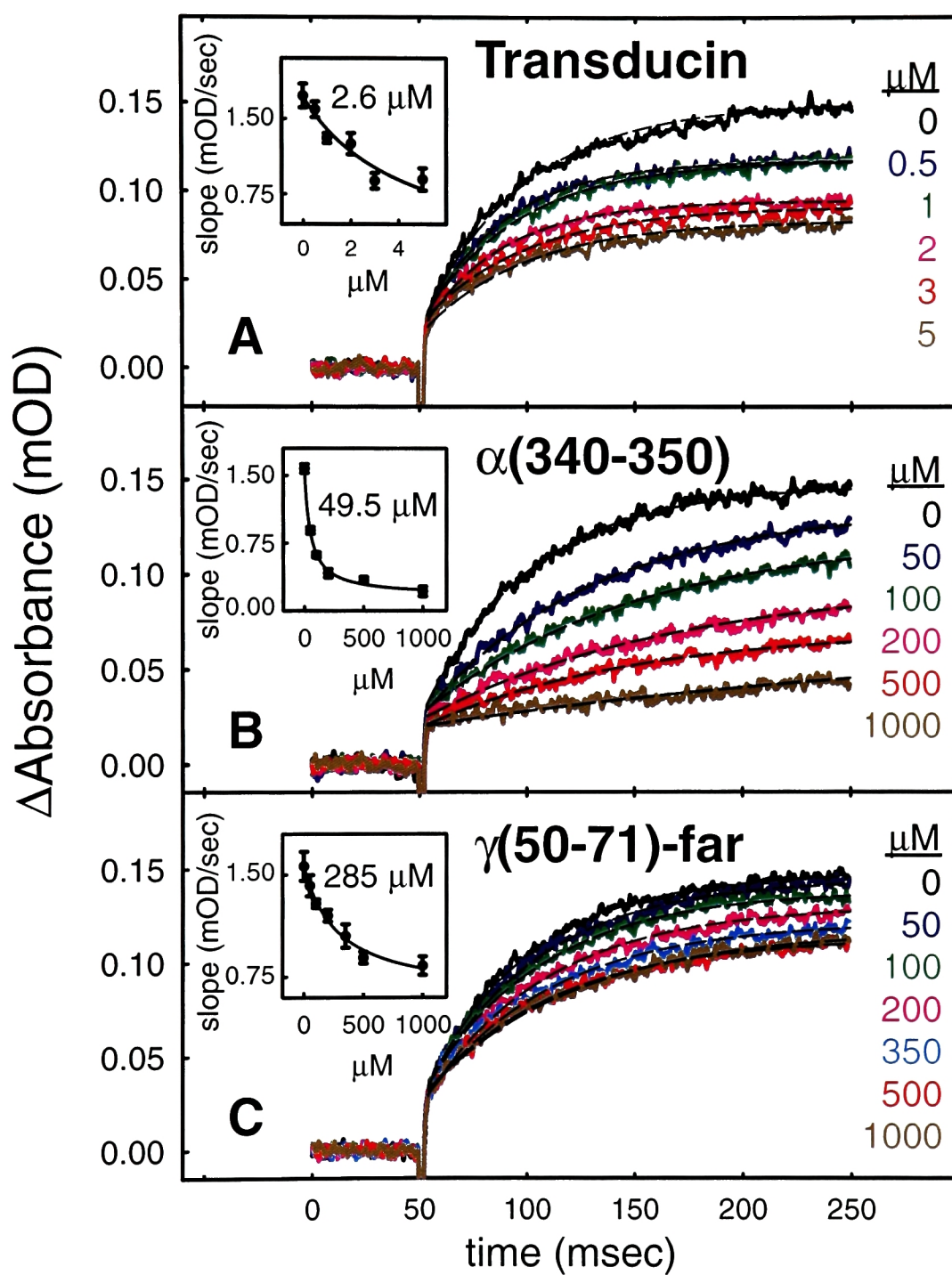
Sample	Fourth Loop Amino Acid Sequence													
	310	311	312	313	314	315	316	317	318	319	320	321	322	323
WT Rho	N	K	Q	F	R	N	C	M	V	T	T	L	C	C
CTr1	N	K	Q	F	R	I	A	F	Q	E	L	L	C	C
CTr2	S	P	D	F	R	I	A	F	Q	E	L	L	C	C
CTr4	S	P	D	F	R	N	C	M	V	T	T	L	C	C
CysXV	N	K	Q	F	R	N	C	M	V	T	T	L	S	S

B

Peptide	Amino Acid Sequence
α (340-350)	I K E N L K D C G L F
α (340-350) K341R/L349A	I R E N L K D C G A F
γ (50-71)-far	E D P L V K G I P E D K N P F K E L K G G C -farnesyl
γ (60-71)	D K N P F K E L K G G C
γ (60-71)-far	D K N P F K E L K G G C -farnesyl
γ (60-71)-far F64A/L67A	D K N P A K E A K G G C -farnesyl

FIG. 4-1. Amino acid sequences of recombinant rhodopsins and G_t-derived peptides. **A**, Amino acid sequence of the loop C4 of wild-type rhodopsin (WT Rho) and mutant opsins (CTr1, CTr2, CTr4 and CysXV). In bovine rhodopsin, this region extends from position 310 at the intracellular junction of the TM helix 7 to Cys322 and Cys323, which are palmitoylated and inserted into the membrane. Changes from the wild-type sequence are highlighted in gray. In CTr1, CTr2 and CTr4, portions of the C4 loop have been replaced with analogous sequences from the β 2 AR. In CysXV, the palmitoylation sites are replaced by serine residues. These mutants represent a subset of those in Fig. 3-4. **B**, Amino acid sequences of peptides were derived from the carboxyl termini of bovine G α_t and G γ_t subunits. The α (340-350) peptide corresponds to the native sequence of G α_t , and the γ (50-71)-far corresponds to the native sequence of G γ_t , which is post-translationally modified by cysteinyl thioetherfarnesylation. Peptides with alterations of primary structure, or a lack of carboxyl-terminal farnesylation, were used as controls. The carboxyl termini of the G γ_t -derived peptides were amidated. The carboxyl termini of the G α_t -derived peptides, and the amino termini of all the peptides, were unmodified.

FIG. 4-2. Photoregeneration of rhodopsin in the presence of increasing concentrations of G_t or G_t -derived peptides. The presence of G_t , $\alpha(340-350)$, or $\gamma(50-71)$ -far causes a dose-dependent reduction in photoregeneration. Each trace shows a representative individual experiment and the time-dependent increase in absorbance at 543 nm. The photoregeneration signal is initiated by a flash at 50 ms. Fits to the slow phase of the signal are shown as dotted lines. Insets show the initial slope of the slow phase of photoregeneration versus added concentration of G_t or peptide as indicated. These plots were fit using a hyperbolic function with additive offset. IC_{50} values and errors are derived from the fits to the dose-response data and presented in the insets. **A**, Photoregeneration of rhodopsin in the presence of increasing concentrations of G_t ($IC_{50} = 2.56 \pm 2.0 \mu M$). **B**, Photoregeneration of rhodopsin in the presence of increasing concentrations of $\alpha(340-350)$ peptide ($IC_{50} = 49.5 \pm 6 \mu M$). **C**, Photoregeneration of rhodopsin in the presence of increasing concentrations of $\gamma(50-71)$ -far peptide ($IC_{50} = 285 \pm 74 \mu M$).



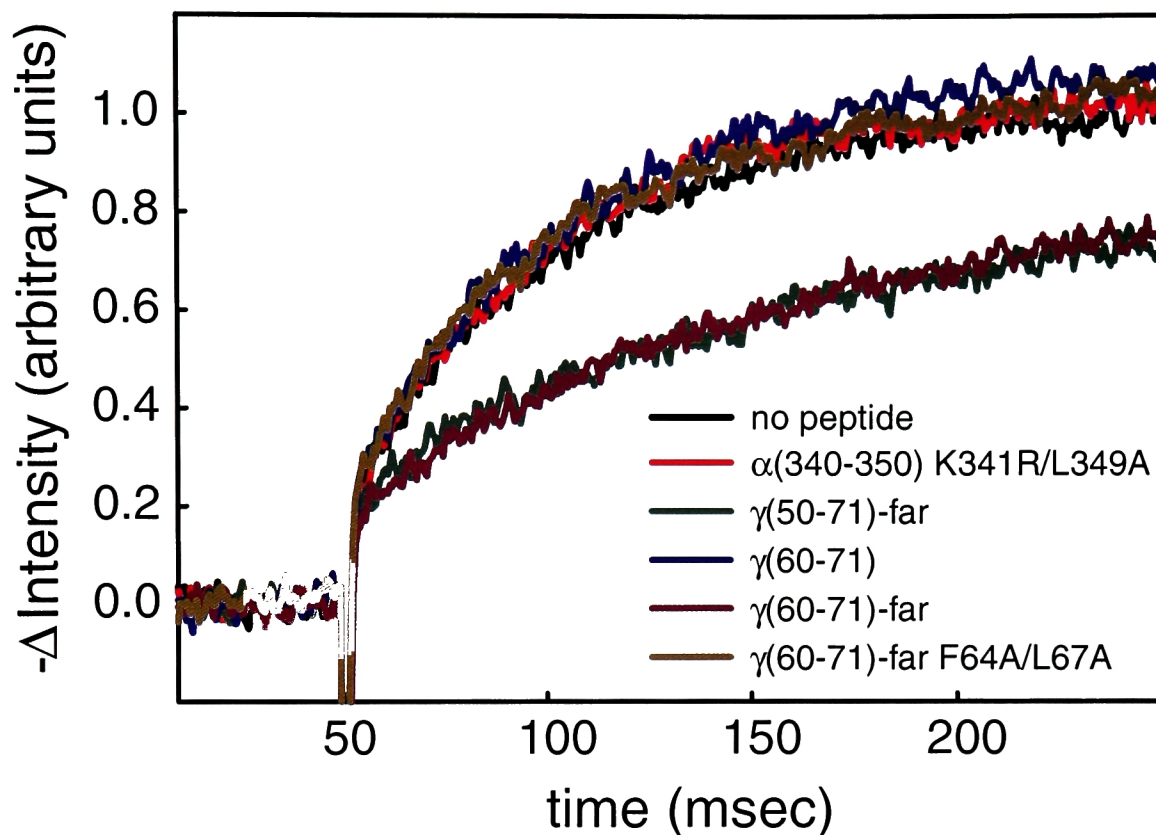


FIG. 4-3. Altered peptides do not inhibit photoregeneration. Photoregeneration experiments were performed as described in Fig. 4-2 in the presence of altered peptides (amino acid sequences are shown in Fig. 4-1). Concentrations were 200 μ M for the $G\alpha_t$ -derived peptides and 500 μ M for the $G\gamma_t$ -derived peptides. The inverse of intensity change at the detector in arbitrary units is plotted as a function of time. Data collected in the absence of peptide were normalized to a value of 1.0 at 250 ms; data collected in the presence of peptides were scaled to data collected with the same rhodopsin sample in the absence of peptide. An arbitrary unit is approximately 0.15 mOD units at 543 nm. Inhibition of photoregeneration is abolished by the conservative substitution of two amino acids in the $\alpha(340-350)$ or $\gamma(60-71)$ -far peptide, or by removal of the farnesyl moiety in the $\gamma(60-71)$ peptide. The longer $\gamma(50-71)$ -far peptide shows functional identity to $\gamma(60-71)$ -far.

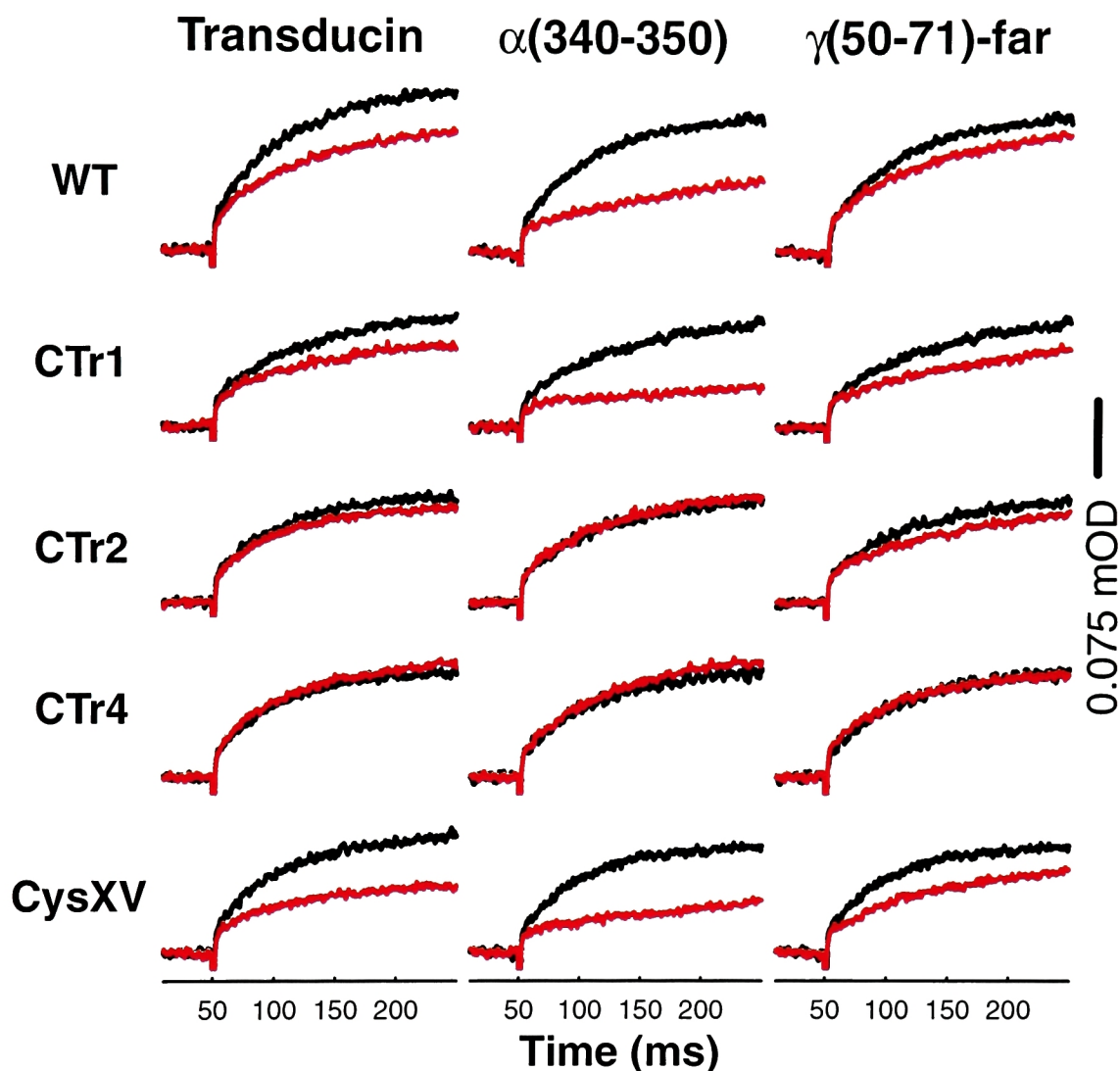
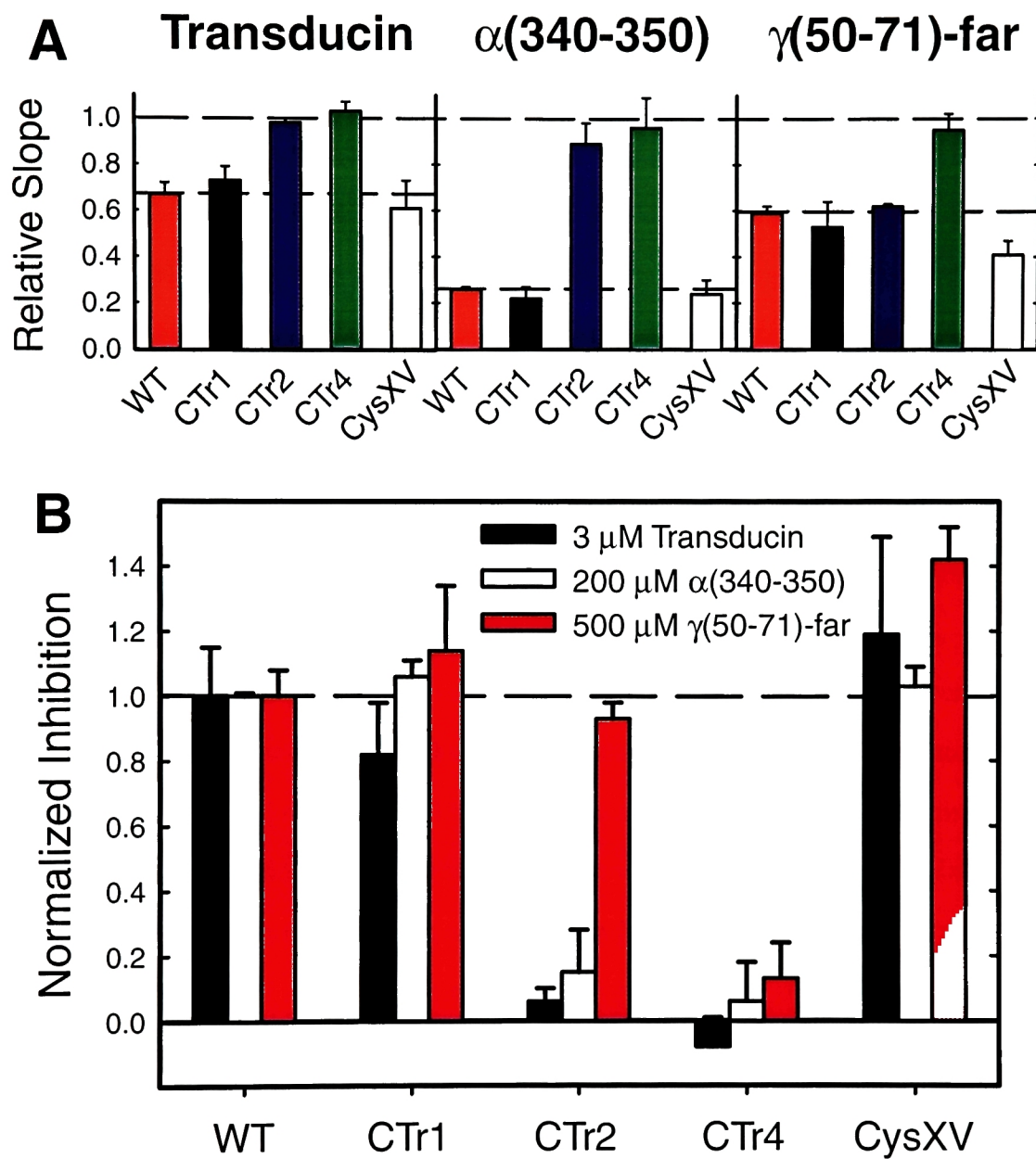


FIG. 4-4. The effect of G_t , $\alpha(340-350)$ and $\gamma(50-71)$ -far on photoregeneration of heterologously expressed rhodopsin and C4 loop mutants. Experiments were carried out as in Fig. 4-2. Concentrations of G_t , $\alpha(340-350)$ and $\gamma(50-71)$ -far were 3 μ M, 200 μ M and 500 μ M, respectively. The vertical scale bar, which depicts 0.075 mOD at 543 nm, applies to all traces. Black traces show photoregeneration of pigment alone. Red traces show photoregeneration of each pigment in the presence of G_t (Transducin), $\alpha(340-350)$ or $\gamma(50-71)$ -far as indicated at the top of each column of panels. The sample used in each row is indicated in the labels at left. Each pair of traces is representative of at least two sets of experiments performed on different samples. WT, CTr1, and CysXV, show distinct effects of G_t or G_t -derived peptides. Photoregeneration of CTr4 is not influenced by G_t or G_t -derived peptides, and CTr2 shows an effect with $\gamma(50-71)$ -far, a minor effect with G_t holoprotein and no effect with $\alpha(340-350)$.

FIG. 4-5. Quantitation of the effects of G_t , $\alpha(340-350)$, and $\gamma(50-71)$ -far on the photoregeneration of recombinant rhodopsin and rhodopsin mutants. The slow phases of the photoregeneration traces were fit with exponential-rise equations, and the initial slopes were determined. **A, Relative slopes.** Bars represent the average ratio of the initial slope of the slow phase of photoregeneration of pigment in the presence of G_t (Transducin), $\alpha(340-350)$ or $\gamma(50-71)$ -far to the initial slope with pigment alone. The error bars display the standard errors. The photoregeneration of mutants CTr2 and CTr4 is unaffected by G_t and $\alpha(340-350)$. Only mutant CTr4 photoregeneration is insensitive to $\gamma(50-71)$ -far. **B, Normalized inhibition.** The vertical bars indicate the ability of G_t and G_t -derived peptides to inhibit photoregeneration of mutant pigments relative to their effect on wild-type rhodopsin (WT). The normalized inhibition values were determined from the following equation: $(1 - \text{mean relative slope})_{\text{mutant}} / (1 - \text{mean relative slope})_{\text{rhodopsin}}$. The error bars depict the propagated standard errors from the determination of relative slope. Numerical values are given in Table 5-I. This analysis allows for direct comparison of the effects of each peptide and G_t on each mutant. The effect of G_t and G_t -derived peptides on CTr1 and CysXV are similar to their effect on rhodopsin. The photoregeneration of CTr4 does not show an effect of G_t or either G_t -derived peptide. This behavior is consistent with a failure of CTr4 to bind G_t , $\alpha(340-350)$ and $\gamma(50-71)$ -far. Replacement of the entire C4 loop in CTr2 shows a graded effect: CTr2 is essentially insensitive to inhibition by $\alpha(340-350)$ and G_t , but shows effects with $\gamma(50-71)$ -far nearly identical to those of wild-type rhodopsin.



Discussion

Several lines of evidence suggest that the conformation of the cytoplasmic surface of the active state of rhodopsin, R^* , is coupled to the conformation of the chromophore-binding pocket in the membrane-embedded domain of the receptor (Sakmar, 1998; Helmreich and Hofmann, 1996). In analogy to GPCRs with diffusible ligands in which G protein binding stabilizes a receptor conformation with a high affinity ligand binding site, MII is stabilized at the expense of its tautomeric forms by the binding of G_t or G_t -derived peptides. This stabilization of MII is the basis of the “extra-MII” assay (Emeis and Hofmann, 1981; Hamm *et al.*, 1988). This assay however, can only be applied under conditions of a dynamic equilibrium between metarhodopsin I and MII, which is exquisitely sensitive to membrane environment, pH, temperature, ionic strength, *etc.* Therefore, an assay was developed that measures the kinetics of photoconversion of MII to rhodopsin in detergent solution. The assay uses the fact that photoconversion of MII ($\lambda_{\max} = 380$ nm) to rhodopsin ($\lambda_{\max} = 500$ nm) following a blue actinic flash is inhibited if the MII molecule is bound to G_t (Arnis and Hofmann, 1995), or certain G_t -derived peptides (Kisselev *et al.*, 1999; Kisselev *et al.*, 1999) as a result of the coupling between the conformation of the cytoplasmic surface and that of the chromophore-binding pocket.

The initial step in photoregeneration, the photo-isomerization of the retinal to its *cis* conformation, may be compared to loading a spring that subsequently drives the protein, including its cytoplasmic domain, back to the ground state conformation (Arnis and Hofmann, 1995). The product formed in this initial step, termed “reverted meta (RM),” is characterized by a MII-like protein conformation and a *cis* retinal with a deprotonated Schiff base; it is spectrally indistinguishable from MII. RM rapidly converts to a rhodopsin-like species characterized by a rhodopsin-like protein conformation and a *cis*

retinal with a protonated Schiff base. The presence of G_t does not affect RM formation, indicating that the isomerization of the retinal itself is unaffected. However, bound G_t prevents RM from converting to rhodopsin, by stabilizing the MII-like conformation of RM. Dissociation of G_t from RM by GTP γ S treatment allows RM to revert to rhodopsin quantitatively (Arnis and Hofmann, 1995). The effects, and presumably the mechanism of action, of certain G_t -derived peptides on photoregeneration are similar to those of G_t itself (Kisselev *et al.*, 1999).

Photoregeneration is Sensitive to Interactions with G_t and Certain G_t -derived Peptides

G_t interacts with R^* to stabilize the active signaling state such that photoregeneration to rhodopsin is effectively blocked (Arnis and Hofmann, 1995). Recently, a peptide corresponding to the carboxyl terminus of $G_{\gamma t}$ and a peptide analogue related to the carboxyl terminus of $G_{\alpha t}$ were demonstrated to mimic the effect of G_t by inhibiting photoregeneration of R^* (Kisselev *et al.*, 1999). Here we showed that synthetic peptide $\alpha(340-350)$ could cause the same effect as G_t (Fig. 4-2). In addition, the effect of $\alpha(340-350)$ was specific to its primary structure since a mutant peptide had no effect (Fig. 4-3). Synthetic peptide $\gamma(50-71)$ -far also inhibited photoregeneration of R^* (Fig. 4-2). The effect was specific to its primary structure and to the presence of cysteinyl thioetherfarnesylation (Fig. 4-3). Using single peptides that represent small regions of G_t provides a powerful probe of subunit- and domain-specific interactions.

The potencies of the $\alpha(340-350)$ and $\gamma(50-71)$ -far peptides are about 20- and 100-fold less than that of G_t , respectively (Fig. 4-2). This finding is reasonable considering that the tertiary structure of a short peptide is less defined, so that a higher binding energy, and thus concentration, is needed for the “induced fit.” Also, the cytoplasmic surface domain of R^* comprises multiple interaction sites for G_t binding, including the loops C2 and C3 (König *et al.*, 1989; Franke *et al.*, 1990; Franke *et al.*, 1992). G_t also has at least two, and probably more, sites that interact with the receptor during binding and

activation. Peptide $\alpha(340-350)$ showed a clear inhibition of photoregeneration with an almost complete suppression at saturating concentrations (Fig. 4-2B). The peptide $\gamma(50-71)$ -far showed a lower efficacy to inhibit photoregeneration. Although the inhibitory effect saturated at high concentrations with a normal first-order-binding isotherm, there was not a complete suppression of the photoregeneration effect (Fig. 4-2C). The binding of $\gamma(50-71)$ -far to R^* is likely to be quite complex due to specificity which arises from both the farnesyl moiety and the peptide sequence (Fig. 4-3). The carboxyl-terminal region of $G_{\gamma t}$ was also studied using a MII difference spectroscopy assay with similar findings (Kisselev *et al.*, 1994; Kisselev *et al.*, 1995a).

The Role of a Conserved Region at the Amino Terminus of Loop C4 of Rhodopsin in G_t Binding

We used the photoregeneration assay to probe the effects of G_t and G_t -derived peptides on expressed rhodopsin and rhodopsin mutants. The rhodopsin loop C4 mutations did not significantly affect the signal transmission path itself, as is seen from the similar kinetics of the photoregeneration signals in the absence of G_t and G_t -derived peptides (Fig. 4-4). The results in Figs. 2 and 3 show that G_t , and peptides $\alpha(340-350)$ and $\gamma(50-71)$ -far are specific probes of rhodopsin signaling. Therefore, inhibition of photoregeneration by G_t or G_t -derived peptides is interpreted as the specific interaction of these reagents with the intracellular surface. A lack of inhibition due to alteration of either the peptide or the C4 loop is interpreted as a disruption of interaction. An advantage of the photoregeneration assay is that only productive binding interactions that stabilize specific conformations of the protein are reported.

In theory, a particular mutation might have the effect of uncoupling the conformation of the cytoplasmic surface from that of the chromophore-binding pocket. For example, an E134Q mutant has been shown to assume a partially activated conformation at the cytoplasmic surface while the chromophore and surrounding structures remain in the

dark, inactive conformation (Kim *et al.*, 1997). This type of mutant might give misleading results, as photoregeneration (monitored by structural rearrangements surrounding the chromophore) could proceed unhindered, even as G_t or peptides bound normally to the cytoplasmic surface. The rhodopsin loop C4 mutants showed no evidence of any uncoupling between the chromophore-binding pocket and cytoplasmic surface conformations. All of the mutants showed similar photoregeneration kinetics in the absence of peptide (Fig. 4-4, black traces). This suggests that the effects of the mutations are localized to the cytoplasmic surface, and do not affect the photoregeneration process itself. However, the mutant E134R/R135E photoregenerated with kinetics that were distinctly different from that of rhodopsin (data not shown), and therefore was not considered further in this study. Of course, mutants could exist that would foil all assays that rely on the detection of binding events at the intracellular surface resulting from conformational changes that are induced elsewhere in the protein. The extra-MII assay commonly used for rhodopsin, and the GTP-induced agonist affinity shift assay extensively used for other GPCRs have the same potential limitations and are much less sensitive and specific.

Taken together, the results in the preceding chapter and the biophysical analysis of selected rhodopsin mutants herein strongly suggest that the amino terminus of C4 plays an important role in G_t binding and activation. Both G_t and $\alpha(340-350)$ binding are disrupted when a tripeptide in this region is replaced by a sequence from the β_2 AR (Fig. 4-5). The most straightforward interpretation of the data is that the amino-terminal region of loop C4 directly influences or is part of a direct binding site for the carboxyl-terminal tail of $G\alpha_t$.

It is surprising that CTr4, in which residues 310-312 are replaced with analogous sequence from the β_2 AR, binds neither $\alpha(340-350)$ nor $\gamma(50-71)$ -far. Can the two peptides bind to overlapping sites on the receptor, each of which includes the 310-312

region? This seems unlikely, because the carboxyl termini of $G\alpha_t$ and $G\gamma_t$ are located at a significant distance apart from each other in the structure of the heterotrimer (Lambright *et al.*, 1996). Two potential explanations, which are not mutually exclusive, arise: 1) the peptides bind to different sites on the receptor and the sites are allosterically coupled; 2) G_t undergoes a large conformational change on contact with R^* to bring the carboxyl termini of $G\alpha_t$ and $G\gamma_t$ into close proximity with the interaction domain near residues 310-312. A conformational switch in G_t , induced by the contact with R^* may be identical to the switch in $G_t\beta\gamma$ that was suggested earlier (Kisselev *et al.*, 1995a).

Possible Role of $G\gamma_t$ -farnesyl in Docking of G_t to the Active Receptor

The relevance of the data to the binding site of $G\beta\gamma_t$ is more subtle. The observation that CTr2, but not CTr4, binds $\gamma(50-71)$ -far highlights the complexity of the binding interaction between $\gamma(50-71)$ -far and rhodopsin. Further evidence of this complexity, as noted above, is that $\gamma(50-71)$ -far fails to fully inhibit the photoregeneration reaction, even at saturating concentrations. This behavior contrasts with that of $\alpha(340-350)$ (Fig. 4-2). In addition, both the farnesyl moiety and the peptide itself are required for binding to R^* (Fig. 4-3). Each is likely to have a distinct binding site that may be differently altered in the mutants studied. The binding of $\gamma(50-71)$ -far to CTr2, but not CTr4, suggests that the structural integrity of the fourth loop is disrupted by substitution of 310-312 with β_2 AR sequence, but that the substitution of the entire loop restores the structural determinants required for $\gamma(50-71)$ -far binding. In this scenario, the tertiary, but not necessarily the primary structure of C4 would be critical for $\gamma(50-71)$ -far binding.

In summary, we developed a novel biophysical assay to probe the G_t -binding domain of rhodopsin and expressed rhodopsin. G_t and peptides corresponding to the carboxyl-terminal regions of $G\alpha_t$ and $G\gamma_t$ specifically bind to R^* and stabilize the active state of the receptor. We conclude that the amino-terminal region of loop C4 acts as part of the binding site for $G\alpha_t$ and modulates the G_t -binding domain of R^* . Future work is

Chapter 4: Photoregeneration Studies of Fourth Loop Mutants

required to reconcile the various models for allosteric regulation of the G_t -binding surface of R^* , especially concerning the binding of $G\beta\gamma_t$.

Chapter 5:

The Function of Interdomain Interactions in Controlling Nucleotide Exchange Rates in Transducin*

Summary

The intramolecular contacts in heterotrimeric G proteins that determine the rates of basal and receptor-stimulated nucleotide exchange are not fully understood. The α subunit of heterotrimeric G proteins consists of two domains: a Ras-like domain with structural homology to the monomeric G protein Ras and a helical domain comprised of six α -helices. The bound nucleotide lies in a deep cleft between the two domains. Exchange of the bound nucleotide may involve opening of this cleft. Thus interactions between the domains may affect the rate of nucleotide exchange in G proteins. We have tested this hypothesis in the α subunit of the rod cell G protein transducin ($G\alpha_t$). Site-directed mutations were prepared in a series of residues located at the interdomain interface. The proteins were expressed *in vitro* in a reticulocyte lysate system. The rates of basal and rhodopsin-catalyzed nucleotide exchange were determined using a trypsin digestion assay specifically adapted for kinetic measurements. Charge-altering substitutions of two residues at the interdomain interface, K273 and K276, increased basal nucleotide exchange rates modestly (5-10 fold). However, we found no evidence that interactions spanning the two domains in $G\alpha_t$ significantly affected either basal or rhodopsin-catalyzed nucleotide exchange rates. These results suggest that opening of the interdomain cleft is not an energetic barrier to nucleotide exchange in $G\alpha_t$. Experiments

*Material in this chapter has been published previously in: Marin E. P., Krishna, A. G., Archambault, V., Simuni, E., Fu, W.-Y., Sakmar, T.-P. (2001) The function of interdomain interactions in controlling nucleotide exchange rates in transducin. *J. Biol. Chem.* **276**:23873-23880.

Chapter 5: Interdomain Interactions in $G\alpha_t$

with $G\alpha_i1$, in conjunction with other published results, suggest that the organization and function of the interdomain region differ among various G protein subtypes.

Introduction

Physiologically, the detection of dim light requires that the basal nucleotide exchange rates of G_t be very low to reduce background noise, and that R^* -catalyzed exchange be very efficient, to ensure consistent detection and amplification of light signals. In the preceding two chapters, we characterized the function of C4 of R^* in binding and supporting rapid activation of G_t . In this chapter, we begin an analysis of the structures of G_t that normally function to maintain low nucleotide exchange rates but which might be perturbed by the binding of R^* to induce rapid nucleotide exchange.

$G\alpha_t$ consists of two domains: a Ras-like domain, which is structurally similar to the monomeric G protein $p21^{ras}$ (Ras), and a helical domain, which is unique to the heterotrimeric G proteins (Noel *et al.*, 1993). The bound nucleotide lies in a deep cleft between the two domains (Fig. 5-1). Although the discovery of this arrangement initially prompted speculation that nucleotide exchange would involve opening of the interdomain cleft (Noel *et al.*, 1993), and that interactions between the domains might affect the rate of nucleotide exchange, the intramolecular contacts in $G\alpha_t$ that determine the rates of nucleotide exchange remain to be elucidated.

There is evidence that structures that do not directly interact with the nucleotide can modulate both the basal and the receptor-catalyzed rates of nucleotide exchange. For example, although the direct contacts between the protein and the nucleotide are virtually the same in closely related subtypes of G protein, the rates of basal nucleotide exchange vary widely. Furthermore, R^* tremendously accelerates nucleotide exchange, yet available evidence indicates that it does not directly contact the nucleotide binding site (Iiri *et al.*, 1998).

One of the regions of the G protein hypothesized to control nucleotide release rates without directly contacting the nucleotide is the interdomain interface. The interface is composed of contacts adjacent to the nucleotide, and also interactions that are distant from the nucleotide (Fig. 5-1). These latter interactions involve residues located on the αD - αE loop (amino acid residues 139-147 of $G\alpha_t$) of the helical domain, and the Switch III region (residues 227-238) and the αG region (residues 269-277) of the Ras-like domain (Fig. 1B). These interactions have been implicated in mediating the lower rate of dissociation of GTP γ S relative to GDP in $G\alpha_{i1}$ (Mixon *et al.*, 1995), and in affecting the basal nucleotide exchange rates in $G\alpha_{i1}$ (Remmers *et al.*, 1999) and $G\alpha_s$ (Warner *et al.*, 1998; Warner and Weinstein, 1999). Additionally, studies in $G\alpha_s$ have suggested that interdomain interactions are involved in mediating rapid nucleotide exchange catalyzed by the β_2 adrenergic receptor (Marsh *et al.*, 1998; Grishina and Berlot, 1998).

We have studied the function of several residues of $G\alpha_t$ that are located at the interdomain interface but do not contact the nucleotide. A number of site-directed mutations of these residues were constructed. The well-documented difficulties in expressing and purifying recombinant $G\alpha_t$ were overcome by expressing the mutant proteins *in vitro* in a rabbit reticulocyte lysate system. The rates of basal and R*-catalyzed nucleotide exchange were measured using a trypsin digestion assay specifically adapted for kinetic measurements. Alteration of two conserved lysine residues, K273 and K276, increased the rate of spontaneous nucleotide exchange 5-10 fold. However, in contrast to what would be predicted based on published structural and biochemical studies, we found no evidence that interactions that span the domain interface were important in either maintaining the low rate of basal nucleotide exchange or in supporting the high rate of R*-catalyzed exchange in $G\alpha_t$. Experiments with $G\alpha_{i1}$ demonstrated that conserved lysine residues serve different roles in $G\alpha_{i1}$ than in $G\alpha_t$. In general, the function of the interdomain region appears to differ among various G protein subtypes.

Results

A series of site-directed mutants of $G\alpha_t$ with replacements of residues located at the interdomain interface was prepared. Sites were selected for mutation based on their position in the crystal structure of GDP-bound $G\alpha_t$ (Lambright *et al.*, 1994) (Fig. 1), as well as their importance in $G\alpha_{i1}$ and $G\alpha_s$ suggested by published studies (see below). Selected residues were replaced with alanine, or with the amino acid present in the homologous position of either $G\alpha_{i1}$ or $G\alpha_s$, and/or with amino acids reported to cause altered phenotypes in $G\alpha_{i1}$ or $G\alpha_s$. For each mutant $G\alpha_t$, the rates of both basal (i.e., uncatalyzed) and R^* -catalyzed nucleotide exchange were measured.

Expression of $G\alpha_t$ in vitro and Trypsin Digestion Assay of Nucleotide Binding and Exchange

All $G\alpha_t$ constructs were expressed *in vitro* in a coupled transcription/translation rabbit reticulocyte lysate system. Time-course experiments confirmed that *in vitro* expression was maximal in 90 min (not shown). Typical reactions with plasmids encoding $G\alpha_t$ or $G\alpha_t$ mutant genes yielded one major protein band at the expected molecular mass of ~40-kDa (Fig. 5-2). Generally 80-90% of the total intensity in the lane was in the one band. Expressed $G\alpha_t$ was digested with trypsin following various treatments. Inactive, GDP-bound $G\alpha_t$ was prepared by incubating *in vitro* translated $G\alpha_t$ with 100 μ M GDP. Trypsin proteolysis of this sample resulted primarily in the formation of a ~23 kDa fragment (Fig. 5-2). The active conformation was prepared by incubating $G\alpha_t$ with GDP and AlF_4^- . AlF_4^- is known to bind to $G\alpha_t$ -GDP and simulate the presence of the γ phosphate of GTP. Therefore, a conformation nearly identical to the activated GTP-bound conformation is induced (Sondek *et al.*, 1994). Digestion of the AlF_4^- -activated $G\alpha_t$ yielded a ~34-kDa band and no ~23-kDa band. Similarly, activation of

$G\alpha_t$ with GTP γ S yielded an identical ~34-kDa band following trypsin digestion (Fig. 5-2).

In all cases, trypsin proteolysis produced a variety of lower molecular weight fragments. Some of these were the smaller polypeptides that were cleaved to produce the ~23- and ~34-kDa fragments. Others likely resulted from extensive proteolysis of protein that was not properly folded. This is consistent with the large number of potential trypsin sites present in the primary structure of $G\alpha_t$ and the relatively small number of accessible sites in the properly folded tertiary structure. The fraction of the total pool of translated $G\alpha_t$ that was properly folded and functional was estimated from the ratio of the intensities of the ~34-kDa band following GDP/AlF₄ treatment (*i.e.*, the properly folded, activatable pool) to that of the ~40-kDa band in the undigested sample (*i.e.*, the total pool of translated full-length protein). This ratio was generally about 0.15 for wild-type $G\alpha_t$ and several-fold higher for $G\alpha_{i1}$. This result parallels the functional expression levels of $G\alpha_t$ and $G\alpha_{i1}$ that have been observed in other heterologous expression systems. Thus, *in vitro* expression might serve as a rapid and useful predictor of the expression level of a given G protein construct in other systems.

The rate of trypsin proteolysis of GDP- and GDP/AlF₄-treated $G\alpha_t$ and the stabilities of the resulting fragments were investigated by digestion time-course experiments. Both the ~23- and ~34-kDa bands formed completely by 20 min and remained stable until at least 40 min in the presence of trypsin (data not shown). We therefore chose to stop the digestion after 30 min in all experiments. Similar experiments with $G\alpha_{i1}$ indicated that digestion occurred more quickly. Accordingly, digests were run for 5 min with $G\alpha_{i1}$ samples.

Three major sites of trypsin proteolysis in properly folded $G\alpha_t$ have been identified: K18, R204, and R310 (Mazzoni *et al.*, 1991). Using site-directed mutagenesis, we

investigated which of these sites were contributing to the fragments produced under the digestion conditions used in this study. The mutants K18A, R204H, and R310A were prepared, expressed *in vitro*, and digested following treatment with either GDP or GDP/ AlF_4^- .

Formation of the ~23-kDa band following treatment with GDP was altered only by the R204H mutation (not shown). R204 is the site at which cleavage occurred in the GDP form to yield the ~23-kDa fragment, but which was protected from digestion in the GTP γ S-bound conformation. R204 is located in the Switch II region of $G\alpha_t$ and crystal structures confirm that it moves from a surface exposed to a more buried position upon activation (Noel *et al.*, 1993; Lambright *et al.*, 1994). Formation of the ~34-kDa band following activation with GDP/ AlF_4^- was affected only by the R310A mutation (not shown). Thus R310 appears to be the site at which trypsin proteolysis occurred to yield the ~34-kDa fragment. The K18A mutant was indistinguishable from wild-type; digestion at K18 does not appear to contribute to the formation of either fragment under the conditions used (not shown). Using these results, the ratio of the number of methionines in the ~34-kDa band relative to the ~23-kDa band was determined to be 1.4. This factor was used to normalize the intensity of the ~23-kDa band in calculating the fraction of activated $G\alpha_t$ in each aliquot.

The fraction of $G\alpha_t$ in the active conformation in a partially activated sample was calculated as the intensity of the ~34-kDa band (*i.e.*, the activated $G\alpha_t$) divided by the sum of the intensities of the ~23- and ~34-kDa bands. The sum of the intensities of the ~23- and ~34-kDa bands is indicative of the total pool of functional $G\alpha_t$ in the sample. This calculation is therefore internally normalized to the total amount of functional $G\alpha_t$ in each aliquot and does not require comparison with the ~34-kDa band of a separate sample (such as one in a completely activated lane).

The rate of nucleotide exchange of each sample was determined by monitoring the fraction of $G\alpha_t$ in the active conformation at specific times following addition of $GTP\gamma S$. In the basal exchange rate assay, $G\alpha_t$ was 31% activated at 6 h following $GTP\gamma S$ addition (Fig. 5-2A). The activity of $G\alpha_t$ following the 6 h incubation was confirmed by demonstrating that addition of rhodopsin and $G\beta\gamma_t$ could fully activate the remaining $G\alpha_t$ (Fig. 5-2). In comparison, $G\alpha_t$ A322S (a mutant known to display high nucleotide exchange rates in $G\alpha_i1$ (Posner *et al.*, 1998) and $G\alpha_s$ (Iiri *et al.*, 1994)) was 100% activated in less than 1 h.

In R^* -catalyzed assays, $G\alpha_t$ was nearly 100% activated in 20 min (Fig. 5-2B). Under the conditions of the assay, the rate of $G\alpha_t$ activation was found to be dependent on the concentration of rhodopsin from 0-100 nM and sensitive to the presence of added $G\beta\gamma_t$ (Fig. 5-3B). Some residual activation was observed in the absence of added $G\beta\gamma_t$, probably as a result of small quantities of $G\beta\gamma$ present in the reticulocyte lysate or the rhodopsin preparations. No rhodopsin-catalyzed activation was observed in the dark (data not shown). Additionally, mutant G348P, which was previously reported to be unable to bind rhodopsin (Osawa and Weiss, 1995), was not activated by R^* in this assay (Fig. 5-3B). To our knowledge, this is the first report in which trypsin proteolysis of *in vitro* translated $G\alpha_t$ has been used to measure the kinetics of R^* -catalyzed nucleotide exchange.

Analysis of Single Amino Acid Replacements in the Interdomain Interface of $G\alpha_t$

Two residues in the helical domain, S140 and Q143, extend toward and interact with residues from the Ras-like domain. S140 was replaced with alanine, arginine (the homologous residue in $G\alpha_i1$), and asparagine (the homologous residue in $G\alpha_s$). Q143 was mutated to alanine and was also combined with S140A in a S140A/Q143A double mutant. None of these mutations substantially altered the rate of basal or R^* -catalyzed nucleotide exchange (Fig. 5-4, Table 5-I).

Several residues in the Switch III region of $G\alpha_t$ were altered by site-directed mutagenesis. The crystal structure suggests that D227 participates in hydrogen bonds with both S140 and K276 (Fig. 1). This residue was replaced with both asparagine (the homologous residue in $G\alpha_s$) and with alanine. The adjacent M228 was replaced with alanine, leucine (the equivalent in $G\alpha_{i1}$), and glutamine (the equivalent of a mutation in $G\alpha_{i1}$ reported to increase the GDP release rate (Remmers *et al.*, 1999)). V231 was replaced with alanine and with tryptophan. The V231W mutant was prepared to simulate a naturally occurring mutation in the homologous residue of $G\alpha_s$, R258, which was found in a patient with Albright's hereditary osteodystrophy (Warner *et al.*, 1998). None of these mutations was found to substantially alter either the basal or the R^* -catalyzed activation rates (Fig. 5-5, 5-6 and Table 5-I). However, several mutations caused slight (~2 fold), but reproducible reductions in the basal nucleotide exchange rate. These mutations include D227A, D227N, V231A and M228L (Table 5-I).

Three lysine residues in the αG region of $G\alpha_t$ were studied. K273 and K276 are oriented toward D227 of Switch III (Fig. 1). In addition, the crystal structure of $G\alpha_t$ -GDP indicates that K276 forms hydrogen bonds with S140 of the helical domain. K275 extends out toward the solvent. K273, K275, and K276 were each replaced with alanine. In addition, K276 was replaced with glutamic acid and with arginine. The K273A, K276A, and K276E mutations all resulted in significantly increased rates of basal nucleotide exchange, from 5- to 10-fold above wild-type (Fig. 5-7A). The K276R mutation did not affect nucleotide exchange rates, nor did mutation of K275. None of the mutations substantially altered the rate of R^* -catalyzed nucleotide exchange (Fig. 5-7B).

Analysis of Double Amino Acid Replacements

In order to probe for functional interactions between pairs of residues, a series of double amino acid replacements was prepared by site directed mutagenesis (Table 5-I).

The K276A/D227N, K276A/D227A, and K273A/D227N double replacements all displayed slower basal rates of nucleotide exchange than the corresponding single replacements of K276 or K273 (Fig. 5-8). The double mutants displayed faster exchange kinetics than wild-type $G\alpha_t$, however. Combining amino acid replacements at positions K276 and S140 revealed that the effects on basal exchange rates of each individual mutation were roughly additive (Fig. 5-8). A combination of amino acid replacements at positions 140 and 227, S140A/D227N had similar exchange kinetics to that of wild-type $G\alpha_t$ (Table 5-I).

Analysis of $G\alpha_{i1}$ Mutants

$G\alpha_{i1}$ is 66% identical to $G\alpha_t$ at the primary structure level and very similar at the tertiary structure level (Fig. 5-10). However, the basal nucleotide exchange rate of $G\alpha_{i1}$ has been reported to be significantly higher than that of $G\alpha_t$ (Skiba *et al.*, 1996). We confirmed this observation in studies with recombinant $G\alpha_{i1}$ and retinal $G\alpha_t$ in a fluorescence activation assay (Fig. 5A). The rate of basal nucleotide exchange as monitored by increases in fluorescence was much greater in $G\alpha_{i1}$ than in $G\alpha_t$ at 25°C. However, the rate and the magnitude of fluorescence change was comparable when each protein was fully activated with excess AlF_4^- .

$G\alpha_{i1}$ was expressed *in vitro* and studied by trypsin digestion. SDS-PAGE analysis indicated that a ~38-kDa band was produced following full activation with either GTP γ S or GDP/ AlF_4^- , and that a smaller fragment resulted from digestion in the presence of GDP. The intensity of the smaller GDP-dependent band of $G\alpha_{i1}$ could not be accurately quantitated due to reproducible nonspecific background in that portion of the gel. Therefore, the method for determining the fraction of *in vitro* translated $G\alpha_{i1}$ activated in an aliquot was modified from the "ratio" method used for $G\alpha_t$. In each aliquot, the intensity of the ~38-kDa band was determined as a fraction of the total

intensity in the lane and the time course of activation was plotted as a change in this fraction over time (Fig. 5B). This analysis suggests that basal nucleotide exchange of GDP for GTP γ S by $G\alpha_{i1}$ was complete in 1 h, significantly faster than that by $G\alpha_t$, which was only 32% complete in 6 h. The $t_{1/2}$ for activation of $G\alpha_{i1}$ (~20 min) was comparable in both the fluorescence and the trypsin protection assays (Fig. 5-9).

A series of site-directed mutants was prepared in $G\alpha_{i1}$ to probe for similarities between the functions of interdomain residues in $G\alpha_{i1}$ and $G\alpha_t$. The equivalent of K273 and K276 of $G\alpha_t$ are conserved in $G\alpha_{i1}$ as K277 and K280, respectively (Fig. 5-10). Both were replaced with alanine, expressed *in vitro*, and the basal nucleotide exchange rates of the resulting mutants were determined. Neither of these mutations (K277A and K280A) increased the basal activation rate of $G\alpha_{i1}$ appreciably (Fig. 5-9B). Additionally R144 of $G\alpha_{i1}$, the homolog of S140 in $G\alpha_t$, was replaced with serine. Since the S140 of $G\alpha_t$ forms hydrogen bonds with K276, it was hypothesized that in $G\alpha_{i1}$ the replacement of R144 with serine might alter the position of K280 (K276 in $G\alpha_t$) to resemble the $G\alpha_t$ conformation and lower the basal rate of nucleotide exchange. However, the opposite was observed. The $G\alpha_{i1}$ R144S mutant exhibited accelerated nucleotide exchange rates (Fig. 5-9B), consistent with previous reports of mutagenesis at the R144 position (Remmers *et al.*, 1999).

Table 5-I. Rate constants for basal nucleotide exchange measured for G α_t and G α_t mutants.

<u>Arranged by Amino Acid Position</u>			<u>Arranged by Basal Exchange Rate</u>		
<u>Mutant</u>	<u>k_{app}^a</u>	<u>fold inc.^b</u>	<u>Mutant</u>	<u>k_{app}^a</u>	<u>fold inc.^b</u>
wild-type	8.6 ± 0.7	1.0 ± 0.1	D227N	3.4 ± 0.6	0.4 ± 0.1
S140A	14.7 ± 4.6	1.7 ± 0.6	M228L	4.0 ± 0.4	0.5 ± 0.1
S140N	7.8 ± 2.1	0.9 ± 0.3	V231A	4.6 ± 0.6	0.5 ± 0.1
S140R	12.1 ± 2.6	1.4 ± 0.3	D227A	5.0 ± 1.1	0.6 ± 1.1
Q143A	6.1 ± 1.4	0.7 ± 0.2	Q143A	6.1 ± 1.4	0.7 ± 0.2
D227A	5.0 ± 1.1	0.6 ± 1.1	M228Q	6.2 ± 0.6	0.7 ± 0.1
D227N	3.4 ± 0.6	0.4 ± 0.1	V231W	6.4 ± 1.1	0.7 ± 0.1
M228A	14.6 ± 0.7	1.7 ± 0.2	S140A/D227N	7.4 ± 0.7	0.9 ± 0.1
M228L	4.0 ± 0.4	0.5 ± 0.1	S140N	7.8 ± 2.1	0.9 ± 0.3
M228Q	6.2 ± 0.6	0.7 ± 0.1	wild-type	8.6 ± 0.7	1.0 ± 0.1
V231A	4.6 ± 0.6	0.5 ± 0.1	K276R	8.8 ± 2.5	1.0 ± 0.3
V231W	6.4 ± 1.1	0.7 ± 0.1	S140A/Q143A	10.4 ± 4.7	1.2 ± 0.6
K273A	39.0 ± 22.6	4.6 ± 2.7	K275A	12.0 ± 1.4	1.4 ± 0.2
K275A	12.0 ± 1.4	1.4 ± 0.2	S140R	12.1 ± 2.6	1.4 ± 0.3
K276A	45.1 ± 7.5	5.3 ± 1.0	D227N/K273A	14.5 ± 2.7	1.7 ± 0.3
K276E	98.8 ± 29.1	11.5 ± 3.5	M228A	14.6 ± 0.7	1.7 ± 0.2
K276R	8.8 ± 2.5	1.0 ± 0.3	S140A	14.7 ± 4.6	1.7 ± 0.6
S140A/Q143A	10.4 ± 4.7	1.2 ± 0.6	D227A/K276A	14.8 ± 7.3	1.7 ± 0.9
S140A/K276A	67.3 ± 14.0	7.9 ± 1.8	D227N/K276A	20.3 ± 4.7	2.4 ± 0.6
S140A/D227N	7.4 ± 0.7	0.9 ± 0.1	K273A	39.0 ± 22.6	4.6 ± 2.7
S140R/K276A	48.0 ± 14.6	5.6 ± 1.8	K276A	45.1 ± 7.5	5.3 ± 1.0
D227A/K276A	14.8 ± 7.3	1.7 ± 0.9	S140R/K276A	48.0 ± 14.6	5.6 ± 1.8
D227N/K273A	14.5 ± 2.7	1.7 ± 0.3	S140A/K276A	67.3 ± 14.0	7.9 ± 1.8
D227N/K276A	20.3 ± 4.7	2.4 ± 0.6	K276E	98.8 ± 29.1	11.5 ± 3.5

^aThe apparent rate constants were derived from fits of each data set to the exponential rise equation, $y = c + 100(1 - \exp(-kt))$. Each mutant was assayed at least 3 times (WT G α_t was assayed 26 times), and an independent fit was made to each data set. The values reported are the mean $k_{app} \cdot 10^4 \text{ min}^{-1} \pm 2 \cdot \text{S.E.M.}$ The catalyzed activation rate of wild-type G α_t was determined to be 5390 ± 802 in the presence of 30nM photoactivated rhodopsin, 30nM G $\beta\gamma_t$, and 14 μM GTP γS . This is a 629 ± 107 fold increase over the basal (uncatalyzed) rate.

^bThe fold increase in the rate of the mutant relative to that of wild-type is calculated at the $k_{app}(\text{mutant})/k_{app}(\text{wild-type})$.

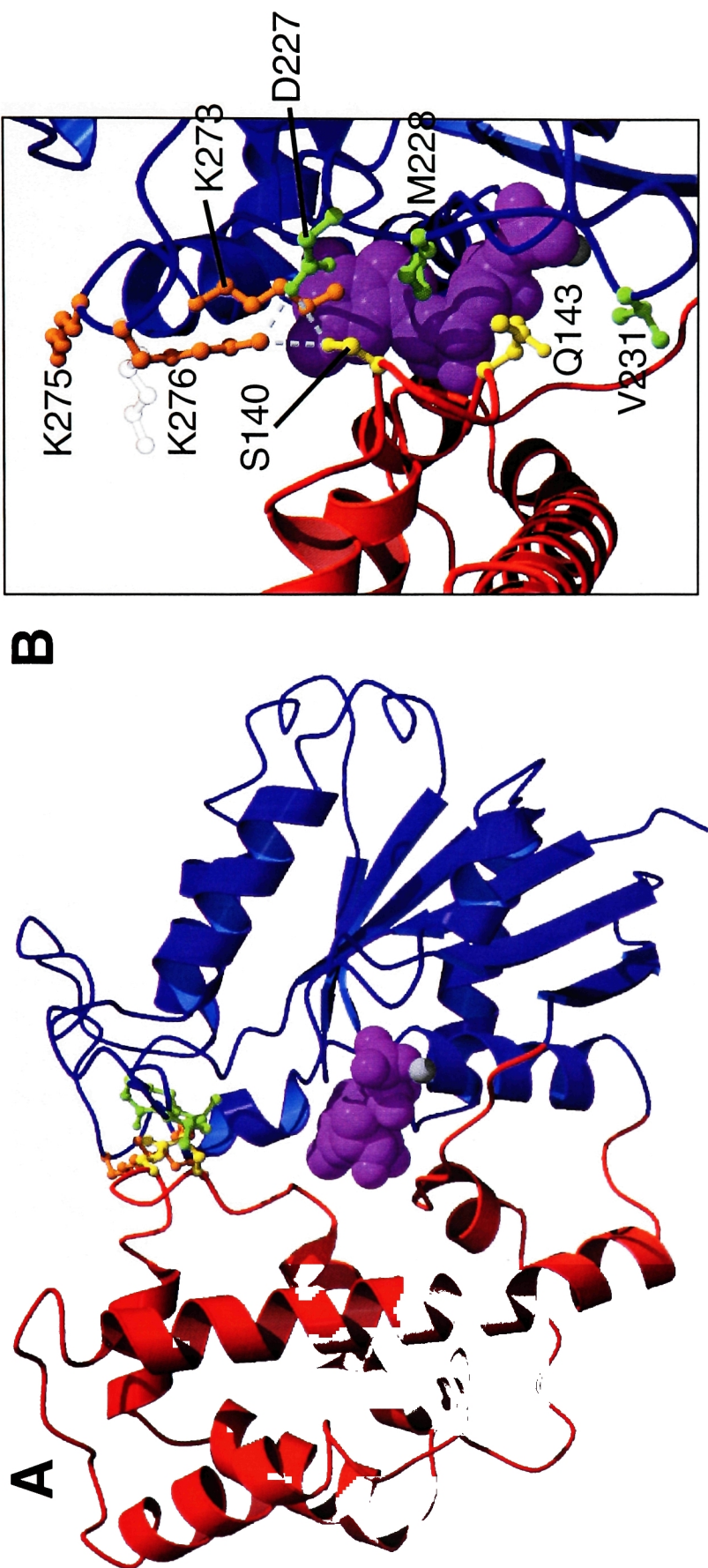


FIG. 5-1. Structure of the interdomain interface of GDP-bound $G\alpha_t$. The Ras-like domain is blue, the helical domain (Insert 1) is red, and the GDP is magenta. Sidechains of residues which have been mutated in this study are shown in ball-and-stick representation. Sidechains of residues in the helical domain are yellow, those from Switch III are green, and those from the αG region are orange. **A**, Overall view of the protein. The nucleotide resides in a cleft between the two domains. The highlighted sidechains potentially interact with each other across the interdomain interface, but do not directly contact the nucleotide. **B**, The protein has been rotated 90° about the horizontal axis relative to panel A and the interdomain region is enlarged. Hydrogen bonds are shown as dotted lines. The position of K276 in the GTP γ S-bound $G\alpha_t$ structure is shown as an outline.

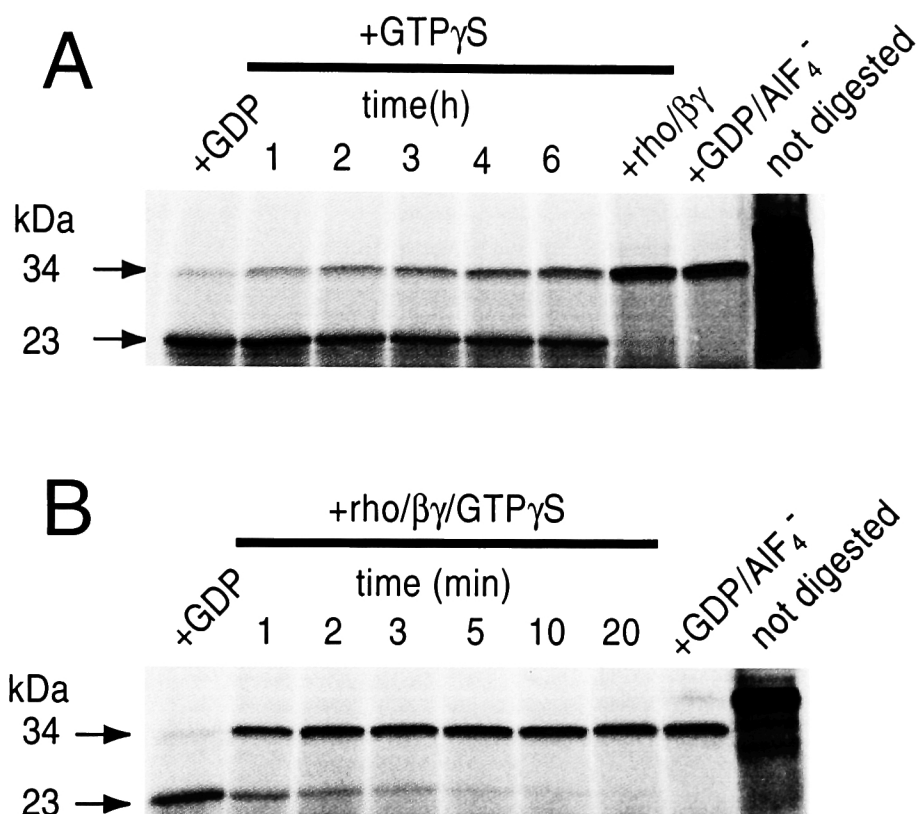


FIG. 5-2. Determination of nucleotide exchange rates by analysis of trypsin digestion patterns. $G\alpha_t$ was expressed *in vitro* in a rabbit reticulocyte lysate system and metabolically labeled with [^{35}S]methionine. Translated material was treated with various conditions as indicated. Aliquots (8 μ l) were removed and digested with trypsin for 30 min on ice, except where indicated otherwise. The resulting fragments were analyzed by SDS-PAGE, and visualized by phosphorimaging. **A.** Uncatalyzed activation. Translated $G\alpha_t$ was mixed with 100 μ M GTP γ S. Aliquots were removed and digested at 1, 2, 3, 4, and 6 h. Following collection of the 6 h aliquot, photoactivated rhodopsin and $G\beta\gamma_t$ were added to a final concentration of 30 nM each. After a 20 min incubation, an aliquot was removed and digested ("rho/ $\beta\gamma$ "). Control reactions show undigested $G\alpha_t$ and $G\alpha_t$ digested following incubation with 100 μ M GDP or GDP/ AlF_4^- . **B.** Rhodopsin/ $G\beta\gamma_t$ -catalyzed activation. Translated $G\alpha_t$ was mixed with 30 nM photoactivated rhodopsin, 30 nM $G\beta\gamma_t$, and 14 μ M GTP γ S. Aliquots were removed and digested at 1, 2, 3, 5, 10, and 20 min. Controls reactions were performed as in panel A.

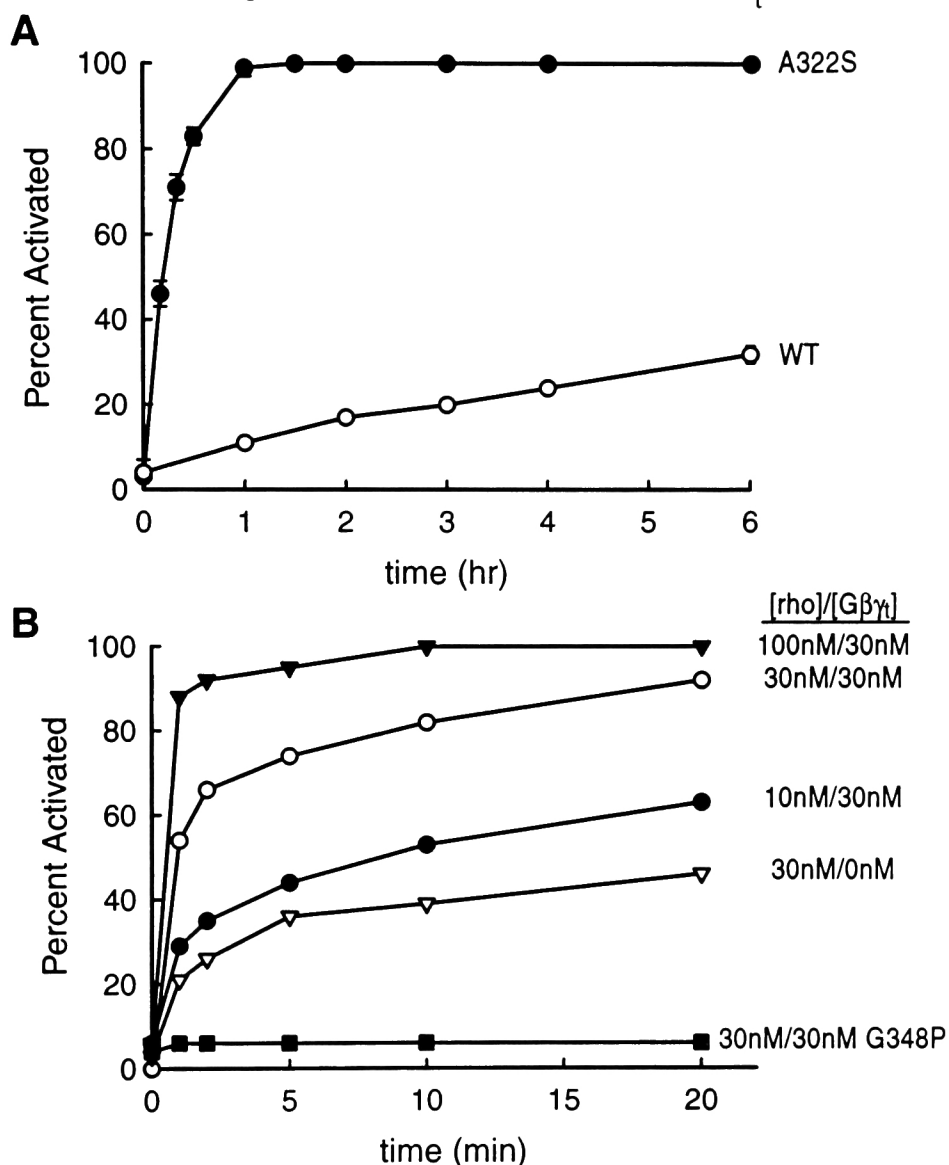


FIG. 5-3. Plots of uncatalyzed and catalyzed nucleotide exchange time courses derived from analysis of trypsin digest patterns of *in vitro* translated $G\alpha_t$. The percent of $G\alpha_t$ activated at each time point is determined as the ratio of the intensity of the ~34 kDa band to the sum of the intensities of the ~34 and ~23 kDa bands. **A.** Uncatalyzed activation time course. The rates of wild-type and the mutant A322S were determined. The results are similar to previously published data determined with other methods (see text). The data points depict the mean of 26 (wild-type) or 3 (A322S) individual determinations; error bars depict $2 \times \text{SEM}$. **B.** Rhodopsin-catalyzed activation time course. The rate of rhodopsin-catalyzed activation of *in vitro*-translated $G\alpha_t$ was determined in the presence of different concentrations of rhodopsin and $G\beta\gamma_t$. A mutant of $G\alpha_t$, G348P, which was previously reported to be resistant to rhodopsin, is not activated in this assay. Data shown are representative of an experiment repeated twice.

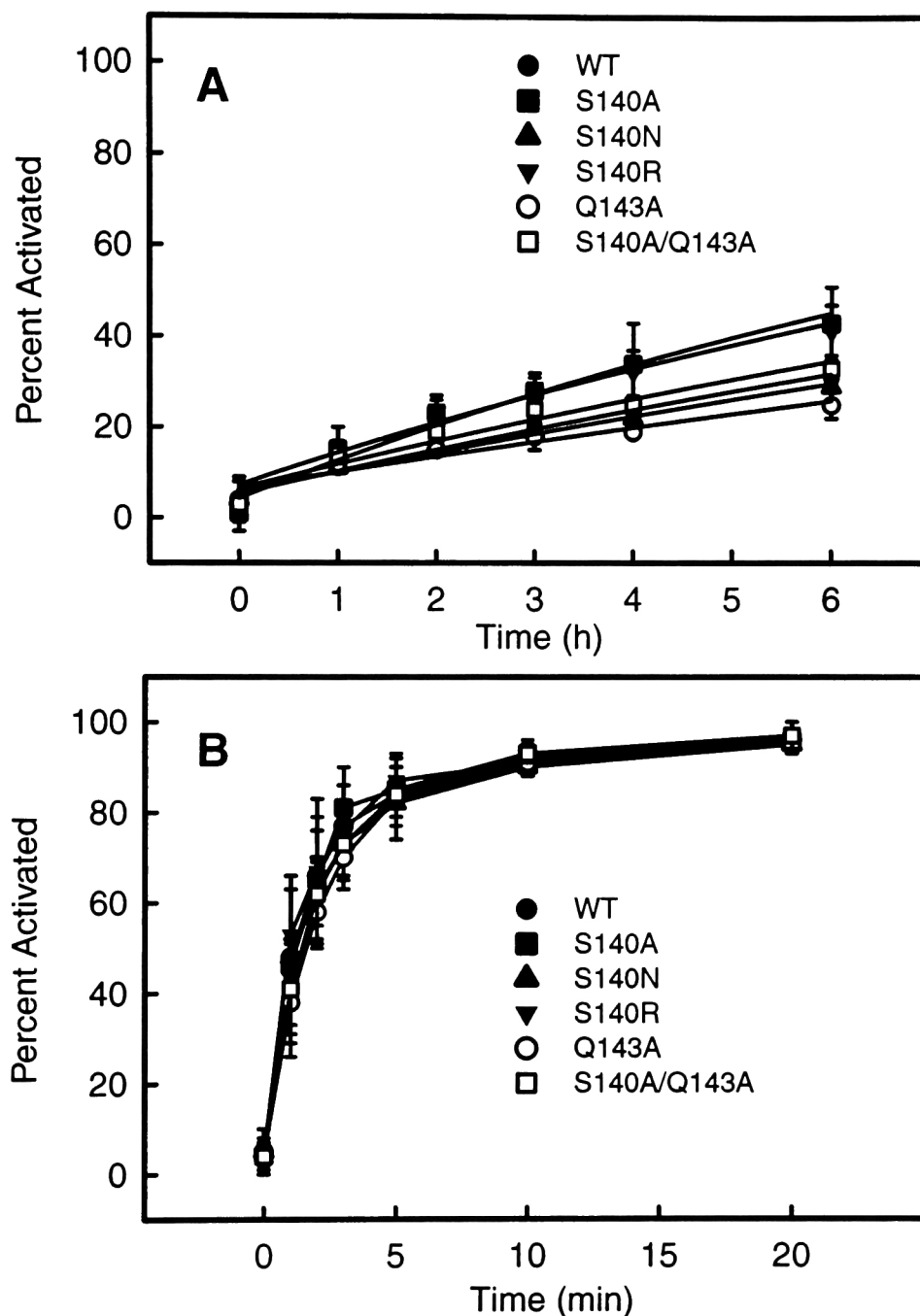


FIG. 5-4. Time courses of activation of mutants of residues located on the helical domain. The percent activation at each time point was determined by analysis of trypsin digestion patterns. The time-zero data point is calculated from protein mixed with 100 μ M GDP for 10 min. Each data point is the average of 3-5 independent experiments. Error bars depict $\pm 2 \times \text{SEM}$. **A**, Uncatalyzed activation. $G\alpha_t$ and mutants were translated *in vitro* and combined with 100 μ M GTP γ S. The solid lines represent fits to one-component exponential rise function. **B**, Rhodopsin/ $G\beta\gamma_t$ -catalyzed activation. $G\alpha_t$ and mutants were translated *in vitro* and combined with 30 nM $G\beta\gamma_t$, 30 nM photoactivated rhodopsin, and 14 μ M GTP γ S.

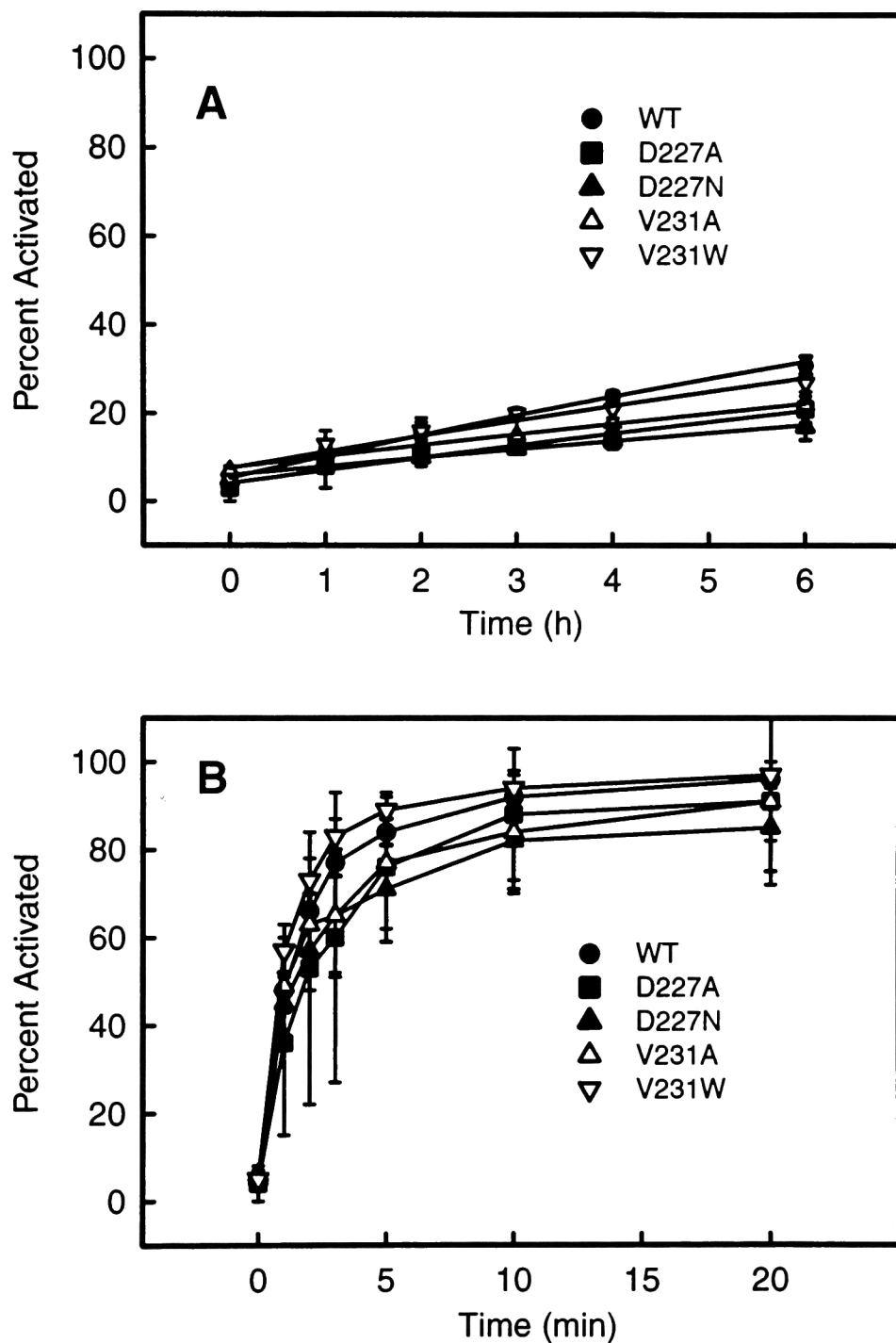


FIG. 5-5. Time courses of activation of mutants of residues located on Switch III (a.k.a. Insert 2). The experiments were performed as in Fig. 5-4. **A.** Uncatalyzed activation. **B.** Rhodopsin/ $G\beta\gamma_t$ -catalyzed activation.

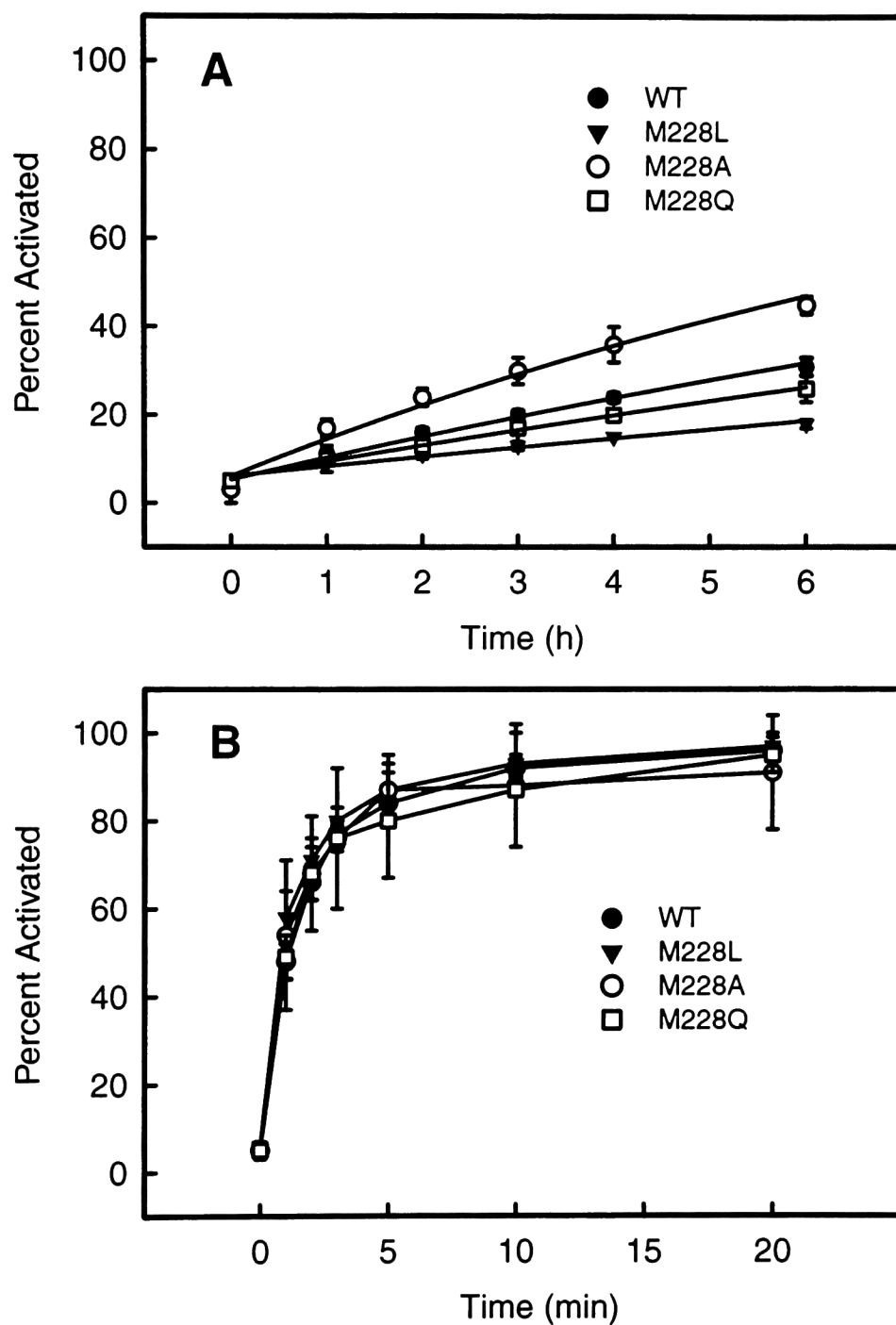


FIG 5-6. Time courses of activation of mutants of residue 228 located on Switch III (a.k.a. Insert 2). The experiments were performed as in Fig. 5-4. **A**, Uncatalyzed activation. **B**, Rhodopsin/ $G\beta\gamma_t$ -catalyzed activation.

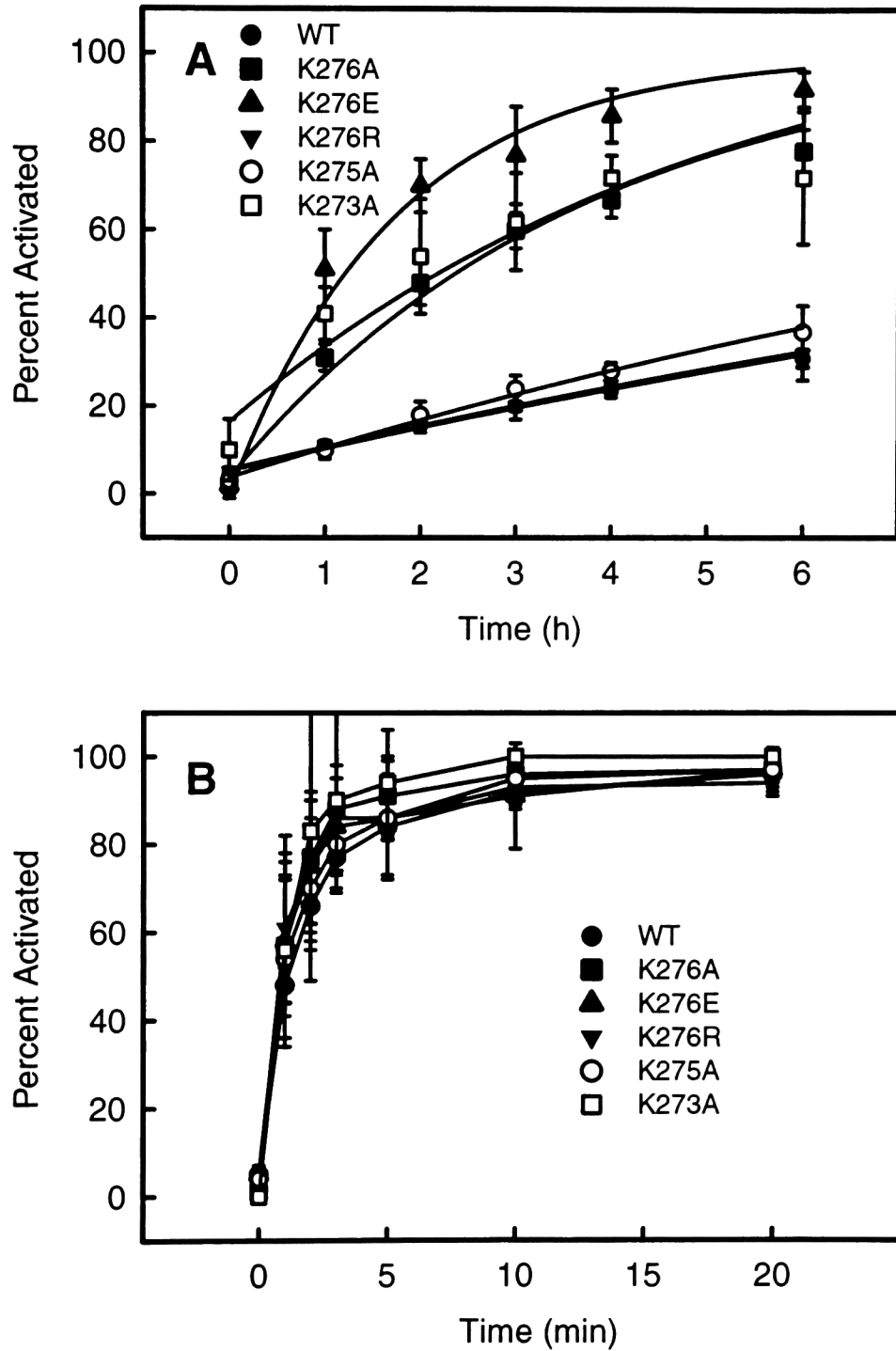


FIG. 5-7. Time courses of activation of mutants of residues located on the αG region (a.k.a., Insert 3). The experiments were performed as in Fig. 5-4. **A**, Uncatalyzed activation. **B**, Rhodopsin/ $G\beta\gamma_t$ -catalyzed activation.

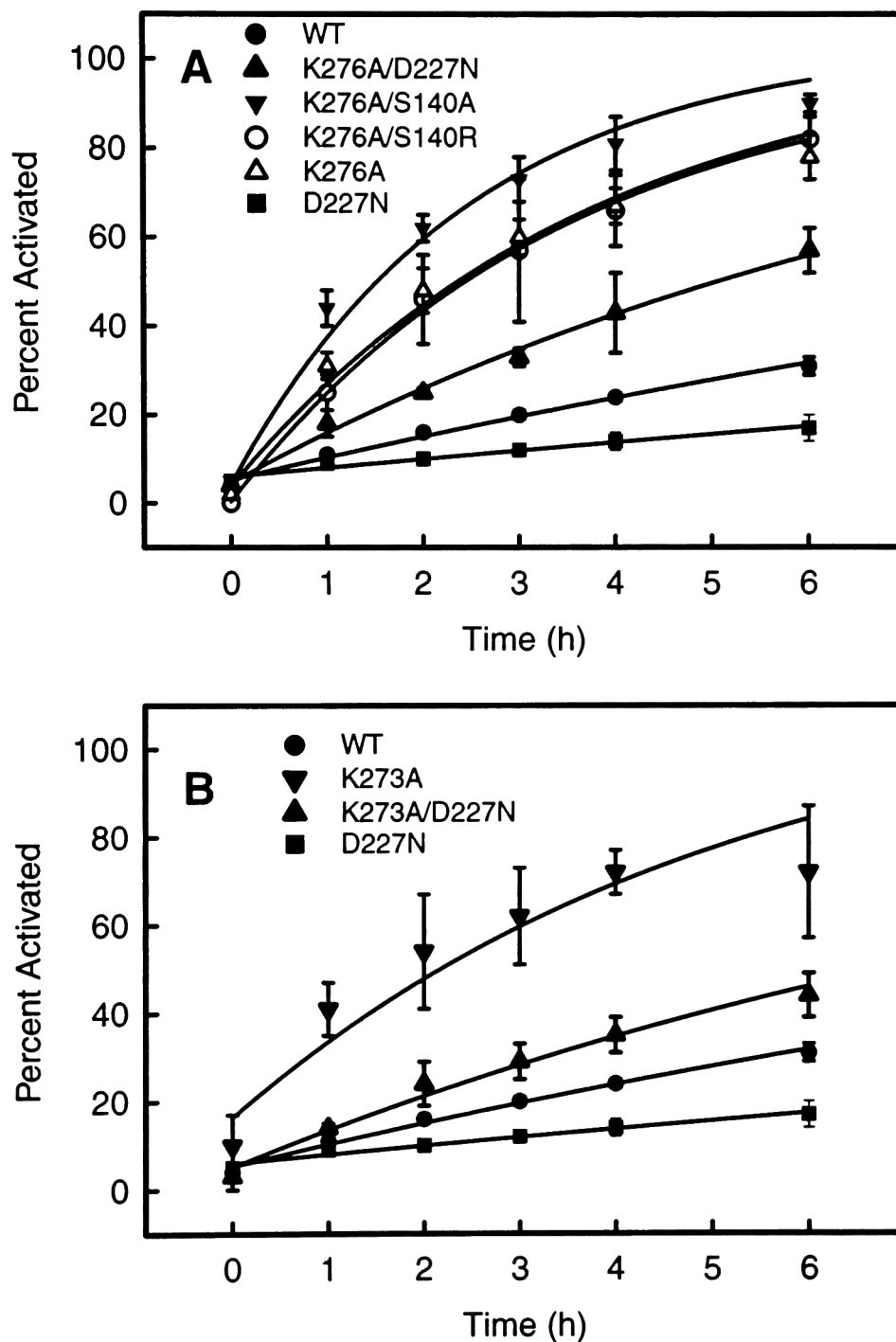


FIG. 5-8. Time courses of uncatalyzed activation of double mutants. The experiments were conducted as described in Fig. 5-4. **A**, The K276A mutation was combined with mutations of residues that are indicated in the crystal structure to interact with K276. The rates of the uncatalyzed activation were determined. Data for K276A and D227N are re-plotted for comparison with the double mutants. **B**, The K273A mutation was combined with the D227N mutation, and the uncatalyzed activation rate determined. K273A and D227N are re-plotted for comparison.

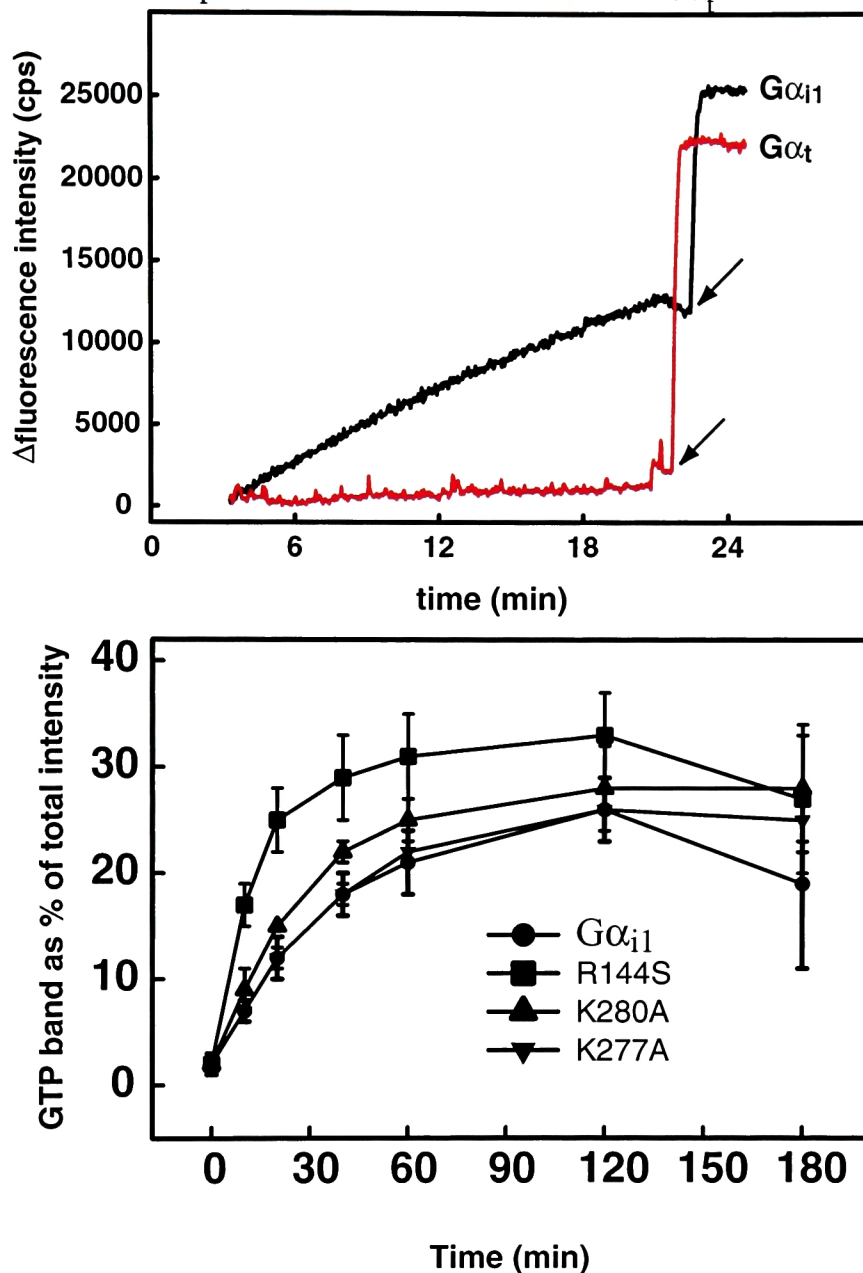


FIG. 5-9. Uncatalyzed activation of $G\alpha_{i1}$ and mutants of $G\alpha_{i1}$. **A.** Fluorescence activation trace of $G\alpha_{i1}$ (expressed and purified from Sf9 cells) and $G\alpha_t$ (purified from bovine retinas). 250 nM of each protein in a total volume of 500 μ L was placed in a stirred cuvette at 25 C. Fluorescence was excited at 300 nm, and emission was measured at 345 nm. At 200 s, 15 μ L of GTP γ S was added to the cuvette to a final concentration of 5 μ M. At the times indicated by the arrows, $AlCl_3$ and NaF were added from separate stock solutions to a final concentration of 0.05mM and 3mM respectively. **B.** Noncatalyzed activation of $G\alpha_{i1}$ and mutants expressed *in vitro* and assayed by analysis of trypsin digestion products. The intensity of the GTP-dependent band is expressed as a percent of the total intensity in the lane. Each point represents the mean of at least three independent experiments ± 2 *S.E.M.

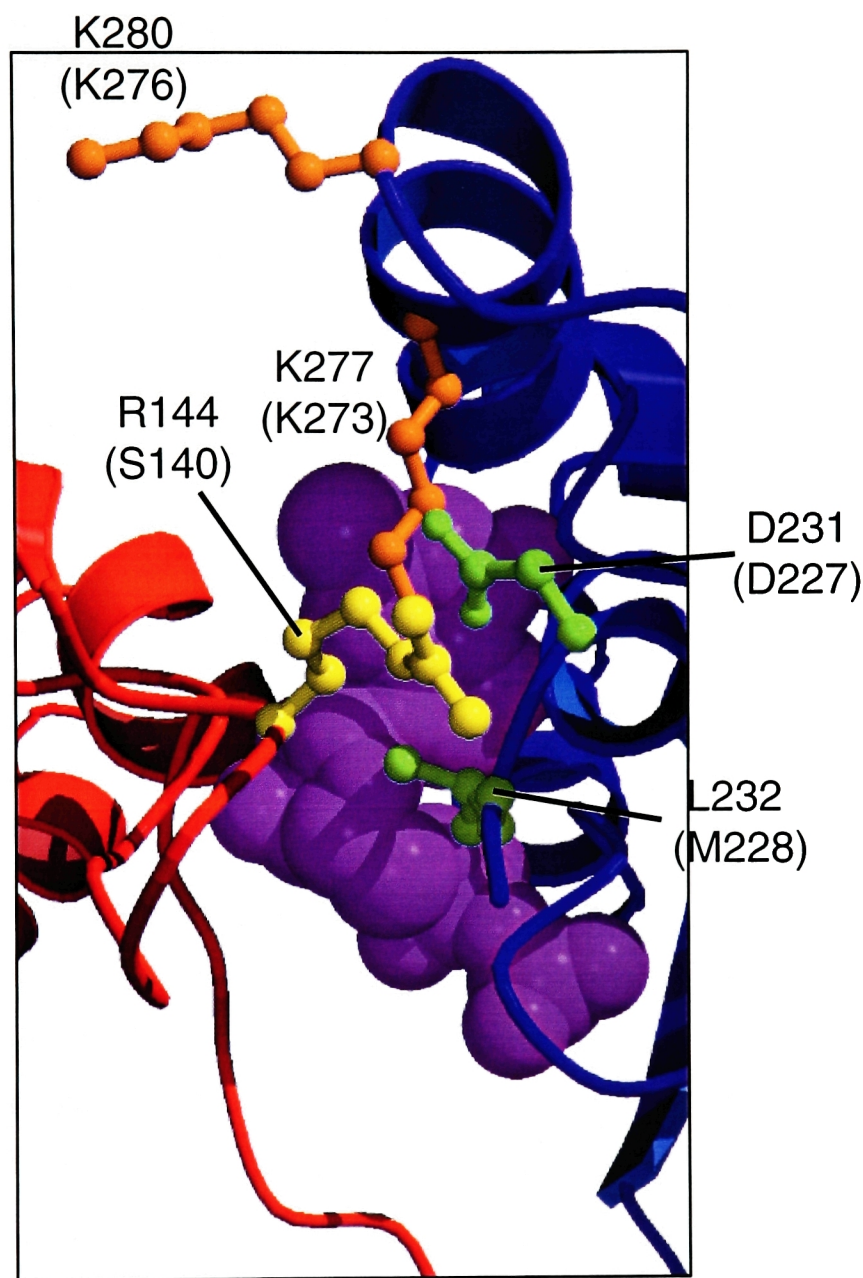


FIG. 5-10. Structure of the interdomain interface of GDP-bound $G\alpha_{i1}$. View and coloring is similar to Fig. 5-1B. $G\alpha_{i1}$ residues are labeled, and the corresponding residues in $G\alpha_t$ are noted in parentheses (see Fig. 5-1B). K280, which is equivalent to K276 of $G\alpha_t$, is oriented toward the solvent whereas K276 of $G\alpha_t$ is oriented toward the equivalent of D231. Residues 234-239 are not ordered in this structure.

Discussion

Analysis of Trypsin-Digest Products of in vitro Translated $G\alpha_t$ to Evaluate Nucleotide Exchange Kinetics

Since $G\alpha_t$ is refractory to expression in bacteria (Skiba *et al.*, 1996), and is cumbersome to express in insect cells (Min *et al.*, 2000) we chose to express $G\alpha_t$ *in vitro*, and analyze nucleotide exchange rates using trypsin digestion. The pattern of proteolytic fragments resulting from trypsin digestion directly reflects the conformation of $G\alpha_t$, and therefore the identity of the bound nucleotide (Neer *et al.*, 1994a; Fung and Nash, 1983). Trypsin proteolysis of expressed $G\alpha_t$ yielded ~23-kDa fragments following incubation with GDP and ~34-kDa fragments following activation with either AlF_4^- or GTP γ S (Fig. 5-2). These observations are consistent with previously published results (Mazzoni and Hamm, 1996; Osawa and Weiss, 1995).

Trypsin proteolysis of *in vitro* translated $G\alpha_t$ allowed for the precise quantitation of basal and R*-catalyzed nucleotide exchange rates. By using both the ~23- and the ~34-kDa bands, the calculation of nucleotide exchange rates was internally normalized and took into consideration both the GDP- and the GTP γ S-bound fractions. As a result, the data were very reproducible and samples in which only a small fraction of the total expressed protein was functional could be analyzed. Additionally, the methodology was rapid enough to allow for the characterization of relatively large numbers of mutants in parallel.

The kinetic parameters for $G\alpha_t$ activation derived from the trypsin digestion assay are consistent with data reported using other traditional methodologies (Ramdas *et al.*, 1991; Skiba *et al.*, 1996) as well as with analysis of retinal $G\alpha_t$ studied with the fluorescence activation assay (Fig. 5-9). Additionally, analysis of the mutant A322S by trypsin

proteolysis indicated that the basal rate of activation was >60-fold greater than that of wild-type $G\alpha_t$ (Fig. 5-3A). This result is also in agreement with published data using different methodologies on the analogous mutation in $G\alpha_s$ and in $G\alpha_{i1}$ (Iiri *et al.*, 1994; Posner *et al.*, 1998).

Several control reactions demonstrated the fidelity of the R^* -catalyzed assay. The rate of rhodopsin-dependent activation was sensitive to light (not shown), to the concentration of rhodopsin from 0-100 nM and to the presence of added $G\beta\gamma_t$ (Fig. 5-3B). A mutation near the carboxyl terminus of $G\alpha_t$ (G348P) that was previously reported to disrupt R^* - G_t interactions (Osawa and Weiss, 1995) was not activated (not shown).

The system does present several potential limitations. The concentrations of the expressed $G\alpha_t$ cannot be easily controlled or readily determined. Other components of the reticulocyte lysate may affect the behavior of $G\alpha_t$ and rhodopsin. Certain mutations of $G\alpha_t$ (such as R204H) directly alter the pattern of fragments produced by trypsin proteolysis, and therefore interfere with determination of the activation state. Despite these limitations, we show here that the analysis of *in vitro* translated $G\alpha_t$ by trypsin proteolysis allowed for the rapid and accurate quantitation of activation kinetics of expressed $G\alpha_t$ in both uncatalyzed and rhodopsin-catalyzed assays.

This expression and assay system offers additional flexibility not explored in the present work. Expressed recombinant rhodopsin could be used in place of retinal rhodopsin to test the combined effects of mutation of rhodopsin and transducin (unpublished observation). Other proteins (e.g., $G\beta\gamma_t$ mutants, regulator of G protein signaling proteins, etc.), could be co-translated with $G\alpha_t$ in the *in vitro* system (Neer *et al.*, 1994a). Furthermore, this system will likely prove useful in the kinetic

characterization of other G protein subtypes, such as cone transducin, which are difficult to express heterologously.

Site-Directed Mutation of K273 or K276 Increases Basal Nucleotide Exchange Rates

Replacement of K276 or K273 with alanine increased the basal rate of nucleotide exchange ~5 fold in $G\alpha_t$ (Fig. 5-7A, Table 5-I). Replacement of the adjacent K275, which in the crystal structure is oriented toward the solvent (Fig. 5-1), had no effect. Replacement of K276 with a negatively charged glutamic acid increased basal nucleotide exchange rates more dramatically (~10 fold) than the neutral alanine replacement mutant. However, mutation to a positively charged arginine did not alter the activation rate. Together, these results suggest that the function of K276 and K273 is dependent on positive charge, and orientation toward the interior of the protein. Interestingly, in the activated, GTP γ S-bound structure of $G\alpha_t$, K276 is rotated outward toward the solvent relative to the GDP-bound conformation (Fig. 5-1B). The K276A mutant may anticipate this active conformation.

K276 and K273 both lie in the third of four regions of $G\alpha_t$ for which there is no homologous sequence in the monomeric G protein Ras. The four regions are known as Insert 1 through Insert 4 (Noel *et al.*, 1993). Specific functions have been attributed to Insert 1 (the helical domain), Insert 2 (the Switch III region) and Insert 4 (which may interact with heptahelical receptors). The present work is the first to identify a functional role for residues in Insert 3 of $G\alpha_t$.

The structure of GDP-bound $G\alpha_t$ reveals that K276 and K273 lie near to and possibly form ionic interactions with D227. This observation suggests that the reason for accelerated nucleotide exchange rates caused by mutations of K276 and K273 might involve disruption of interactions with D227. To test this hypothesis, the K276A and K273A mutations were combined with mutation of D227N to produce the K276A/D227N and K273A/D227N double mutants. If the effects of K276A were due

solely to breaking of an ionic interaction with D227, then the K276 mutation should not increase the rate of nucleotide exchange in the context of D227N or D227A mutants. Indeed, the increase in the basal rate of activation caused by the K276A and K273A mutations was reduced (from ~5 fold to ~2 fold relative to wild-type) when combined with D227N (Fig. 5-8). However, since the rate of the D227N mutant alone is 2 fold slower than that of wild-type, the effect of the K276A mutation is roughly the same (i.e., a ~5 fold increase in rate) whether introduced into a wild-type or a D227N background. Similar results were obtained with a D227A mutation. Thus, the origin of the increase in basal nucleotide exchange rates by the K276A and K273A mutation is not merely due to disruption of interactions with D227.

K276 also appears to interact across the interdomain interface with S140. Replacement of S140 with alanine, which would have disrupted hydrogen bonding to K276A, did not affect the rate of activation. Thus, breaking of the putative S140-K276 interaction does not fully explain the effects of the K276A mutation. There appear to be other unidentified requirements for positively charged sidechains in the αG region in order to maintain low basal rates of nucleotide exchange.

Mutation of D227 slows the rate of basal nucleotide exchange, both in the context of the wild-type protein as well as in the K276A mutant (Fig. 5-8). This is surprising since G α_t has an extremely low rate of basal nucleotide exchange, as is demanded by the low background noise required for sensitive light detection by photoreceptors. Other mutations in the Switch III regions also appear to slightly reduce the basal rate of nucleotide exchange, including M228L and V231A (Fig. 5-5, 5-6; Table 5-I). The origins of these effects, which are relatively small, are unclear. Previously, it has been demonstrated that the entire Switch III region can be deleted from G α_t without disrupting the ability to bind nucleotides (Li and Cerione, 1997). The rates of nucleotide exchange

in these Switch III-deleted constructs were not characterized, but such studies might illuminate the role of Switch III in facilitating or impeding nucleotide exchange.

Interdomain Interactions in $G\alpha_t$ Do Not Affect Basal or Rhodopsin-Catalyzed Nucleotide Exchange Rates

When the structure of $G\alpha_t$ was determined, the nucleotide was found to reside in a deep cleft between the Ras-like domain and the helical domain (Noel *et al.*, 1993). It was proposed that rhodopsin might accelerate the nucleotide exchange rate by opening the cleft (Noel *et al.*, 1993; Bourne, 1993). Similarly, interactions between these domains could control the rate of basal nucleotide exchange. $G\alpha_t$ has a very low rate of basal nucleotide exchange as compared to related G proteins and a very high rate of R*-catalyzed exchange. If interdomain interactions were important mediators of either of these processes, one might expect nucleotide exchange rates in $G\alpha_t$ to be particularly sensitive to mutation of residues involved in those interactions. However, none of the $G\alpha_t$ mutants characterized in this report significantly affected either basal or R*-catalyzed rates.

Close analyses of G protein structures indicate that opening of the interdomain cleft is not necessarily an energetic barrier to nucleotide release. The helical domain does not contribute many contacts to the nucleotide binding pocket and certain monomeric G proteins, which do not have a helical domain at all, release GDP more slowly than some heterotrimeric G proteins subtypes (Sprang, 1997). A crystal structure of the $G\alpha_{i1}$ mutant A326S, which releases GDP ~250-fold faster than wild-type $G\alpha_{i1}$, does not reveal any alteration in the interdomain interactions, suggesting that an open cleft is not a prerequisite of fast nucleotide exchange (Posner *et al.*, 1998). In addition, the reported increases in nucleotide release rates resulting from mutations at the interdomain interface of $G\alpha_{i1}$ and $G\alpha_s$ are relatively modest (~5-10 fold) as compared with mutations in other

regions of G proteins hypothesized to be involved in regulating nucleotide exchange rates. For example, we observed up to 165-fold increases in nucleotide exchange rates in mutations of certain residues of the $\alpha 5$ helix of $G\alpha_t$, a structure implicated in the mechanism of rhodopsin-catalyzed activation (Chapter 6). In summary, the opening of the interdomain cleft may not necessarily be a rate-determining step in nucleotide exchange in G proteins.

The Function of Residues at the Interdomain Interface Differs Among $G\alpha_t$, $G\alpha_{i1}$ and $G\alpha_s$

Many of the residues mutated in this study, such as S140, Q143, M228, and V231, have been previously found to alter basal or receptor-catalyzed nucleotide exchange rates in the related G proteins, $G\alpha_s$ and $G\alpha_{i1}$. In $G\alpha_s$, a mutation in the Switch III region, R258W (corresponding to V231 in $G\alpha_t$), was found in a patient with Albright hereditary osteodystrophy (Warner *et al.*, 1998). Biochemical studies indicated that replacement of R258 to tryptophan and to alanine, as well as alteration of a proposed interacting residue, Q170 of the helical domain (corresponding to Q143 in $G\alpha_t$), led to increases in the basal nucleotide exchange rate (Warner *et al.*, 1998; Warner and Weinstein, 1999). These mutations were hypothesized to widen the interdomain cleft. Other studies in $G\alpha_s$ found that mutation of R258 or N167 (corresponding to S140 in $G\alpha_t$) disrupted receptor catalyzed activation (Grishina and Berlot, 1998), suggesting that the receptor induces structural changes that are communicated across the interdomain interface. In $G\alpha_{i1}$, mutation of either L232 or R144 (corresponding to M228 and S140, respectively, in $G\alpha_t$) increased the basal nucleotide exchange rate by disrupting a proposed interdomain hydrophobic interaction (Remmers *et al.*, 1999). The effects of mutating R144 were corroborated by the results of the R144S mutant in the current work (Fig. 5B).

The residues analogous to those proposed to interact with each other across the interdomain interface in $G\alpha_s$ and $G\alpha_{i1}$ are also potentially interacting in $G\alpha_t$ (Fig. 5-1B). In many cases, however, the amino acids are not conserved. For example, V231 and Q143 of $G\alpha_t$, which correspond to the proposed interaction between R258 and Q170 in $G\alpha_s$, are adjacent. S140 and M228 (corresponding to R144 and L232 of $G\alpha_{i1}$) and S140 and D227 (corresponding to the proposed interaction of N167 and N254 of $G\alpha_s$ (Grishina and Berlot, 1998)) are similarly adjacent. However, in contrast to the results with $G\alpha_{i1}$ and $G\alpha_s$, replacement of these residues in $G\alpha_t$ did not affect nucleotide exchange rates. These results suggest that the interdomain interface residues are functionally different in $G\alpha_t$ than in $G\alpha_{i1}$ and $G\alpha_s$. Counterintuitively, $G\alpha_{i1}$ and $G\alpha_s$, which exchange nucleotides faster than $G\alpha_t$, appear to have tighter and more sensitive interactions across the interdomain interface than those of $G\alpha_t$.

Both K273 and K276 of $G\alpha_t$ are conserved in $G\alpha_{i1}$. However, the structure of GDP-bound $G\alpha_{i1}$ reveals that K280 (cognate to K276 of $G\alpha_t$) is oriented toward the solvent instead of toward the Switch III region as in $G\alpha_t$ (Fig. 5-10). Functionally, mutation of K280 and K277 to alanine did not lead to increases in nucleotide exchange rates in $G\alpha_{i1}$, as was observed in $G\alpha_t$. Thus, conserved residues, K276 and K273 of $G\alpha_t$, are found to serve different roles and to assume different structures in closely related G proteins.

In conclusion, the data in this report ascribe a role to K273 and K276 in the αG region of $G\alpha_t$ in maintaining low basal rates of nucleotide exchange. However, unlike in $G\alpha_{i1}$ and $G\alpha_s$, interactions which span the interdomain interface do not appear to be important in regulating either basal or rhodopsin-catalyzed nucleotide exchange rates. Differences exist in the organization of the interdomain interface among $G\alpha_t$, $G\alpha_{i1}$, and $G\alpha_s$ -- and even between conserved residues in $G\alpha_{i1}$ and $G\alpha_t$.

Chapter 6:

Rapid Activation of Transducin by Mutations on the $\alpha 5$ Helix Distant From the Nucleotide-Binding Site: Evidence for a Mechanistic Model of Receptor-Catalyzed Nucleotide Exchange by G Proteins*

Summary

Rhodopsin, a prototypical G protein-coupled receptor, catalyzes the release of GDP from the α subunit of transducin ($G\alpha_t$), a heterotrimeric G protein. Hypothetical models of the complex between photoactivated rhodopsin (R^*) and transducin (G_t) suggest that R^* does not directly contact the nucleotide-binding pocket of $G\alpha_t$. Instead, R^* is thought to act “at-a-distance” through an unknown mechanism. The $\alpha 5$ helix of $G\alpha_t$ connects the carboxyl terminal region, which binds R^* , to the nucleotide-interacting $\beta 6/\alpha 5$ loop. Thus the $\alpha 5$ helix has been proposed to mediate communication between R^* and the nucleotide binding pocket. We investigated the role of the $\alpha 5$ helix in R^* -catalyzed activation of $G\alpha_t$ by extensive site-directed mutagenesis of $\alpha 5$ and the surrounding region. The mutants were expressed *in vitro* and the kinetics of uncatalyzed and R^* -catalyzed nucleotide exchange were determined by quantitative analysis of trypsin digests of $G\alpha_t$. A set of conserved residues (T325, V328 and F332) was identified that constitutes a nucleotide-release control microdomain on the buried surface of the $\alpha 5$ helix about 0.7-1.5 nm from the nucleotide. Mutations of these residues did not disturb the folding of the protein, interactions with R^* , or binding of GDP, GTP γ S and GDP/AlF $_4^-$. However, their mutation greatly (up to 165-fold) increased nucleotide exchange rates in the absence of rhodopsin. Mutation of a series of hydrophobic residues on the opposite face of $\alpha 5$ reduced R^* -catalyzed activation, as did replacement of $\alpha 5$

* A portion of the material in this chapter has been published previously in: Marin, E. P., Krishna, A. G., and Sakmar, T. P. (2001) Rapid Activation of Transducin by Mutations Distant From the Nucleotide-Binding Site: Evidence for a Mechanistic Model of Receptor-Catalyzed Nucleotide Exchange by G Proteins. *J. Biol. Chem.* 276:27400-27405.

Chapter 6: The $\alpha 5$ helix of $G\alpha_t$

residues with prolines. The data suggest that the mechanism by which R^* catalyzes GDP release "at-a-distance" involves perturbation of the residues in the nucleotide-release control microdomain on $\alpha 5$. The structural basis of this perturbation may involve the binding of R^* directly to $\alpha 5$.

Introduction

In chapters 3 and 4, evidence was presented supporting a role for the amino terminus of the C4 loop in the binding and activation of G_t , and specifically in binding a peptide derived from the carboxyl terminus of $G\alpha_t$. The carboxyl terminus of $G\alpha_t$ is 2.5 nm away from the nucleotide (Fig. 1-2); available evidence suggests that rhodopsin is unlikely to directly contact the nucleotide binding pocket (Chapter 1). It is not clear how the C4-mediated binding of G_t by the cytoplasmic surface of R^* affects the nucleotide binding pocket. In Chapter 5, it was demonstrated that the mechanism is not likely to involve opening the interdomain cleft.

The $\alpha 5$ helix connects the carboxyl-terminal tail of $G\alpha_t$ (residues 340-350) to the $\beta 6/\alpha 5$ loop (residues 321-324) (Fig. 6-1). As discussed in Chapter 1, the carboxyl-terminal tail is a well characterized rhodopsin-binding domain of $G\alpha_t$ (Hamm *et al.*, 1988; Ernst *et al.*, 2000). The $\beta 6/\alpha 5$ loop directly contacts the guanine ring of the nucleotide. Certain mutations in this loop have been shown to dramatically increase GDP release rates in G proteins (Iiri *et al.*, 1994; Posner *et al.*, 1998). Consequently, it has been proposed (Onrust *et al.*, 1997; Iiri *et al.*, 1998) that R^* might achieve GDP dissociation by binding to the C-terminus of $G\alpha_t$ and communicating with the $\beta 6/\alpha 5$ loop via the $\alpha 5$ helix.

We examined in detail the role of the $\alpha 5$ helix in R^* catalyzed activation of $G\alpha_t$ by extensive mutagenesis of the $\alpha 5$ helix and the surrounding region. Using *in vitro* expression of $G\alpha_t$ coupled with quantitative analysis of trypsin digestion patterns, we characterized the kinetics of spontaneous and R^* -catalyzed nucleotide exchange in a large number (>30) of relevant mutants.

We found that mutation of three residues on the buried surface of $\alpha 5$ (T325, V328 and F332) mimicked the receptor-bound state in that the rate of GDP release was

dramatically (up to 165-fold) increased, even though the site of the mutation was distant from the nucleotide-binding pocket.

Consistent with the proposed role of $\alpha 5$ we also found that mutation of a hydrophobic, solvent exposed surface of $\alpha 5$ disrupted R^* -catalyzed nucleotide exchange. Furthermore, structural perturbation of the $\alpha 5$ helix induced by the replacement of individual residues with proline or by the insertion of alanines disrupted R^* -catalyzed exchange.

These data support an important role for the $\alpha 5$ helix in determining the rates of basal and R^* -catalyzed nucleotide exchange. We suggest that R^* does not use $\alpha 5$ merely to communicate with the $\beta 6/\alpha 5$ loop, but that R^* perturbs the conformation of residues on the buried surface of $\alpha 5$ itself and thus accomplishes rapid GDP release "at-a-distance". We speculate that the structural basis by which R^* perturbs the $\alpha 5$ helix might involve binding of rhodopsin directly to an exposed surface of $\alpha 5$.

Results

Proline Scanning Mutagenesis of the $\alpha 5$ Helix

In an effort to test the role of the $\alpha 5$ helix in mediating communication between R^* and the nucleotide binding pocket of $G\alpha_t$, we introduced structural perturbations into the helix. Each residue (amino acids 325-339) was individually replaced by proline. Each of the resulting constructs yielded proteins of an appropriate molecular weight and expression level, as judged by SDS-PAGE analysis of undigested samples (not shown). Several of the mutants were severely impaired in nucleotide binding, including N327, V328, K329, V331, F332 and V335. In these cases, the trypsin digestion patterns generally indicated that GDP binding was absent and that $GTP\gamma S$ binding was compromised. $GTP\gamma S$ binding was less defective than GDP binding, likely due to the extra binding energy contributed by contacts involving the γ phosphate. Additionally, AlF_4^- -induced activation in these mutants was greatly attenuated, presumably due to reduced GDP binding.

The proline mutants which could bind GDP were characterized in both R^* -catalyzed and uncatalyzed activation assays (Fig. 6-2). In the uncatalyzed assay, one mutant located in the first turn of the helix, T325P, exhibited an extremely fast basal activation rate. Several other proline substitution mutants exhibited moderately accelerated rates relative to that of $G\alpha_t$, including D333P, A334P, T336P, D337P and I338P. Three proline mutants, Q326P, F330P and I339P, were similar to wild-type $G\alpha_t$. In the R^* -catalyzed nucleotide exchange assay, the proline mutants (with the exception of T325P) exhibited defects in activation of varying severity.

Deletions and Insertions in the $\alpha 5$ Helix and Carboxyl Terminus of $G\alpha_t$

In a further effort to evaluate the effects of structural alterations in $\alpha 5$, deletion and insertion mutants were prepared (Fig. 6-3). Three deletion mutants were constructed in

which 5, 10 or 25 amino acids were deleted from the carboxyl terminus of $G\alpha_t$. None of these constructs yielded proteins which could bind nucleotides as judged by trypsin digest analysis.

Four insertion mutants were prepared. In three of the mutants, the insertion point was immediately following I339. This position was chosen to minimize disruptions between the $\alpha 5$ helix and the rest of the protein. Three alanines, four alanines or four isoleucines were inserted at this location in three different constructs, called $\alpha 5$ ala3, $\alpha 5$ ala4, and $\alpha 5$ ile4, respectively. In the fourth mutant, four alanines were inserted following residue 345 in the carboxyl-terminal tail (CT ala4). Of these constructs, only the two with insertions of four alanines yielded proteins that were functional (CT ala4 and $\alpha 5$ ala4), and in these cases only a small fraction of the protein could bind GDP. These two constructs could be activated by GDP/AlF_4^- ; however, they were unresponsive to R^* -catalyzed nucleotide exchange (Fig. 6-3C).

Alanine Scanning Mutagenesis of the $\alpha 5$ Helix

In order to evaluate the effects of less drastic mutations in $\alpha 5$, each non-alanine residue of the helix was individually replaced by alanine. Each of these mutants expressed well *in vitro*, could bind GDP, and could be activated by AlF_4^- as judged by trypsin proteolysis. A significantly reduced level of functional protein was observed only in the case of I339A. The rates of uncatalyzed and R^* -catalyzed nucleotide exchange were determined for the resulting mutant proteins. In the uncatalyzed assay, the majority of the mutants behaved similarly to wild-type $G\alpha_t$. However, three mutants showed dramatic increases in the rate of uncatalyzed GTP γ S uptake: T325, V328 and F332. Additionally, the N327A and I339A mutants showed accelerated kinetics of uncatalyzed activation (Fig. 6-4, Table 5-I). The rapid rate of nucleotide exchange observed in these mutants was not the result of global misfolding of the proteins. The conformations of

these proteins were similar to wild-type $G\alpha_t$ in the presence of GDP, GDP/ AlF_4^- or GTP γ S as judged by trypsin digest analysis (Fig. 6-5).

In the R^* -catalyzed assay (Fig. 6-6), T325A, N327A, V328A, and F332A were activated faster than wild-type $G\alpha_t$. The estimated times (in units of min) for half-maximal activation ($t_{1/2}$) for these mutants were: T325A, 0.4; V328A, 0.4; F332A, 0.2. In comparison, the estimated $t_{1/2}$ for wild-type was 1.1. Four mutants exhibited activation rates that were reduced 3-4 fold relative to wild-type. These mutants, and the estimated values for $t_{1/2}$ were: F330A, 4.1; V331A, 3.2; D337A, 4.6; and I338A, 4.0. The remaining mutants displayed activation rates that were similar to wild-type: Q326A, 1.3; K329A, 1.2; D333A, 1.2; V335A, 1.5; and T336A, 1.4.

Mutagenesis of the $\beta 6/\alpha 5$ Loop and of Residues Interacting with the $\alpha 5$ Helix

The $\beta 6/\alpha 5$ loop immediately precedes the $\alpha 5$ helix. Mutations in the analogous region in $G\alpha_i$ and $G\alpha_s$ were previously shown to increase nucleotide exchange rates (Iiri *et al.*, 1994; Posner *et al.*, 1998). In order to test the role of this region in $G\alpha_t$, several site directed mutations were made. The mutants A322S, A322G and C321A all caused substantial increases in the rates of uncatalyzed activation and modest increases in rhodopsin-catalyzed activation (Fig. 6-7). The results of the A322S mutant were previously reported in Chapter 5 (Fig. 5-3) as a control for the trypsin digest assay.

In order to examine the function of interactions between $\alpha 5$ and the rest of the protein, five additional residues, which interact with the $\alpha 5$ helix and are located elsewhere on $G\alpha_t$, were mutated to alanine. The F185A and F192A mutants did not form the typical ~23-kDa band when digested by trypsin following incubation with GDP (Fig. 6-7). Under these conditions, the F185A mutant generally yielded no bands >20-kDa, and the F192A mutant produced a ~21-kDa band. The absence of a ~23-kDa band could indicate lack of GDP binding. However, it appears that F185A and F192A did indeed

bind GDP since activation by AlF_4^- , which requires binding of GDP, was normal. Additionally, the kinetics of GTP γ S uptake required at least 20 min for completion, as judged by the intensity of the ~34-kDa band at times following GTP γ S addition. If the $G\alpha_t$ mutants were not binding GDP, then much more rapid GTP γ S uptake would be expected.

The F185A and F192A mutations seem to interfere not with GDP binding, but with the production of a ~23-kDa fragment by trypsin proteolysis that is otherwise characteristic of the GDP bound form. As a result, the fraction of mutant $G\alpha_t$ activated in a given aliquot of the F185A and F192A mutants cannot be accurately determined, since this calculation depends on the intensities of both the ~34- and ~23-kDa bands. However, an examination of the time course ~34-kDa bands following GTP γ S treatment for mutants F185A and F192A clearly shows that uncatalyzed GTP γ S uptake is accelerated in these mutants (Fig. 6-7). Similarly, the catalyzed activation rates of F185A and F192A are at least as fast as wild-type $G\alpha_t$, if not faster (not shown).

A third mutant protein in which a phenylalanine was replaced with an alanine, F187A, formed a ~23-kDa band normally when digested with trypsin following incubation with GDP. F187A caused a very slight retardation in both the catalyzed and uncatalyzed activation reactions. Two other mutations of residues predicted to interact with $\alpha 5$, K188A and Q168A, caused moderately increased rates in both catalyzed and uncatalyzed assays (Fig. 6-7).

Engineering of Disulfide Bridges Between $\alpha 5$ and Other Parts of $G\alpha_t$

The effects of constraining the conformation of the $\alpha 5$ helix were explored by attempts to engineer disulfide cross links between the $\alpha 5$ helix and the rest of the protein. The residue I339 of the $\alpha 5$ helix lies near to V30 (Natochin *et al.*, 2000), and a naturally occurring cysteine, C216. Mutants I339C, V30C and I339C/V30C were constructed.

Chapter 6: The $\alpha 5$ helix of $G\alpha_t$

Disulfide formation was monitored by trypsin proteolysis of the GDP-bound and GDP/ AlF_4^- bound $G\alpha_t$ and analysis by nonreducing SDS-PAGE. Since trypsin cleaves GDP-bound $G\alpha_t$ at R204 (Chapter 5), disulfide bonds between 339 and 30 (in the I339C/V30C mutant) would be expected to yield larger fragments following tryptic cleavage of the GDP-bound form. Similarly, since trypsin digests GDP/ AlF_4^- bound $G\alpha_t$ at R310, disulfide bonds between C339 and C216 (in a I339C mutant) would be expected to result in a larger fragments following cleavage of the GDP/ AlF_4^- -bound $G\alpha_t$.

The data did not reveal any evidence of disulfide formation in either the I339C or I339C/V30C constructs (not shown). Analysis was complicated, however, by the poor quality of electrophoresis performed under nonreducing conditions, as well as by the low levels of functional I339C produced.

Chapter 6: The $\alpha 5$ helix of $G\alpha_t$

Table 6-I. Rate constants of uncatalyzed nucleotide exchange of $G\alpha_t$ and $G\alpha_t$ mutants.

<u>Position</u>	<u>mutant^d</u>	<u>k_{app}^a</u>	<u>fold inc.^c</u>	<u>mutant^d</u>	<u>k_{app}^a</u>	<u>fold inc.^c</u>
wild-type		8.6±0.7	1.0±0.1			
catalyzed ^b		5390±802	629±107			
Q168	A	26.4±5.2	3.1±0.7			
F187	A	4.8±0.8	0.6±0.1			
K188	A	48.5±13.1	5.7±1.6			
C321	A	36.5±5.9	4.3±0.8			
A322	S	536±109	62.6±13.7			
A322	G	74.1±22.3	8.7±2.7			
T325	A	1410±474	165±57	P	988±78	115±13
Q326	A	6.6±1.3	0.8±0.2	P	4.9±0.8	0.6±0.1
N327	A	198±60	23±7.2			
V328	A	661±185	77±23			
K329	A	9.0±0.9	1.0±0.1			
F330	A	5.3±1.2	0.6±0.1	P	11.3±0.9	1.3±0.1
V331	A	9.6±2.0	1.1±0.3			
F332	A	1300±256	151±32			
D333	A	6.4±0.3	0.7±0.1	P	43.3±6.5	5.1±0.9
A334				P	72.3±30.9	8.4±3.7
V335	A	17.7±2.2	2.1±0.3			
T336	A	7.4±2.0	0.9±0.2	P	32.8±6.2	3.8±0.8
D337	A	17.3±4.2	2.0±0.5	P	43.5±8.6	5.1±1.1
I338	A	9.3±1.1	1.1±0.2	P	36.7±13.1	4.3±1.6
I339	A	35.4±23	4.1±2.7	P	10.4±2.3	1.2±0.3

^aThe apparent rate constants were derived from fits of each data set to the exponential rise equation, $y = c + 100(1 - \exp(-kt))$. Each mutant was assayed at least 3 times (WT $G\alpha_t$ was assayed 26 times), and an independent fit was made to each data set. The values reported are the mean $k_{app} \cdot 10^4 \text{ min}^{-1} \pm 2 \cdot \text{SEM}$.

^bThe catalyzed assay of wild-type $G\alpha_t$ was conducted in the presence of 30nM photoactivated rhodopsin, 30nM $G\beta\gamma_t$, and 14 μ M GTP γ S.

^cThe fold increase over uncatalyzed wild-type is calculated at the $k_{app}(\text{mutant})/k_{app}(\text{wild-type})$.

^dThe amino acid used to replace the wild-type residue.

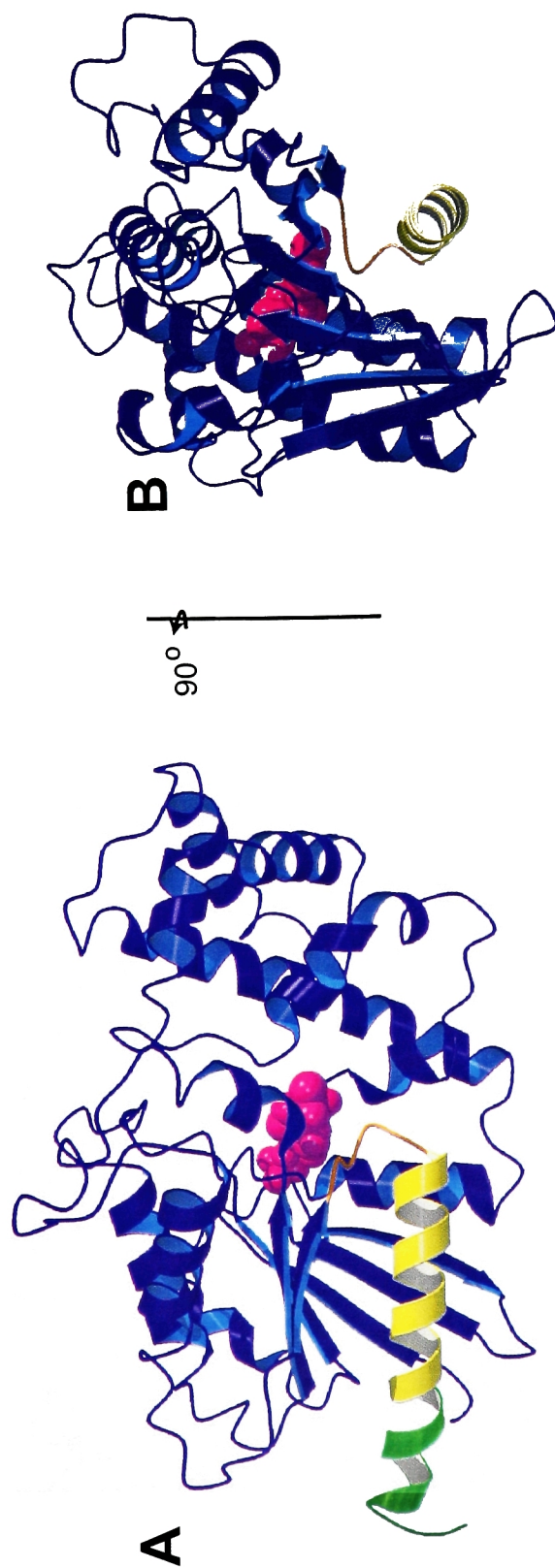


FIG. 6-1. Structure of the $\alpha 5$ helix of $G\alpha_t$. A. Overall view of the structure of $G\alpha_t$ bound to GDP. The nucleotide is purple, the $\beta 6/\alpha 5$ loop is orange, and the $\alpha 5$ helix (which is part of the Ras-like domain) is yellow. The nucleotide lies in a cleft between the Ras-like and helical domains of $G\alpha_t$, adjacent to the $\beta 6/\alpha 5$ loop at the N-terminal end of the $\alpha 5$ helix. An NMR structure of a peptide corresponding to the extreme carboxyl terminus of $G\alpha_t$, residues 340-350, in the rhodopsin-bound conformation is shown in green, docked onto the end of the $\alpha 5$ helix (Kisselev, et. al., 1998). (This region was not ordered in the crystal structures, and it is not shown in the other panel). B. The view in panel A has been rotated 90 degrees about the vertical axis. The $\alpha 5$ helix is viewed end-on. The helix packs into a groove formed by the central curved beta sheet of the Ras-like domain and the $\alpha 1$ helix.

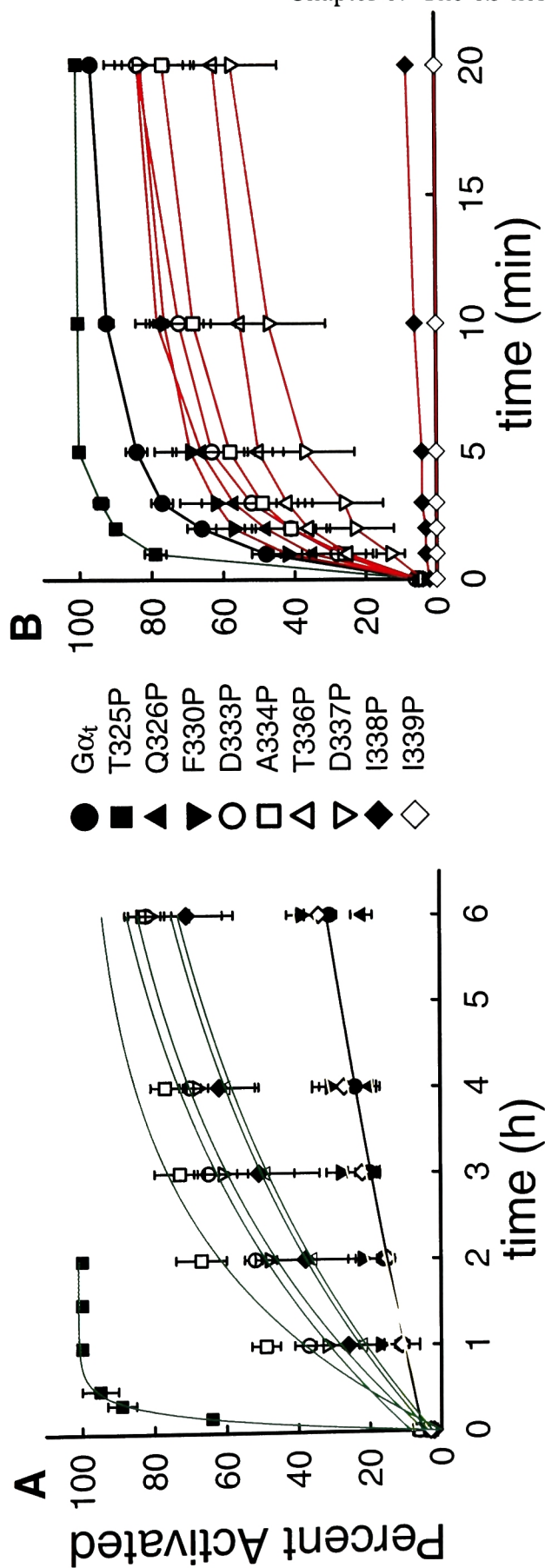


FIG. 6-2. Nucleotide exchange time courses of proline mutants in $\alpha 5$. $G\alpha_t$ and mutants were translated *in vitro* and combined with 100 μ M GTP γ S (panel A) or 30 nM $R^*/10$ nM $G\beta\gamma_t/14$ μ M GTP γ S (panel B). Aliquots (8 μ l) were removed at the indicated times and the percent activation was determined by analysis of trypsin digestion patterns, as described in Chapter 5. The time-zero data point is calculated from protein mixed with 100 μ M GDP for 10 min. Each data point is the average of 3-5 independent experiments. Error bars depict ± 2 SEM. The solid lines represent fits to an exponential rise function. **A.** Uncatalyzed nucleotide exchange time courses. **B.** $R^*/G\beta\gamma_t$ -catalyzed nucleotide exchange time courses.

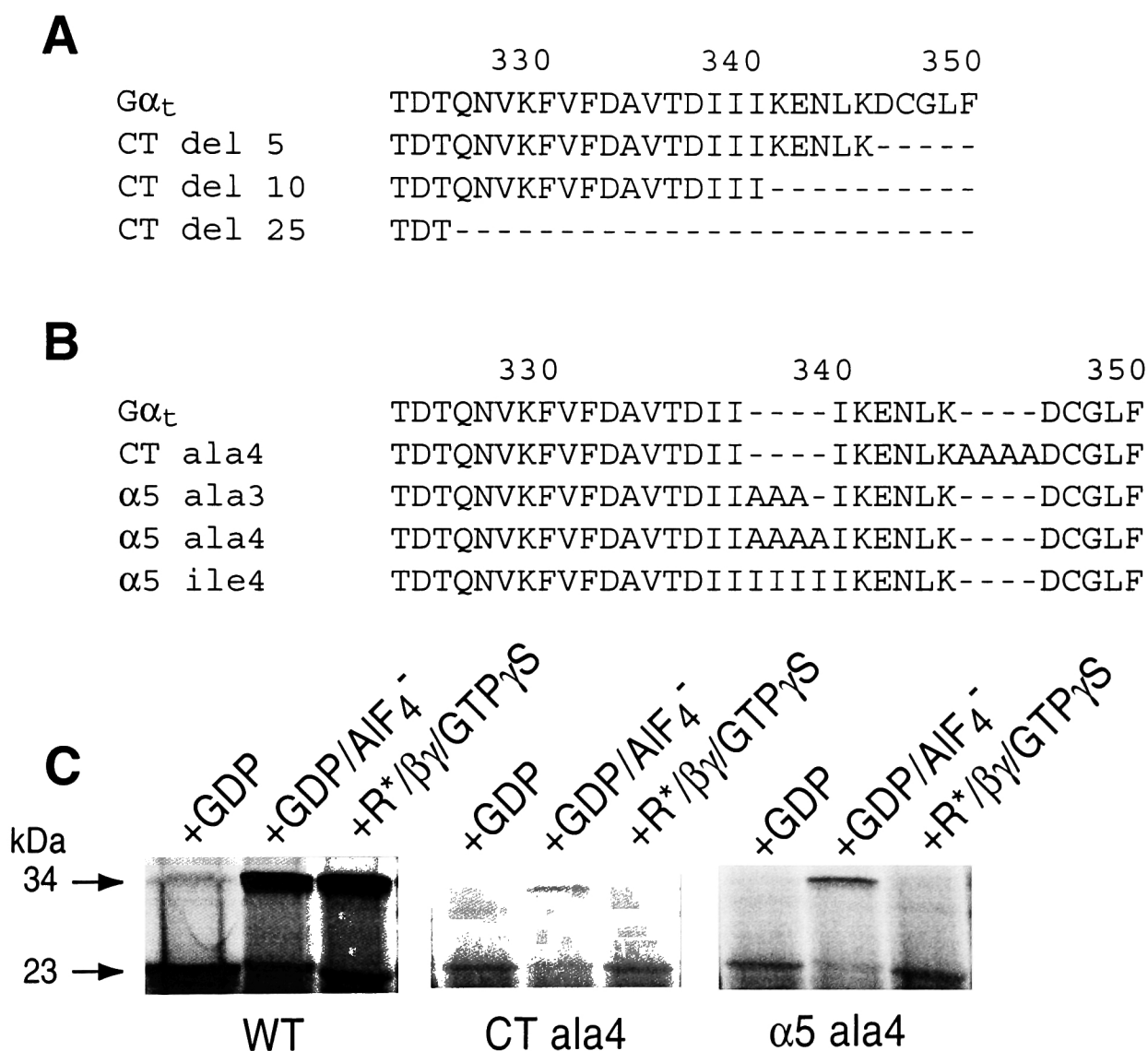


FIG. 6-3. Truncation and insertion mutants of $G\alpha_t$. **A.** Sequence alignment of truncation mutants of the carboxyl terminus of $G\alpha_t$. **B.** Sequence alignment of insertion mutants of $G\alpha_t$. **C.** Trypsin proteolysis of wild-type (WT), CT ala4, and $\alpha 5$ ala4 following treatment with GDP, GDP/ AlF_4^- , or $R^*/G\beta\gamma_t/GTP\gamma S$ (20 min incubation). The ala4 insertion mutants were resistant to activation by rhodopsin and $GTP\gamma S$.

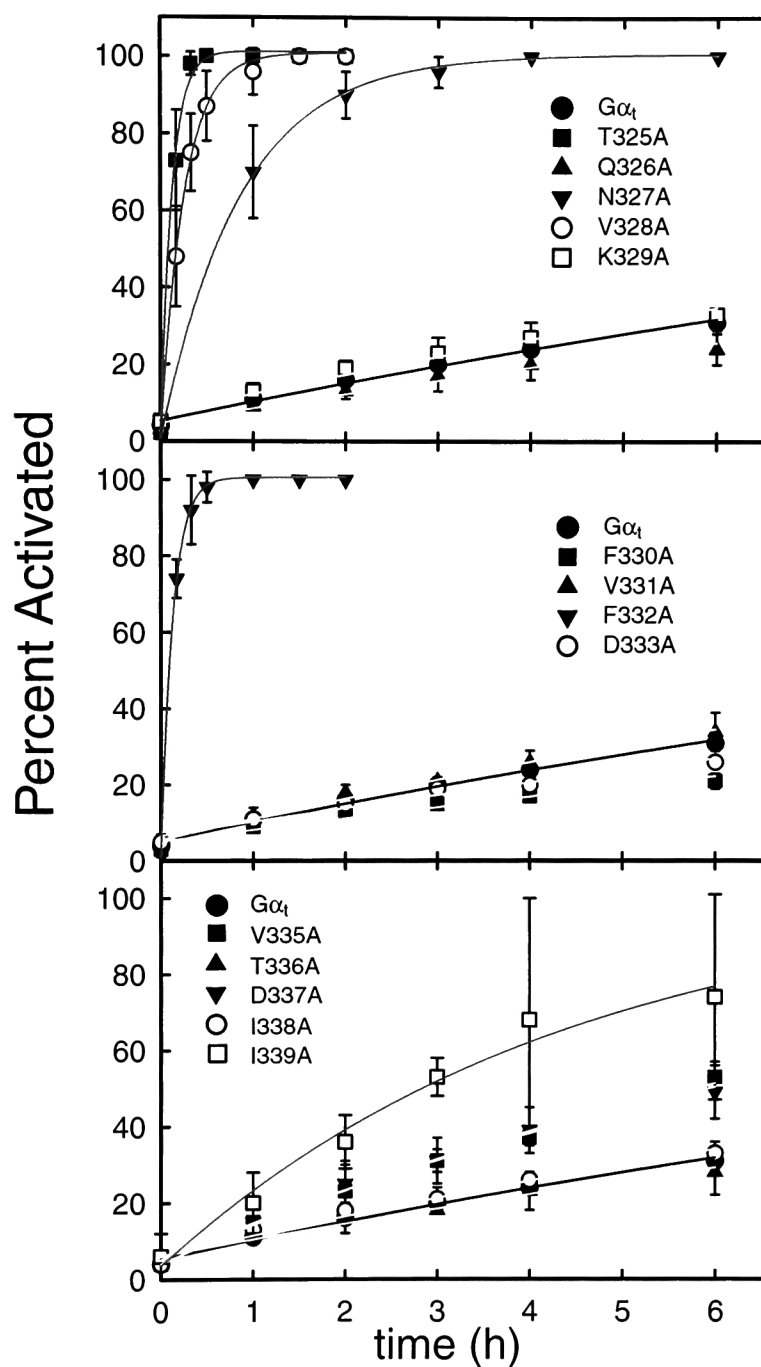


FIG. 6-4. Uncatalyzed nucleotide exchange time courses of alanine mutants in $\alpha 5$. Experiments were performed as described in Fig. 6-2 A.

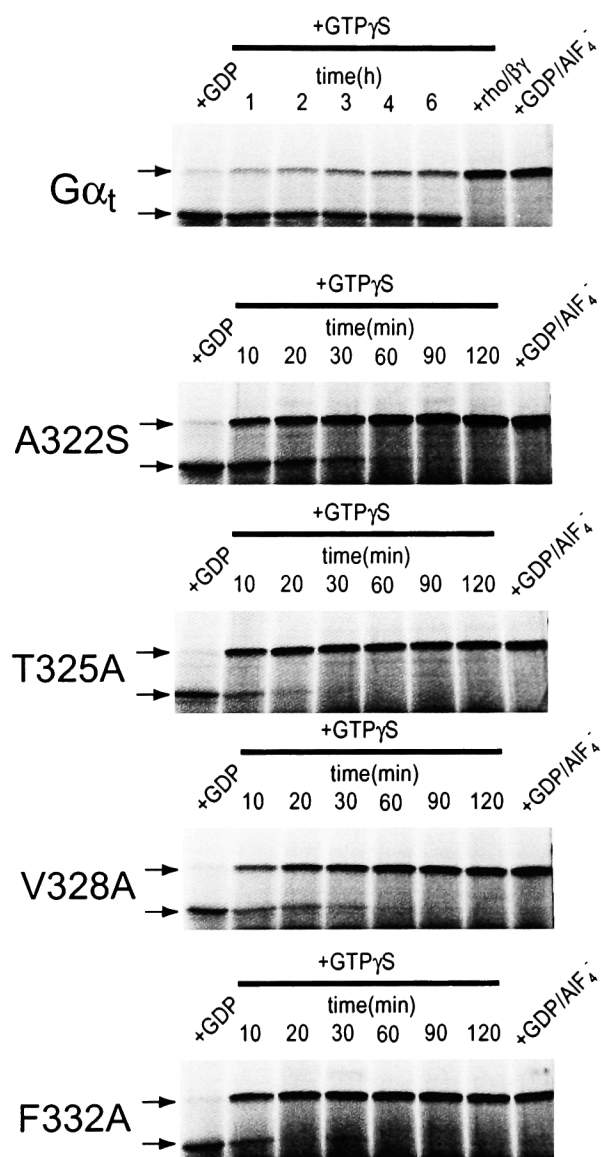


FIG. 6-5. Trypsin digest analysis of wild-type, A322S, and the rapidly activating alanine mutants (T325A, V328A, and F332A). The arrows indicate the position of the ~ 34 and ~ 23 kDa bands. All the mutants displayed patterns of trypsin digestion identical to wild-type in the presence of GDP, $GTP\gamma S$, and GDP/AlF_4^- , which suggests that the tertiary structure of the proteins is not grossly altered.

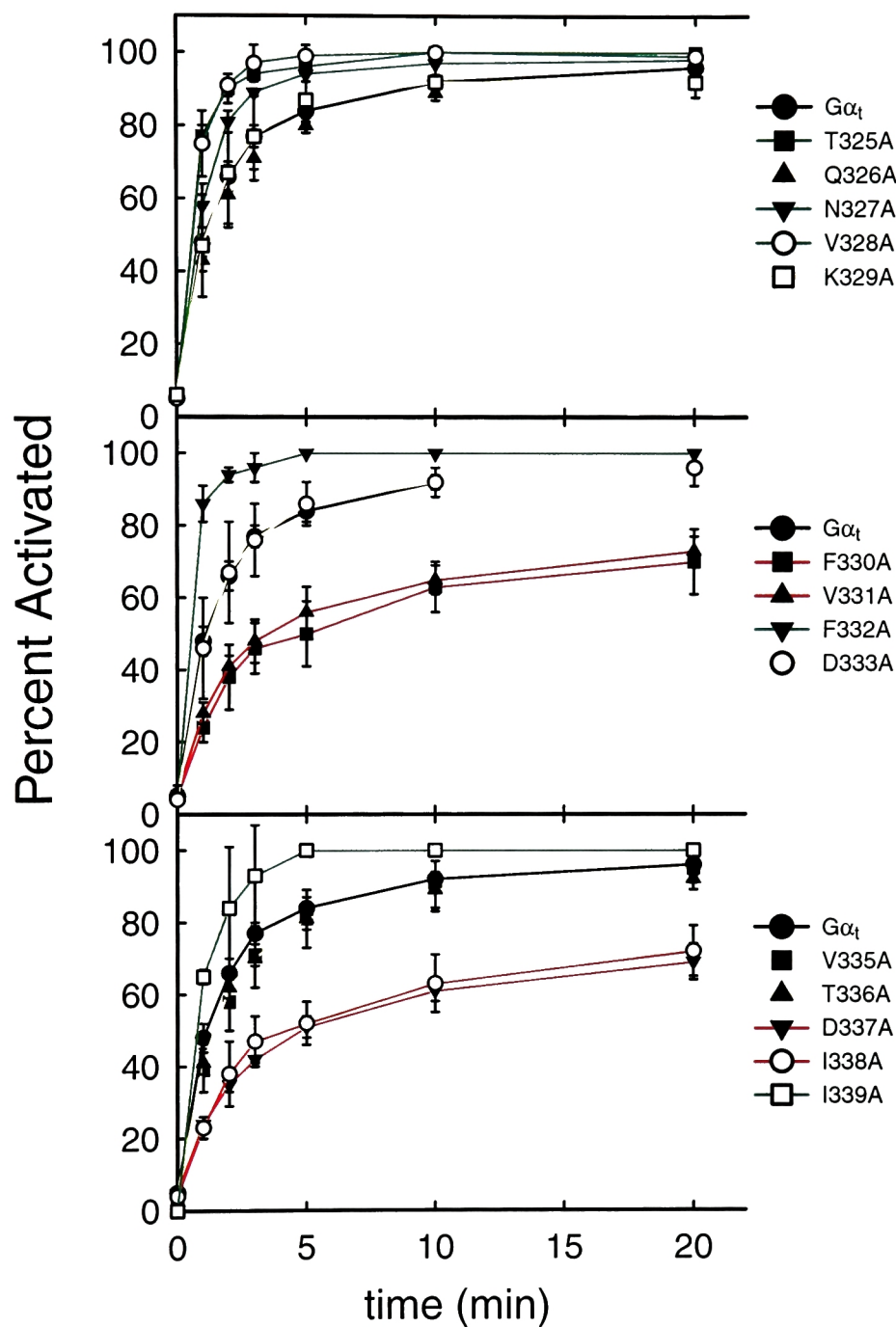


FIG. 6-6. $R^*/G\beta\gamma_t$ -catalyzed nucleotide exchange time courses of alanine mutants in $\alpha 5$. Experiments were performed as described in Fig. 6-2 B.

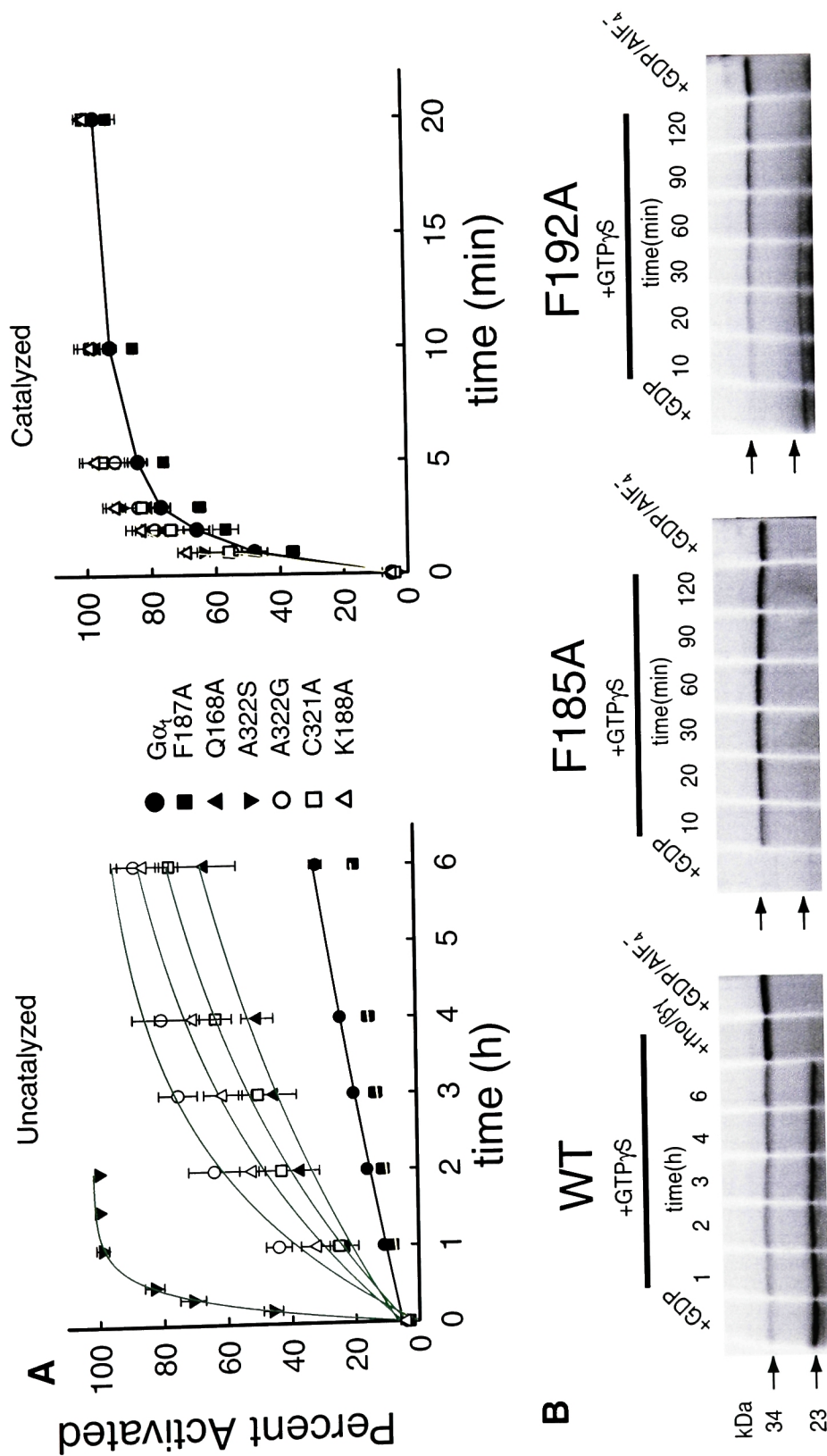


FIG. 6-7. Nucleotide exchange time courses of mutants of residues near $\alpha 5$ and in the $\beta 6/\alpha 5$ loop. A. Mutations were prepared in several residues that interact with the $\alpha 5$ helix or which are part of the $\beta 6/\alpha 5$ loop. Assays were conducted as in Fig. 6-2. **B.** Mutation of residues F185 and F192 led to disruption of the normal ~ 23 kDa band produced by GDP-bound $G\alpha_t$. Representative gels visualized by phosphorimaging from experiments with F185A, F192A, and WT suggest that the rate of GTP γ S binding, as indicated by the change in intensity of the ~ 34 kDa band, is much faster than WT.

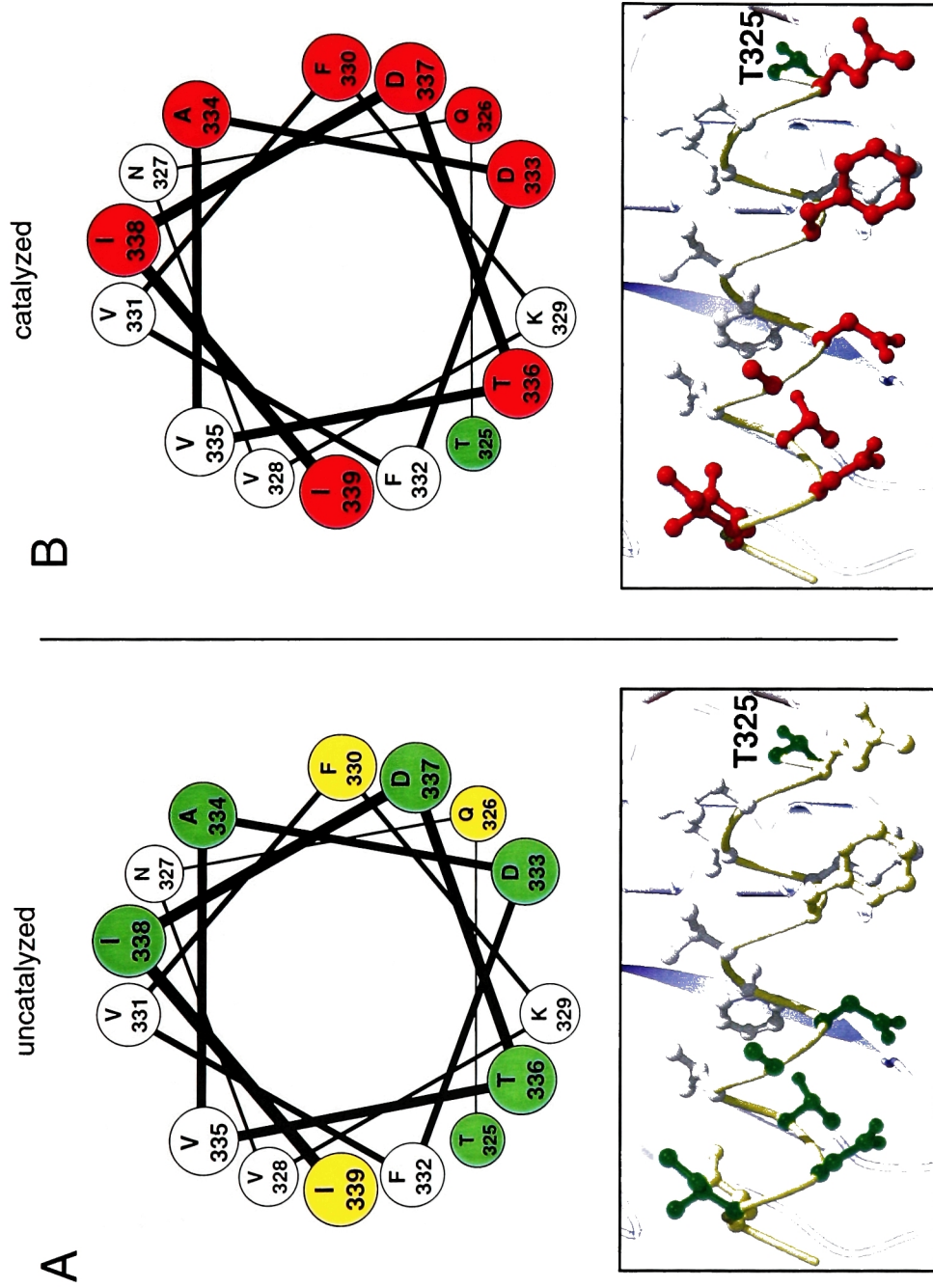
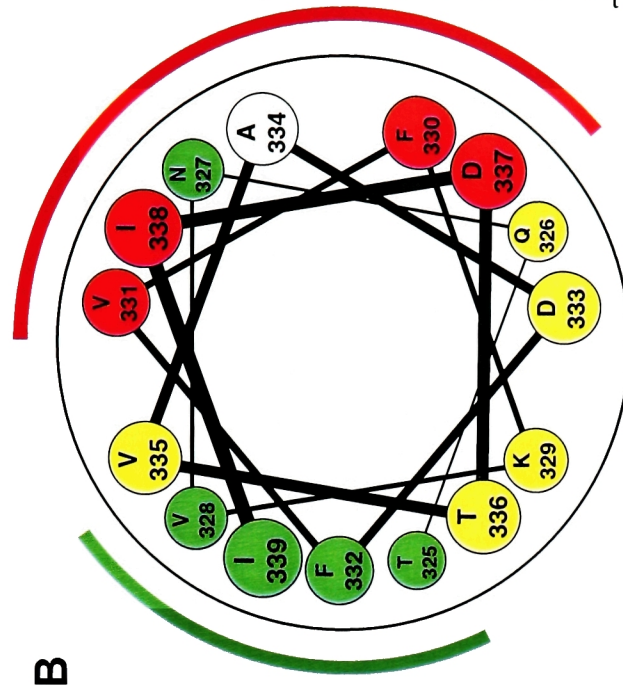
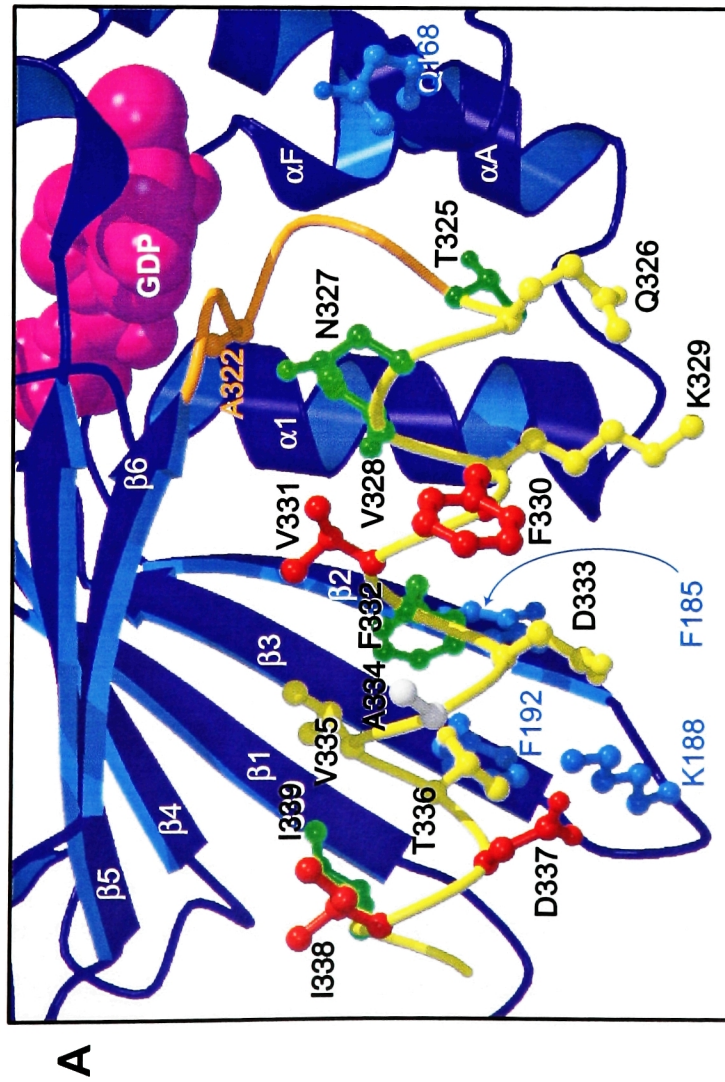


FIG. 6-8. Schematic representation of the phenotypes of proline mutants in $\alpha 5$. *Top*, helical wheel representation of $\alpha 5$, as viewed in Fig. 6-1B; *bottom*, close-up of the structure of $\alpha 5$. Residues are color-coded by phenotype: mutants similar to WT are yellow, those exhibiting rates faster than WT are green, and those slower than WT are red. Residues colored white did not yield functional proteins when mutated to proline. **A.** Uncatalyzed rates. **B.** Rhodopsin/ $G\beta\gamma$ -catalyzed rates.

FIG. 6-9. Schematic representation of the phenotypes of alanine mutants in $\alpha 5$: a model for R^* -catalyzed G_t activation . *A*, Close-up view of the $\alpha 5$ region. Most of the residues mutated in this study are shown in ball-and-stick representation. Within the $\alpha 5$ helix, residues that led to increases in both basal and R^* -catalyzed nucleotide exchange rates when substituted with alanine are colored green; residues that led to decreases in R^* -catalyzed exchange rate when substituted with alanine are colored red; and residues that were indistinguishable from wild-type when substituted with alanine are yellow. Also shown are residues which interact with $\alpha 5$ (blue). Mutation of these residues lead to increases in the basal nucleotide exchange rate. *B*, Helical wheel representation of the $\alpha 5$ helix, as viewed in Fig. 6-1B. The coloring is the same as in panel *A*. The sites of mutations that caused increases in both basal and R^* -catalyzed nucleotide exchange map predominantly to a buried surface of the helix. The sites of mutations that caused impairment of R^* -catalyzed nucleotide exchange map to a solvent exposed hydrophobic patch (including V331, I338, A334 and F330) adjacent to the buried surface of $\alpha 5$. Hydrophilic residues that map to the "bottom" of the helix did not affect either basal or R^* -catalyzed nucleotide exchange when replaced with alanine. Together, the data provide evidence that R^* catalyzes nucleotide exchange by perturbing the conformation of residues on the buried surface of $\alpha 5$ (green line). These residues communicate with the nucleotide-binding pocket. The perturbation may result from direct binding of R^* to the exposed hydrophobic surface of $\alpha 5$ (red line).



Discussion

The $\alpha 5$ helix has been proposed to mediate the effects of R^* on $G\alpha_t$ (Onrust *et al.*, 1997). This role was suggested by its location as a link between the carboxyl-terminal tail of $G\alpha_t$, which binds to R^* , and the nucleotide-contacting $\beta 6/\alpha 5$ loop. To test this hypothesis, we prepared a large set of $G\alpha_t$ mutants in the $\alpha 5$ helix and surrounding regions. The mutants were expressed *in vitro*, and the kinetics of nucleotide exchange, both uncatalyzed and R^* -catalyzed, were determined directly by quantitative analysis of trypsin digestions of $G\alpha_t$.

Alterations of the Structure of the $\alpha 5$ Helix by Site-Directed Mutagenesis Disrupted R^ -Catalyzed Activation*

One set of mutations in $G\alpha_t$ was designed to introduce structural perturbations into $\alpha 5$. If $\alpha 5$ were indeed involved in coupling R^* to the nucleotide binding pocket, then one would predict that structural alteration on $\alpha 5$ would lead to reduced R^* -catalyzed activation rates. Additionally, one might predict that structural alterations in $\alpha 5$ would lead to increases in basal nucleotide exchange since the natural structure of $\alpha 5$ has evolved for low nucleotide exchange in the absence of R^* .

Prolines frequently introduce kinks into α helices, which bend away from the side of the helix containing the proline (Woolfson and Williams, 1990). The kinks arise because the side chain of proline bonds covalently to the backbone nitrogen, and disrupts the typical pattern of hydrogen bonding in α helices between the backbone oxygen of position n and the backbone nitrogen of position $n+4$. Thus prolines in positions 325-328 would not be expected to induce kinks per se since the $n-4$ residue does not exist; however, several of these mutations do appear to alter the structure of $G\alpha_t$ by other means. Proline substitutions at a variety of positions on the $\alpha 5$ helix, predominantly on the buried surface, severely diminished nucleotide binding in general (Fig. 6-8).

Possibly, prolines in some of these positions caused bending of the helix away from the rest of $G\alpha_t$ so as to disrupt a large number of intramolecular contacts and to interfere with protein folding and/or stability.

Among the proline mutants that were capable of binding GDP, increases in uncatalyzed nucleotide exchange rates were generally observed (Fig. 6-2A). This is consistent with the involvement of the $\alpha 5$ helix in interacting with the nucleotide binding pocket. In many cases, these effects were likely due to structural perturbation of $\alpha 5$, as opposed to disruption of contacts involving the substituted amino acid. For example, placement of alanines at the same positions generally did not cause the same phenotype as the prolines (with the exception of T325). Furthermore, in contrast to the alanine mutants (see below), the sites on $\alpha 5$ where substitutions with proline increased basal nucleotide exchange rates were not restricted to a particular surface of the helix (Fig. 6-8A). In addition, the effect on basal activation rates was most pronounced for replacement with proline of residues in the middle of the helix (Fig. 6-8). Kinks in the middle of the helix would be predicted to be most disruptive of interactions between $\alpha 5$ and the rest of $G\alpha_t$. Proline mutants at the carboxyl terminus of the helix had a milder phenotype, plausibly because kinks at this sites were less disruptive to $G\alpha_t$ structure.

The proline mutants, with the exception of T325P, were generally partially defective in their response to R^* -catalyzed activation (Fig. 6-2B, 6-8B). These mutants were not likely to be defective in binding to $G\beta\gamma_t$, since the site of the mutation was on the opposite side of $G\alpha_t$ from the known $G\beta\gamma_t$ binding surface. The substitution of $\alpha 5$ residues with prolines seem to induce conformations in the $\alpha 5$ helix that disrupt communication between R^* and the nucleotide; this result is further evidence for the involvement of $\alpha 5$ in mediating R^* -catalyzed activation.

As in the uncatalyzed assay, the effects of the prolines in the catalyzed assay seem to result from structural perturbations of $\alpha 5$ and not merely from disruption of contacts involving the substituted amino acid. For example, the proline mutants of a given position were generally more defective in R^* -catalyzed activation than were the corresponding alanine mutants. In addition, the sites on $\alpha 5$ where proline substitution led to disruption of R^* -catalyzed activation were not restricted to a particular surface of $\alpha 5$ (Fig. 6-8B). The defect in R^* -catalyzed activation of the proline mutants increased as the proline was placed at positions progressively closer to the carboxyl terminus of the $\alpha 5$ helix. For example, the Q326P mutant was only mildly defective, whereas the I338P mutant was nearly unresponsive to activation by R^* (Fig. 6-2B). This phenomenon might relate to the fact that the alteration in the relative alignment of $\alpha 5$ and the R^* binding site on the 340-350 region would be expected to be larger as the site of the kink moved closer to the 340-350 region-- i.e., closer to the carboxyl terminus of $\alpha 5$.

Additional alterations of the $\alpha 5$ helix, in the form of insertion and deletion mutants, were tested (Fig. 6-3). In general, such manipulations interfered with the folding and/or nucleotide binding of the resulting mutant proteins. Previously, it was reported that deletion of just the carboxyl terminal amino acid (F350) from $G\alpha_t$ eliminated nucleotide binding (Osawa and Weiss, 1995). In contrast, a related G protein, $G\alpha_o$, was reported to tolerate a variety of deletions (Denker *et al.*, 1992). It is not clear why $G\alpha_t$ is more sensitive than $G\alpha_o$ to deletions, but it might relate to the general difficulties in heterologously expressing functional $G\alpha_t$.

For the $G\alpha_t$ insertion constructs that did yield interpretable data, $\alpha 5$ ala4 and CT ala4, trypsin digests indicated that the proteins could bind GDP and become activated in the presence of GDP/AlF_4^- . However, $R^*/G\beta\gamma_t$ could not induce $GTP\gamma S$ uptake in these mutants (Fig. 6-3). It is possible that these mutants could not bind $GTP\gamma S$ (uncatalyzed $GTP\gamma S$ uptake was not tested), but it seems more likely that the mutations caused a

specific defect in R^* interactions. The CT ala4 mutant would be expected to have disruptions in the R^* -binding site at positions 340-350 of $G\alpha_t$, and thus might not bind to R^* . However, the 340-350 region in the mutant $\alpha 5$ ala4 would not be expected to be altered by the mutation. The phenotype of the $\alpha 5$ ala4 mutant suggests that R^* might need to interact not only with the 340-350 region of $G\alpha_t$, but also with additional sites amino-terminal to I440. The binding of these latter sites might be disrupted by the insertion of four alanines following I339. Binding between R^* and residues in the 330-338 region are also suggested by alanine substitution mutants (see below).

Mutations of the $\beta 6/\alpha 5$ Loop Increased Basal Nucleotide Exchange Rates

Several mutations of the nucleotide-contacting $\beta 6/\alpha 5$ loop have been described in other G protein subtypes as accelerating GDP release. A322 is highly conserved in both monomeric and heterotrimer G proteins. The mutation of this alanine to serine was first described (Iiri *et al.*, 1994) as a naturally occurring mutant of $G\alpha_s$ (A366S) found in patients with a combination of both gain and loss of endocrine function, in the form of testitoxycosis (gain) and pseudohypoparathyroidism type Ia (loss). Characterization *in vitro* of this mutant, as well as analogous mutants in $G\alpha_i$ (Posner *et al.*, 1998) and G_t (Garcia *et al.*, 1995) showed in all cases that the mutation accelerated uncatalyzed nucleotide exchange rates. This mutant has therefore been described as an approximation of the receptor-bound state (Posner *et al.*, 1998). In the case of $G\alpha_s$, this mutant was also found to be temperature sensitive. Hence the paradoxical disease phenotype was caused by high levels of receptor-independent activation of $G\alpha_s$ in the relatively cool environment of the testis, and loss of $G\alpha_s$ signaling due thermolability in the higher-temperature environment of the body.

The C321A mutant was previously reported to decrease the affinity for GDP in an equivalent mutant of $G\alpha_o$ (Thomas *et al.*, 1993). Our results confirm the finding of rapid GDP release rates in A322S and C321A mutants of $G\alpha_t$, as well as demonstrate an

increased GDP dissociation rate in A322G. Together, these mutants suggest that a variety of perturbations of conserved regions in the $\beta 6/\alpha 5$ loop can induce increased GDP release in $G\alpha_t$. Additionally, we demonstrate that receptor-catalyzed activation of $G\alpha_t$ is not impaired by mutation of the $\beta 6/\alpha 5$ loop (Fig. 6-7). These results are consistent with the previously proposed role of the $\beta 6/\alpha 5$ loop and of the $\alpha 5$ helix in R^* -catalyzed nucleotide exchange.

Identification of Nucleotide-Release Control Microdomain on the $\alpha 5$ Helix

Replacement of several residues in the $\alpha 5$ helix to alanine resulted in a gain-of-function phenotype, namely a marked (up to 165-fold) increase in the rate of uncatalyzed nucleotide exchange. These rates are comparable to or in excess of the basal exchange rate of mutant A322S (63-fold increase) (Table 6-I). These results suggest that alteration of the $\alpha 5$ helix, which is distant from the nucleotide, can accelerate GDP release to even a greater degree than replacement of amino acids known to be in direct contact with the nucleotide. Together the residues T325, V328 and F332, which cluster on an inward facing quadrant of $\alpha 5$ (Fig. 6-9), constitute a potent nucleotide-release control microdomain.

Significantly, mutations in the $\alpha 5$ nucleotide-release control region do not destroy the basic nucleotide-binding and conformational properties of $G\alpha_t$ (Fig. 6-5). Preservation of the patterns of trypsin digestion indicates that the overall folding patterns of the mutants are similar to that of wild-type $G\alpha_t$. Each of the mutants is capable of binding GDP and $GTP\gamma S$, and of being activated by GDP/AlF_4^- . The mutants also are responsive to rapid activation by R^* (Fig. 6-6). Together, these data suggest that the mutations do not merely disrupt folding of the protein, but that they induce conformations that anticipate, or at least are compatible with, the R^* -bound conformation. This contrasts with several of the proline mutants, which displayed increased basal activation rates, but reduced R^* -catalyzed rates.

T325 is located in the first turn of the $\alpha 5$ helix immediately adjacent to the $\beta 6/\alpha 5$ loop (Fig. 6-9A). An extensive network of hydrogen bonds maintains the arrangement of this first helical turn. Mutation of the sidechains in this region would be expected to disrupt some of these hydrogen bonds, and alter the structure of the first turn and possibly of the $\beta 6/\alpha 5$ loop. The T325P mutant also displayed accelerated basal activation rates. Mutation of N327, which is also located in the first turn of $\alpha 5$, resulted in an increase in the non-catalyzed activation rate (Fig. 6-2).

Two other residues, F332 and V328, point in towards the center of the molecule and contribute to the hydrophobic core of the protein (Fig. 6-9A). F332 and V328 make extensive hydrophobic contacts with residues from the $\alpha 1$ helix, as well as the $\beta 2$ and $\beta 3$ sheets. Loops emanating from these structural elements contribute to the canonical nucleotide-binding surfaces of $G\alpha_t$ (Sprang, 1997). Replacement of F332 or V328 by alanine may alter the packing of the hydrophobic core of the protein, including the $\beta 2$ and $\beta 3$ sheets and the $\alpha 1$ helix, such that a conformational change is communicated to the nucleotide-binding pocket.

The F332A mutant was previously studied in microsomes prepared from transiently-transfected COS cells (Onrust *et al.*, 1997). In this assay system, it was described as being impaired in a rhodopsin activation assay. However, in the same study this mutant was found to bind to rhodopsin normally in an assay based on *in vitro* translated material. The rate of noncatalyzed activation was not assessed and the origins of these apparent inconsistencies were not clear.

Amino acids V328 and F332 are extremely conserved, not only in heterotrimeric G protein α subunits, but also among monomeric G proteins of the Ras superfamily (Valencia *et al.*, 1991). A mutant of the analog of F332 in Ras, F156L, was found to have transforming properties *in vivo* and to greatly accelerate the rate of nucleotide

release *in vitro* (Quilliam *et al.*, 1995). NMR studies of this mutant revealed that the structures of $\alpha 1$, $\alpha 5$ and $\beta 1$ - $\beta 3$ were altered. The mutation did not appear to reduce the stability of the protein, apparently due to induction of new intramolecular contacts not present in the wild-type version (Quilliam *et al.*, 1995).

Interactions Between the $\alpha 5$ Helix and the Rest of $G\alpha_t$

Since the $\alpha 5$ helix contains elements that, when perturbed, dramatically increase the GDP release rate, one would expect that $\alpha 5$ must be held in a very specific conformation to avoid inappropriate release of GDP. Thus, there should exist specific contacts between the $\alpha 5$ helix and the rest of the protein necessary to maintain such a conformation. In fact, mutation of a variety of residues located at different positions of $G\alpha_t$ that interact with the $\alpha 5$ helix do moderately increase the uncatalyzed nucleotide exchange rate (Fig. 6-7, 6-9). In particular, alanine substitution at positions Q168, F185, K188 or F192 lead to increases in nucleotide-exchange rate. Q168, which is located on αF of the helical domain, hydrogen bonds with the main chain carbonyl of T323. K188, which extends from a loop between $\beta 2$ and $\beta 3$ appears to form ionic interactions with two aspartic acid residues on the $\alpha 5$ helix, D333 and D337. These interactions likely serve to maintain the proper register of the $\alpha 5$ helix with respect to the rest of the protein. F185 and F192, which are located on $\beta 2$ and $\beta 3$ respectively, are part of a phenylalanine cluster which lies adjacent to F332. These contacts may serve both to stabilize the local tertiary structure near the $\alpha 5$ helix, to sense alterations in the position of F332 and to communicate structural changes on to the nucleotide-binding pocket. This latter role is suggested by the structural changes observed in $\beta 2$ and $\beta 3$ in NMR studies of the F156L mutant in Ras (Quilliam *et al.*, 1995).

It has been previously suggested that interactions between the carboxyl terminus of the $\alpha 5$ helix and the rest of the protein are important for mediating the basal rate of nucleotide exchange (Denker *et al.*, 1992; Denker *et al.*, 1995; Natochin *et al.*, 2000).

We suggest that these contacts, like those discussed above, contribute to the stability of amino acid side chains at the amino terminus of $\alpha 5$. Weakening of these contacts, as in the I339A mutant, moderately accelerated GDP release (Table 6-I), in agreement with previous results. However, the magnitude of the increase in GDP release resulting from these mutations is very small (~4-fold) compared with mutations closer to the amino terminus of $\alpha 5$.

A Mechanistic Model of R-Catalyzed Nucleotide Exchange*

Previously, it has been suggested that rhodopsin might induce GDP dissociation by deforming the $\beta 6/\alpha 5$ loop via $\alpha 5$ (Onrust *et al.*, 1997). The data in this study are consistent with this hypothesis. Mutations predicted to alter the structure of $\alpha 5$ disrupted R*-catalyzed nucleotide exchange, and a variety of mutants in the $\beta 6/\alpha 5$ loop were found to increase basal activation rates in $G\alpha_t$, as had been previously reported in related G proteins.

The identification of a potent nucleotide-release control region in the $\alpha 5$ helix of $G\alpha_t$ allows refinement of this hypothesis. The replacement of T325, V328 and F332 with alanine mimics the effects of R* binding on $G\alpha_t$ in several key respects. The rate of GDP dissociation is tremendously increased, the primary perturbation is at a distance from the nucleotide-binding site, and the overall structure and function of the protein is preserved. Thus the data in this chapter suggest that $\alpha 5$ may not merely serve as a conduit between R* and the $\beta 6/\alpha 5$ loop, but that perturbation of the nucleotide-release control region (T325, V328 and F332) on $\alpha 5$ itself by R* would be sufficient to induce rapid nucleotide exchange "at-a-distance."

Evidence that R* does in fact use this mechanism comes from alanine mutations in a F330, V331, D337 and I338 (Fig 6-9). These mutations did not affect the rate of basal activation, but they all decreased R*-catalyzed activation kinetics ~3-4 fold (Fig. 6-4B).

Since the mutations did not completely abolish activation by R^* , the functions of these residues may be partially redundant. The overall structures of these mutant proteins were not significantly disturbed as indicated by trypsin proteolysis patterns and basal nucleotide exchange rates that were similar to wild-type $G\alpha_t$ (Table 6-I and not shown). The mutations were unlikely to affect interactions with $G\beta\gamma_t$, which is known to bind to the opposite face of $G\alpha_t$ from $\alpha 5$ (Lambright *et al.*, 1996). The most direct interpretation of these loss-of-function results is that F330, V331, D337 and I338 make important contacts in the R^* - $G\alpha_t$ complex, and that these contacts are disrupted by the substitutions with alanine.

In the absence of R^* , these residues do not appear to be involved in any contacts that are relevant to nucleotide exchange rates, as indicated by the crystal structure and the basal nucleotide exchange rates of the corresponding mutants (Fig. 6-4, Table 6-I). In particular, F330 is more than 4 Å from any other residue. Thus, the formation of important contacts involving F330, V331, D337 and I338 in the R^* -bound conformation necessitates a R^* -induced conformational change in $\alpha 5$. Consistently, a site-directed spin labeling study with $G\alpha_t$ demonstrated that R^* -induced conformational changes occur in a similar set of residues at the amino terminus of $\alpha 5$ corresponding to Q326, N327 and F330 of $G\alpha_t$ (W. Hubbell, personal communication).

Since R^* appears to induce conformational changes at V331 and F330 and other residues of $\alpha 5$, it is plausible that R^* also alters the T325/V328/F332 region on the adjacent face of the $\alpha 5$ helix (Fig. 6-9). This is evidence that R^* does in fact catalyze nucleotide exchange at-a-distance by perturbing the T325/V328/F332 region and by exploiting the built-in structural connection between these residues and the nucleotide-binding pocket of $G\alpha_t$. Subsequent alteration of the $\beta 6/\alpha 5$ loop as previously hypothesized could also occur (Onrust *et al.*, 1997).

The proposed conformational changes of T325, V328 and F332 induced by binding of R^* need be only subtle to induce nucleotide exchange. Since mutation of each residue by itself led to a dramatic increase in nucleotide exchange rate, even a minor structural perturbation of more than one residue simultaneously by R^* would be expected to produce a potent effect on the nucleotide exchange rate. As a precedent, the 2.6 Å-resolution crystal structure of the $G\alpha_i$ A326S mutant heterotrimer (analogous to A322S in $G\alpha_t$) did not reveal any significant structural alterations although the nucleotide exchange rate was dramatically increased (Posner *et al.*, 1998).

Some or all of the contacts involving F330, V331, D337 and I338 that are inferred to exist in the R^* -bound conformation may result from direct binding of R^* to $\alpha 5$. The amino acid residues F330, V331, D337 and I338 map to a conspicuous solvent-exposed, yet predominantly hydrophobic surface of the $\alpha 5$ helix (Fig. 3). This surface is contiguous with the carboxyl-terminal region (amino acids 340-350), a well-documented R^* -binding domain. Furthermore, the placement of either prolines in $\alpha 5$ or a four alanine insertion following I339 diminished R^* -catalyzed activation (see above). These results are consistent with a R^* binding surface that extends to include parts of $\alpha 5$. Thus, the exposed surface of $\alpha 5$ may be part of the R^* -binding region on $G\alpha_t$, as has been previously suggested (Lichtarge *et al.*, 1996; Onrust *et al.*, 1997).

The data are also consistent with the possibility that R^* indirectly induces the formation of *intramolecular* contacts involving F330, V331, D337 and I338 or a subset thereof. In this scenario, R^* would induce changes in the amino terminus of $\alpha 5$ by binding to other sites on the protein, such as the carboxyl terminal region. As a speculative example, R^* might induce a counterclockwise rotation of $\alpha 5$ such that the exposed hydrophobic surface of $\alpha 5$ would become buried, and contacts between F330, V331, D337 and I338 would form with the mostly hydrophobic residues in the core of $G\alpha_t$. Such a rotation would of course also displace T325, V328, and F332 on the inside

surface of $\alpha 5$. Additional experiments are needed to conclusively determine whether the interactions between R^* and $\alpha 5$ are direct or indirect.

Conclusions

The data in this report support a significant role for the $\alpha 5$ helix in the mechanism of R^* -catalyzed $G\alpha_t$ activation. Mutations predicted to disrupt the structure of $\alpha 5$ reduced R^* -catalyzed nucleotide exchange rates. Furthermore, the $\alpha 5$ helix itself was found to contain residues that when mutated tremendously increased the GDP dissociation rate. These mutations, in residues F332, V328, and T325, mimic the receptor bound conformation in that the nucleotide exchange rate is very high, the primary perturbation is at a distance from the nucleotide binding pocket, and the overall integrity of the protein is maintained. Thus, R^* needs only to distort the local structure of the $\alpha 5$ helix to achieve catalysis of nucleotide exchange. R^* is known to bind to the adjacent carboxyl terminus of $G\alpha_t$. R^* may also bind directly to $\alpha 5$, as suggested by the results of substitution of exposed residues in $\alpha 5$ with alanines or prolines, or the insertion of alanines after I339. Together, these results strongly suggest that R^* achieves GDP-nucleotide release "at-a-distance" by perturbing the $\alpha 5$ helix.

Chapter 7: Perspectives

The fourth loop of rhodopsin in context of the rhodopsin crystal structure

The experiments described in Chapters 3 and 4 were performed, analyzed, and published (Marin *et al.*, 2000; Ernst *et al.*, 2000) before the crystal structure of rhodopsin became available (Palczewski *et al.*, 2000). The structure does not alter any of the central conclusions from those studies. However, the new structure allows for a re-evaluation of the results in Chapters 3 and 4.

Helix 8

One of the more surprising features of the crystal structure of rhodopsin was the presence of an additional helix, the non-transmembrane Helix 8 (H8) (Fig. 7-1). H8 was not accurately predicted by earlier structural studies of C4 based on site directed spin labeling (Altenbach *et al.*, 1999) and NMR analysis of peptides (Yeagle *et al.*, 1996). This helix involves residues 312-321 in the C4 region. It is separated from TM 7 by a short linker, consisting of M309 to K311. The helix runs approximately parallel to the hypothetical intracellular membrane surface, and roughly perpendicular to TM 7. H8 points out from the helix bundle and increases the size of the cytoplasmic surface of rhodopsin. The helix is amphipathic and cationic; hydrophobic residues F313, M317, and L321 point in toward the lipid bilayer, parallel to the TM helices. Additionally, there is a highly conserved arginine in H8, which extends outward such that it could interact with negatively charged phospholipids. C322 and C323 are positioned such that attached palmitoyl groups, which are not included in current crystal structure model, could insert into the bilayer as predicted (Moench *et al.*, 1994). Sequence analysis of related GPCRs reveals that hydrophobic residues are frequently conserved in positions 313, 317, and 321, suggesting that the presence of an amphipathic, membrane associated H8 may be a conserved feature of related receptors.

The structure of H8 is redundant: 3 separate hydrophobic residues plus the 2 palmitoyl groups contribute to the formation and orientation of the amphipathic helix. Therefore, neither point mutations, chimeras with other related receptors, nor removal of the palmitoyl groups is guaranteed to effectively disrupt the H8 structure. For example, none of our the chimeric rhodopsin constructs CTr1, CTr2, CTr3, or CTr4 are likely to disrupt H8, since in all cases the amphipathic pattern is preserved.

The role of the helix itself in G_t activation is unclear. Truncation of rhodopsin following position 315 was reported to activate G_t normally (Weiss *et al.*, 1994). This mutation would destroy H8, but it did not affect signaling. Additionally, the studies conducted in Chapter 3, and well as those from another group (Cai *et al.*, 1999), suggest that the region of C4 that is important in activation of G_t is the amino-terminal region, which involves the linker between TM7 and H8, and only the first two amino acids of H8. Thus the majority of H8, despite its conservation, might not function in G_t activation. Additional studies of combinations of mutants designed to foil the redundancy in the stability of H8 structure, e.g., F313A/M317A/L321A, would clarify this point. Alternatively, mutations of two highly conserved residues, F313 and R314, which contribute directly to the cationic amphipathic nature of the helix should be explored. Neither of these residues was examined in our chimeras (Chapter 3) since they are conserved.

A likely possibility is that H8 serves to down-regulate the activity of rhodopsin in the dark state, perhaps by constraining the conformation of residues in the amino terminus of C4. The crystal structure of rhodopsin represents a conformation that does not interact with G_t . A conformational change in H8 upon MII formation might be required for efficient G_t activation. Light dependent changes in the structure of H8 have been suggested (Resek *et al.*, 1993; Yang *et al.*, 1996). Also supporting this hypothesis is the observation the depalmitoylation of rhodopsin leads to moderate hyperactivity (Chapter

3; (Morrison *et al.*, 1991)), as does truncation of C4 (Weiss *et al.*, 1994). Additionally, H8 is near the conserved NPXXY motif on TM7. Hydrogen bond interactions between this motif and residues on TM6 are hypothesized to be important in maintaining low dark and opsin activity (Palczewski *et al.*, 2000; Han *et al.*, 1998).

Structural predictions regarding the amino terminus of C4

We suggested (Chapter 3) that the amino terminus of C4 (residues 310-312) might interact with other parts of rhodopsin to contribute the G_t binding surface. The structure indicates that both N310 and Q312 are close to residues on TM 6 (E249) and the C1 loop (L68). Additional experiments with point mutations at these locations would be informative; perhaps it is disruption of these interactions involving 310 and 312 that are responsible for the reduction in G_t activation observed in two mutants of the 310-312 region, CTr2 and CTr4.

Also, we had speculated that 311 might be in the midst of a helical extension of TM 7, and that the proline placed there in CTr2 and CTr4 might disrupt this helix and cause the observed phenotype. This hypothesis proved inconsistent with the finding that the K311P point mutant activated G_t normally (Chapter 3). The structure reveals that 311 lies not in a helical extension of TM 7, but rather in a turn region between TM 7 and H8.

In Chapter 4, we hypothesized that replacement of the amino-terminal third of C4 with β_2 -AR sequence, as in CTr4, might disrupt interactions between the amino and carboxyl ends of C4. We speculated that these interactions could be restored by substitution of the entire C4 loop with amino acid sequence of the β_2 AR, as in CTr2. This possibility was raised to explain the fact that the $\gamma(50-71)$ -far peptide bound to CTr2 but not CTr4. However, the structure does not reveal any obvious reasons to support that hypothesis. The structural basis of the difference between the two mutants in binding to $\gamma(50-71)$ -far is not clear.

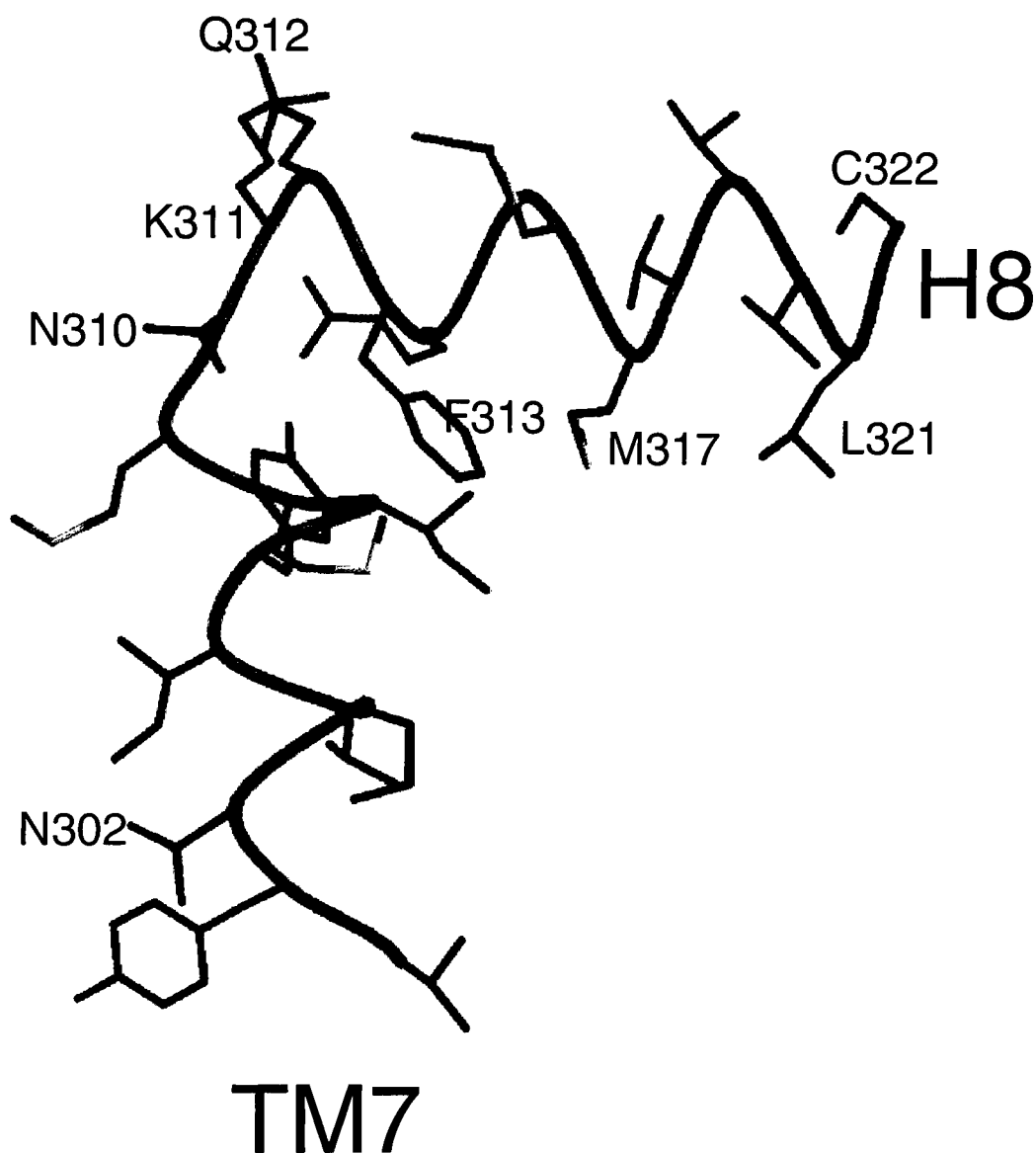


FIG. 7-1. Close-up of Helix 8 (H8) of rhodopsin. The amino terminus of TM7 and the C4 loop, which includes H8, are shown based on the crystal structure of rhodopsin (PDB code 1f88). The orientation is similar to Fig. 1-2. N302 of the conserved NPXXY motif is labeled as are certain residues in C4.

Rhodopsin— G_t interactions: the big picture

A Path of Interaction Between the Chromophore and the Nucleotide Binding Pocket

The data in this thesis partially delineate a path between the chromophore binding pocket of rhodopsin and the nucleotide binding pocket of $G\alpha_t$. This pathway represents a specific example of how information is transferred across distances within and between proteins. In Chapter 3, experiments with peptides and site-directed mutagenesis supported a specific role for the C4 loop of rhodopsin in interactions with G_t . In Chapter 4, a kinetic spectroscopic assay was used to demonstrate that the binding of both G_t and of a peptide derived from the extreme C terminus of $G\alpha_t$ were sensitive to mutation of the C4 loop. In Chapter 5, we found that mutations predicted to disrupt interdomain interactions did not alter either basal or R^* -catalyzed nucleotide exchange rates. In Chapter 6, we found that mutation of key residues on $\alpha 5$, which are located at a distance from the nucleotide, but adjacent to the carboxyl terminus and other probable rhodopsin binding sites, can dramatically increase the nucleotide exchange rate.

Together, the data support the following scenario. Information regarding the isomerization of the chromophore moves from the chromophore binding pocket to the cytoplasmic surface of rhodopsin, where conformational and electrostatic changes occur. The cytoplasmic surface of R^* then interacts with G_t , and in particular with the carboxyl-terminus of $G\alpha_t$, in a manner modulated by the amino terminus of C4. Interactions may also occur with the exposed surface of $\alpha 5$. As a result, the conformation of key residues at the amino terminus of $\alpha 5$ is altered. The altered structure of these residues (T325, V328, and F332) leads to structural changes in adjacent regions, such as the $\beta 6/\alpha 5$ loop and the $\beta 2$ and $\beta 3$ sheets. Ultimately, the nucleotide binding pocket is perturbed, culminating in the rapid release of GDP. Thus, the chromophore binding pocket of rhodopsin is functionally connected to the nucleotide binding pocket of $G\alpha_t$.

Additional structures of R^* and G_t are likely to participate in establishing the connection between the chromophore and the nucleotide. For example, interactions between the cytoplasmic surface of R^* and the carboxyl terminus of $G\alpha_t$ certainly involve structures besides C4, such as C2 and C3 (Acharya *et al.*, 1997). Other structures of $G\alpha_t$, such as the $\alpha 4/\beta 6$ loop, are also likely to participate in the complex (see Chapter 1). The interdomain cleft may open to facilitate the egress of GDP, although the opening per se does not appear to be an energetic barrier to nucleotide release as indicated by mutational analysis (Chapter 5).

The Possible Role of $G\beta\gamma_t$

A second path connecting the chromophore to the nucleotide may involve $G\beta\gamma_t$. Several authors have suggested that $G\beta\gamma_t$ does not merely facilitate R^* - $G\alpha_t$ binding, but rather is mechanistically involved in nucleotide exchange (Bohm *et al.*, 1997; Iiri *et al.*, 1998). Several key observations support this idea. First, $G\beta\gamma_t$ is known to be required for efficient rhodopsin-catalyzed activation of $G\alpha_t$ (Fung, 1983). Second, the site at which the guanine nucleotide exchange factors Ef-Ts and Sos bind their cognate monomeric G proteins, Ef-Tu and Ras, overlaps with the equivalent region on $G\alpha_t$ where $G\beta\gamma_t$ binds (Iiri *et al.*, 1998). In contrast, rhodopsin binds structures on the other side of the molecule. Third, several mutants have been identified in $G\beta_t$ which do not disturb $G\alpha_t$ - $G\beta\gamma_t$ interactions, or rhodopsin- G_t interactions, but which do interfere with rhodopsin catalyzed nucleotide exchange (Ford *et al.*, 1998). Possibly these mutants disrupt contacts necessary for the transmission of information from rhodopsin to the nucleotide binding pocket.

One attractive feature of the $G\beta\gamma_t$ dependent pathway is that the Switch I and Switch II regions, which mediate interactions with the $G\beta_t$ subunit, are flexible and adopt different conformations in the free GDP-bound $G\alpha_t$, the heterotrimeric GDP-bound, and the GTP γ S-bound conformations of $G\alpha_t$ (Bohm *et al.*, 1997). Therefore, in the empty

pocket conformation, it seems likely that a new conformation of the Switch I/II region could be induced. In contrast, the $\alpha 5$ region appears very rigid. However, only very small perturbations of the $\alpha 5$ helix (which might not be revealed in a crystal structure) could underlie the conformational shift necessary to induce GDP release.

Additional Questions

More detailed questions remain. For example it is not clear whether R^* induces the proposed conformational changes in $\alpha 5$ of $G\alpha_t$ via direct or indirect mechanisms. A complete answer to these questions will eventually require high resolution structural data for the complex. As discussed, the crystal structure of the complex between R^* and G_t is not known. A variety of studies, using mutational (Acharya *et al.*, 1997), genetic (Liu *et al.*, 1995) and crosslinking (Cai *et al.*, 2001; Itoh *et al.*, 2001) approaches, have sought to define specific point-to-point contacts between the R^* and G_t . For example, the results in this thesis suggest a specific interaction between C4 and the carboxyl termini of $G\alpha_t$ and $G\gamma_t$. These types of data serve as a starting point for the construction of models of the complex (Bourne, 1997). One vexing question that arises from the construction of these models, besides the aforementioned fact that rhodopsin needs to act "at a distance", is the apparent size mismatch between the cytoplasmic surface of rhodopsin and the R^* -interacting surface of G_t (Hamm, 2001; Kisselev *et al.*, 1999). The cytoplasmic surface of rhodopsin appears to be at best just barely large enough to simultaneously contact all the regions of G_t that are thought to interact with R^* . Thus several possibilities must be considered. First, there may be large conformational changes in rhodopsin or G_t (Kisselev *et al.*, 1995b; Kisselev *et al.*, 1999) or both upon complex formation. Second, it may be possible that some interactions between R^* and G_t occur sequentially, and not simultaneously (Kisselev *et al.*, 1999). Finally, it may be the case that the stoichiometry of the reaction is not 1:1, but rather 2 R^* : 1 G_t . A variety of recent experiments in related GPCRs (but not rhodopsin) have provided evidence that GPCRs can exist as dimers *in*

vivo (Bouvier, 2001). However, the functional importance of dimerization in G protein activation is unknown.

Reference List

- Abdulaev, N. G. and Ridge, K. D. (1998) Light-induced exposure of the cytoplasmic end of transmembrane helix seven in rhodopsin. *Proc. Natl. Acad. Sci. U. S. A.* **95**:12854-12859.
- Acharya, S. and Karnik, S. S. (1996) Modulation of GDP release from transducin by the conserved Glu134- Arg135 sequence in rhodopsin. *J. Biol. Chem.* **271**:25406-11.
- Acharya, S., Saad, Y., and Karnik, S. S. (1997) Transducin- α C-terminal peptide binding site consists of C-D and E- F loops of rhodopsin. *J. Biol. Chem.* **272**:6519-6524.
- Altenbach, C., Cai, K., Khorana, H. G., and Hubbell, W. L. (1999) Structural features and light-dependent changes in the sequence 306-322 extending from helix VII to the palmitoylation sites in rhodopsin: a site-directed spin-labeling study. *Biochemistry* **38**:7931-7937.
- Altenbach, C., Yang, K., Farrens, D. L., Farahbakhsh, Z. T., Khorana, H. G., and Hubbell, W. L. (1996) Structural features and light-dependent changes in the cytoplasmic interhelical E-F loop region of rhodopsin: a site-directed spin- labeling study. *Biochemistry* **35**:12470-12478.
- Arnis, S., Fahmy, K., Hofmann, K. P., and Sakmar, T. P. (1994) A conserved carboxylic acid group mediates light-dependent proton uptake and signaling by rhodopsin. *J. Biol. Chem.* **269**:23879-23881.
- Arnis, S. and Hofmann, K. P. (1993) Two different forms of metarhodopsin II: Schiff base deprotonation precedes proton uptake and signaling state. *Proc. Natl. Acad. Sci. U. S. A.* **90**:7849-7853.
- Arnis, S. and Hofmann, K. P. (1995) Photoregeneration of bovine rhodopsin from its signaling state. *Biochemistry* **34**:9333-9340.
- Baldwin, J. M., Schertler, G. F., and Unger, V. M. (1997) An α -carbon template for the transmembrane helices in the rhodopsin family of G-protein-coupled receptors. *J. Mol. Biol.* **272**:144-64.
- Baylor, D. A., Lamb, T. D., and Yau, K. W. (1979) Responses of retinal rods to single photons. *J. Physiol.* **288**:613-34.
- Bell, M. W., Desai, N., Guo, X. X., and Ghalayini, A. J. (2000) Tyrosine phosphorylation of the α subunit of transducin and its association with src in photoreceptor rod outer segments. *J. Neurochem.* **75**:2006-19.
- Ben-Tal, N., Ben-Shaul, A., Nicholls, A., and Honig, B. (1996) Free-energy determinants of α -helix insertion into lipid bilayers. *Biophys. J.* **70** :1803-1812.

References

- Bohm, A., Gaudet, R., and Sigler, P. B. (1997) Structural aspects of heterotrimeric G-protein signaling. *Curr. Opin. Biotechnol.* **8**:480-487.
- Borhan, B., Souto, M. L., Imai, H., Shichida, Y., and Nakanishi, K. (2000) Movement of retinal along the visual transduction path. *Science* **288**:2209-12.
- Borjigin, J. and Nathans, J. (1994) Insertional mutagenesis as a probe of rhodopsin's topography, stability, and activity. *J. Biol. Chem.* **269**:14715-14722.
- Bourne, H. R. (1993) A turn-on and a surprise. *Nature* **366**:628-629.
- Bourne, H. R. (1997) How receptors talk to trimeric G proteins. *Curr. Opin. Cell. Biol.* **9**:134-142.
- Bouvier, M. (2001) Oligomerization of G-protein-coupled transmitter receptors. *Nat. Rev. Neurosci.* **2**:274-86.
- Cai, K., Itoh, Y., and Khorana, H. G. (2001) Mapping of contact sites in complex formation between transducin and light-activated rhodopsin by covalent crosslinking: Use of a photoactivatable reagent. *Proc. Natl. Acad. Sci. U. S. A.* **98**:4877-82.
- Cai, K., Klein-Seetharaman, J., Farrens, D., Zhang, C., Altenbach, C., Hubbell, W. L., and Khorana, H. G. (1999) Single-cysteine substitution mutants at amino acid positions 306-321 in rhodopsin, the sequence between the cytoplasmic end of helix VII and the palmitoylation sites: sulfhydryl reactivity and transducin activation reveal a tertiary structure. *Biochemistry* **38**:7925-7930.
- Cepko, C. L., Austin, C. P., Yang, X., Alexiades, M., and Ezzeddine, D. (1996) Cell fate determination in the vertebrate retina. *Proc. Natl. Acad. Sci. U. S. A.* **93**:589-95.
- Conklin, B. R., Farfel, Z., Lustig, K. D., Julius, D., and Bourne, H. R. (1993) Substitution of three amino acids switches receptor specificity of Gq α to that of Gi α . *Nature* **363**:274-6.
- Denker, B. M., Boutin, P. M., and Neer, E. J. (1995) Interactions between the amino- and carboxyl-terminal regions of G α subunits: analysis of mutated G α o/G α i2 chimeras. *Biochemistry* **34**:5544-5553.
- Denker, B. M., Schmidt, C. J., and Neer, E. J. (1992) Promotion of the GTP-liganded state of the Go α protein by deletion of the C terminus. *J. Biol. Chem.* **267**:9998-10002.
- Dixon, R. A. F., Kobilka, B. K., Strader, D. J., Benovic, J. L., Dohlman, H. G., Frielle, T., Bolanowski, M. A., Bennett, C. D., Rands, E., Diehl, R. E., Mumford, R. A., Slater, E. E., Sigal, I. S., Caron, M. G., Lefkowitz, R. J., and Strader, C. D. (1986) Cloning of the gene and cDNA for mammalian β -adrenergic receptor and homology with rhodopsin. *Nature* **321**:75-79.
- Eason, M. G. and Liggett, S. B. (1996) Chimeric mutagenesis of putative G-protein

References

- coupling domains of the $\alpha 2A$ -adrenergic receptor. Localization of two redundant and fully competent Gi coupling domains. *J. Biol. Chem.* **271**:12826-32.
- Emeis, D. and Hofmann, K. P. (1981) Shift in the relation between flash-induced metarhodopsin I and metarhodopsin II within the first 10% rhodopsin bleaching in bovine disc membranes. *FEBS Lett.* **136**:201-207.
- Ernst, O. P., Bieri, C., Vogel, H., and Hofmann, K. P. (1999) Intrinsic biophysical monitors of transducin activation: fluorescence, UV-visible spectroscopy, light scattering, and evanescent field techniques. *Methods Enzymol.* **315**:471-489.
- Ernst, O. P., Hofmann, K. P., and Sakmar, T. P. (1995) Characterization of rhodopsin mutants that bind transducin but fail to induce GTP nucleotide uptake. Classification of mutant pigments by fluorescence, nucleotide release, and flash-induced light-scattering assays. *J. Biol. Chem.* **270**:10580-6.
- Ernst, O. P., Meyer, C. K., Marin, E. P., Henklein, P., Fu, W.-Y., Sakmar, T. P., and Hofmann, K. P. (2000) Mutation of the fourth cytoplasmic loop of rhodopsin affects binding of transducin and peptides derived from the carboxyl-terminal sequences of transducin α and gamma subunits. *J. Biol. Chem.* **275**:1937-1943.
- Fahmy, K. (1998) Binding of transducin and transducin-derived peptides to rhodopsin studies by attenuated total reflection-fourier transform infrared difference spectroscopy. *Biophys. J.* **75**:1306-1318.
- Fahmy, K. and Sakmar, T. P. (1993a) Regulation of the rhodopsin-transducin interaction by a highly conserved carboxylic acid group. *Biochemistry* **32**:7229-7236.
- Fahmy, K. and Sakmar, T. P. (1993b) Light-dependent transducin activation by an ultraviolet-absorbing rhodopsin mutant. *Biochemistry* **32**:9165-71.
- Farahbakhsh, Z. T., Ridge, K. D., Khorana, H. G., and Hubbell, W. L. (1995) Mapping light-dependent structural changes in the cytoplasmic loop connecting helices C and D in rhodopsin: a site-directed spin labeling study. *Biochemistry* **34**:8812-8819.
- Farrens, D. L., Altenbach, C., Yang, K., Hubbell, W. L., and Khorana, H. G. (1996) Requirement of rigid-body motion of transmembrane helices for light activation of rhodopsin. *Science* **274**:768-770.
- Faurobert, E., Otto-Bruc, A., Chardin, P., and Chabre, M. (1993) Tryptophan W207 in transducin T α is the fluorescence sensor of the G protein activation switch and is involved in the effector binding. *EMBO J.* **12**:4191-4198.
- Ferretti, L., Karnik, S. S., Khorana, H. G., Nassal, M., and Oprian, D. D. (1986) Total synthesis of a gene for bovine rhodopsin. *Proc. Natl. Acad. Sci. U. S. A.* **83**:599-603.
- Fesenko, E. E., Kolesnikov, S. S., and Lyubarsky, A. L. (1985) Induction by cyclic GMP of cationic conductance in plasma membrane of retinal rod outer segment. *Nature*

References

313:310-313.

Ford, C. E., Skiba, N. P., Bae, H., Daaka, Y., Reuveny, E., Shekter, L. R., Rosal, R., Weng, G., Yang, C. S., Iyengar, R., Miller, R. J., Jan, L. Y., Lefkowitz, R. J., and Hamm, H. E. (1998) Molecular basis for interactions of G protein $\beta\gamma$ subunits with effectors. *Science* **280**:1271-4.

Franke, R. R., König, B., Sakmar, T. P., Khorana, H. G., and Hofmann, K. P. (1990) Rhodopsin mutants that bind but fail to activate transducin. *Science* **250**:123-125.

Franke, R. R., Sakmar, T. P., Graham, R. M., and Khorana, H. G. (1992) Structure and function in rhodopsin. Studies of the interaction between the rhodopsin cytoplasmic domain and transducin. *J. Biol. Chem.* **267**:14767-14774.

Franke, R. R., Sakmar, T. P., Oprian, D. D., and Khorana, H. G. (1988) A single amino acid substitution in rhodopsin (lysine 248----leucine) prevents activation of transducin. *J. Biol. Chem.* **263**:2119-2122.

Fung, B. K., Hurley, J. B., and Stryer, L. (1981) Flow of information in the light-triggered cyclic nucleotide cascade of vision. *Proc. Natl. Acad. Sci. U. S. A.* **78**:152-156.

Fung, B. K. and Nash, C. R. (1983) Characterization of transducin from bovine retinal rod outer segments. II. Evidence for distinct binding sites and conformational changes revealed by limited proteolysis with trypsin. *J. Biol. Chem.* **258**:10503-10510.

Fung, B. K. K. (1983) Characterization of transducin from bovine retinal rod outer segments. I. separation and reconstitution of the subunits. *J. Biol. Chem.* **258**:10495-10502.

Fung, B. K. K. and Stryer, L. (1980) Photolyzed rhodopsin catalyzes the exchange of GTP for bound GDP in retinal rod outer segments. *Proc. Natl. Acad. Sci. USA* **77**:2500-2504.

Garcia-Higuera, I., Fenoglio, J., Li, Y., Lewis, C., Panchenko, M. P., Reiner, O., Smith, T. F., and Neer, E. J. (1996) Folding of proteins with WD-repeats: comparison of six members of the WD-repeat superfamily to the G protein β subunit. *Biochemistry* **35**:13985-94.

Garcia, P. D., Onrust, R., Bell, S. M., Sakmar, T. P., and Bourne, H. R. (1995) Transducin- α C-terminal mutations prevent activation by rhodopsin: a new assay using recombinant proteins expressed in cultured cells. *EMBO J.* **14**:4460-4469.

Godchaux, W. and Zimmerman, W. F. (1979) Membrane-dependent guanine nucleotide binding and GTPase activities of soluble protein from bovine rod cell outer segments. *J. Biol. Chem.* **254**:7874-84.

Grishina, G. and Berlot, C. H. (1998) Mutations at the domain interface of GS α impair receptor-mediated activation by altering receptor and guanine nucleotide binding. *J. Biol.*

References

Chem. **273**:15053-15060.

Hamm, H. E. (1998) The many faces of G protein signaling. *J. Biol. Chem.* **273**:669-672.

Hamm, H. E. (2001) How activated receptors couple to G proteins. *Proc. Natl. Acad. Sci. U. S. A.* **98**:4819-21.

Hamm, H. E., Deretic, D., Arendt, A., Hargrave, P. A., König, B., and Hofmann, K. P. (1988) Site of G protein binding to rhodopsin mapped with synthetic peptides from the α subunit. *Science* **241**:832-835.

Han, M., Groesbeek, M., Smith, S. O., and Sakmar, T. P. (1998) Role of the C9 methyl group in rhodopsin activation: characterization of mutant opsins with the artificial chromophore 11-*cis*-9- demethylretinal. *Biochemistry* **37**:538-545.

Han, M., Lin, S. W., Minkova, M., Smith, S. O., and Sakmar, T. P. (1996) Functional interaction of transmembrane helices 3 and 6 in rhodopsin. Replacement of phenylalanine 261 by alanine causes reversion of phenotype of a glycine 121 replacement mutant. *J. Biol. Chem.* **271**:32337-32342.

Han, M., Lou, J., Nakanishi, K., Sakmar, T. P., and Smith, S. O. (1997) Partial agonist activity of 11-*cis*-retinal in rhodopsin mutants. *J. Biol. Chem.* **272**:23081-5.

Han, M. and Sakmar, T. P. (2000) Assays for activation of recombinant expressed opsins by all-*trans*- retinals. *Methods Enzymol.* **315**:251-267.

Han, M., Smith, S. O., and Sakmar, T. P. (1998) Constitutive activation of opsin by mutation of methionine 257 on transmembrane helix 6. *Biochemistry* **37**:8253-61.

He, W., Cowan, C. W., and Wensel, T. G. (1998) RGS9, a GTPase accelerator for phototransduction. *Neuron* **20**:95-102.

Heck, M. and Hofmann, K. P. (1993) G-protein-effector coupling: a real-time light-scattering assay for transducin-phosphodiesterase interaction. *Biochemistry* **32**:8220-8227.

Heck, M. and Hofmann, K. P. (2001) Maximal rate and nucleotide dependence of rhodopsin catalyzed transducin activation: initial rate analysis based on a double displacement mechanism. *J. Biol. Chem.* **276**:10000-10009.

Helmreich, E. J. and Hofmann, K. P. (1996) Structure and function of proteins in G-protein-coupled signal transfer. *Biochim. Biophys. Acta* **1286**:285-322.

Horn, F., Weare, J., Beukers, M. W., Horsch, S., Bairoch, A., Chen, W., Edvardsen, O., Campagne, F., and Vriend, G. (1998) GPCRDB: an information system for G protein-coupled receptors. *Nucleic Acids Res.* **26**:275-279.

Iiri, T., Farfel, Z., and Bourne, H. R. (1998) G-protein diseases furnish a model for the

References

turn-on switch. *Nature* **394**:35-38.

Iiri, T., Herzmark, P., Nakamoto, J. M., van Dop, C., and Bourne, H. R. (1994) Rapid GDP release from Gs α in patients with gain and loss of endocrine function. *Nature* **371**:164-168.

Itoh, Y., Cai, K., and Khorana, H. G. (2001) Mapping of contact sites in complex formation between light-activated rhodopsin and transducin by covalent crosslinking: Use of a chemically preactivated reagent. *Proc. Natl. Acad. Sci. U. S. A.* **98**:4883-7.

Jager, F., Fahmy, K., Sakmar, T. P., and Siebert, F. (1994) Identification of glutamic acid 113 as the Schiff base proton acceptor in the metarhodopsin II photointermediate of rhodopsin. *Biochemistry* **33**:10878-10882.

Karnik, S. S., Ridge, K. D., Bhattacharya, S., and Khorana, H. G. (1993) Palmitoylation of bovine opsin and its cysteine mutants in COS cells. *Proc. Natl. Acad. Sci. U. S. A.* **90**:40-44.

Karnik, S. S., Sakmar, T. P., Chen, H. B., and Khorana, H. G. (1988) Cysteine residues 110 and 187 are essential for the formation of correct structure in bovine rhodopsin. *Proc. Natl. Acad. Sci. U. S. A.* **85**:8459-8463.

Kelleher, D. J. and Johnson, G. L. (1988) Transducin inhibition of light-dependent rhodopsin phosphorylation: evidence for β gamma subunit interaction with rhodopsin. *Mol. Pharmacol.* **34**:452-60.

Kibelbek, J., Mitchell, D. C., Beach, J. M., and Litman, B. J. (1991) Functional equivalence of metarhodopsin II and the Gt-activating form of photolyzed bovine rhodopsin. *Biochemistry* **30**:6761-8.

Kim, J. M., Altenbach, C., Thurmond, R. L., Khorana, H. G., and Hubbell, W. L. (1997) Structure and function in rhodopsin: rhodopsin mutants with a neutral amino acid at E134 have a partially activated conformation in the dark state [In Process Citation]. *Proc. Natl. Acad. Sci. U. S. A.* **94**:14273-14278.

Kisselev, O., Ermolaeva, M., and Gautam, N. (1995a) Efficient interaction with a receptor requires a specific type of prenyl group on the G protein γ subunit. *J. Biol. Chem.* **270**:25356-25358.

Kisselev, O., Pronin, A., Ermolaeva, M., and Gautam, N. (1995b) Receptor-G protein coupling is established by a potential conformational switch in the β gamma complex. *Proc. Natl. Acad. Sci. U. S. A.* **92**:9102-9106.

Kisselev, O. G., Ermolaeva, M. V., and Gautam, N. (1994) A farnesylated domain in the G protein γ subunit is a specific determinant of receptor coupling. *J. Biol. Chem.* **269**:21399-21402.

Kisselev, O. G., Kao, J., Ponder, J. W., Fann, Y. C., Gautam, N., and Marshall, G. R.

References

- (1998) Light-activated rhodopsin induces structural binding motif in G protein α subunit. *Proc. Natl. Acad. Sci. U. S. A.* **95**:4270-4275.
- Kisselev, O. G., Meyer, C. K., Heck, M., Ernst, O. P., and Hofmann, K. P. (1999) Signal transfer from rhodopsin to the G-protein: evidence for a two-site sequential fit mechanism. *Proc. Natl. Acad. Sci. U. S. A.* **96**:4898-4903.
- König, B., Arendt, A., McDowell, J. H., Kahlert, M., Hargrave, P. A., and Hofmann, K. P. (1989) Three cytoplasmic loops of rhodopsin interact with transducin. *Proc. Natl. Acad. Sci. U. S. A.* **86**:6878-6882.
- Kokame, K., Fukada, Y., Yoshizawa, T., Takao, T., and Shimonishi, Y. (1992) Lipid modification at the N terminus of photoreceptor G-protein α -subunit. *Nature* **359**:749-52.
- Kühn, H. (1980) Light- and GTP-regulated interaction of GTPase and other proteins with bovine photoreceptor membranes. *Nature* **283**:587-589.
- Lambright, D. G., Noel, J. P., Hamm, H. E., and Sigler, P. B. (1994) Structural determinants for activation of the α -subunit of a heterotrimeric G protein. *Nature* **369**:621-628.
- Lambright, D. G., Sondek, J., Böhm, A., Skiba, N. P., Hamm, H. E., and Sigler, P. B. (1996) The 2.0 Å crystal structure of a heterotrimeric G protein. *Nature* **379**:311-319.
- Li, Q. and Cerione, R. A. (1997) Communication between switch II and switch III of the transducin α subunit is essential for target activation. *J. Biol. Chem.* **272**:21673-21676.
- Lichtarge, O., Bourne, H. R., and Cohen, F. E. (1996) Evolutionarily conserved $G\alpha\beta\gamma$ binding surfaces support a model of the G protein-receptor complex. *Proc. Natl. Acad. Sci. U. S. A.* **93**:7507-7511.
- Liggett, S. B., Caron, M. G., Lefkowitz, R. J., and Hnatowich, M. (1991) Coupling of a mutated form of the human β 2-adrenergic receptor to G_i and G_s . Requirement for multiple cytoplasmic domains in the coupling process. *J. Biol. Chem.* **266**:4816-4821.
- Lin, S. W. and Sakmar, T. P. (1996) Specific tryptophan UV-absorbance changes are probes of the transition of rhodopsin to its active state. *Biochemistry* **35**:11149-59.
- Liu, J., Conklin, B. R., Blin, N., Yun, J., and Wess, J. (1995) Identification of a receptor/G-protein contact site critical for signaling specificity and G-protein activation. *Proc. Natl. Acad. Sci. U. S. A.* **92**:11642-11646.
- Lo, K.-M., Jones, S. S., Hackett, N. R., and Khorana, H. G. (1984) Specific amino acid substitutions in bacteriorhodopsin: Replacement of a restriction fragment in the structural gene by synthetic DNA fragments containing altered codons. *Proc. Natl. Acad. Sci. U. S. A.* **91**:2285-2289.

References

- Marin, E. P., Krishna, A. G., Zvyaga, T. A., Isele, J., Siebert, F., and Sakmar, T. P. (2000) The amino terminus of the fourth cytoplasmic loop of rhodopsin modulates rhodopsin-transducin interaction. *J. Biol. Chem.* **275**:1930-1936.
- Marin, E. P. and Neubig, R. R. (1995) Lack of association of G-protein $\beta 2$ - and $\gamma 2$ -subunit N-terminal fragments provides evidence against the coiled-coil model of subunit- $\beta \gamma$ assembly. *Biochem. J.* **309** (Pt 2):377-80.
- Marsh, S. R., Grishina, G., Wilson, P. T., and Berlot, C. H. (1998) Receptor-mediated activation of Gs α : evidence for intramolecular signal transduction. *Mol. Pharmacol.* **53**:981-990.
- Matsuda, T., Hashimoto, Y., Ueda, H., Asano, T., Matsuura, Y., Doi, T., Takao, T., Shimonishi, Y., and Fukada, Y. (1998) Specific isoprenyl group linked to transducin gamma-subunit is a determinant of its unique signaling properties among G-proteins. *Biochemistry* **37**:9843-50.
- Mazzoni, M. R. and Hamm, H. E. (1996) Interaction of transducin with light-activated rhodopsin protects it from proteolytic digestion by trypsin. *J. Biol. Chem.* **271**:30034-30040.
- Mazzoni, M. R., Malinski, J. A., and Hamm, H. E. (1991) Structural analysis of rod GTP-binding protein, Gt. Limited proteolytic digestion pattern of Gt with four proteases defines monoclonal antibody epitope. *J. Biol. Chem.* **266**:14072-14081.
- Menon, S. T., Han, M., and Sakmar, T. P. (2001) Rhodopsin: the structural basis of molecular physiology. *Physiol. Rev.* in press.
- Miki, N., Keirns, J. J., Marcus, F. R., and Bitensky, M. W. (1974) Proceedings: Light regulation of adenosine 3',5' cyclic monophosphate levels in vertebrate photoreceptors. *Exp. Eye Res.* 281-297.
- Miller, J. L., Fox, D. A., and Litman, B. J. (1986) Amplification of phosphodiesterase activation is greatly reduced by rhodopsin phosphorylation. *Biochemistry* **25**:4983-8.
- Miller, W. H. and Nicol, G. D. (1979) Evidence that cyclic GMP regulates membrane potential in rod photoreceptors. *Nature* **280**:64-66.
- Min, K. C., Gravina, S. A., and Sakmar, T. P. (2000) Reconstitution of the vertebrate visual cascade using recombinant heterotrimeric transducin purified from Sf9 cells. *Protein Expr. Purif.* **20**:514-526.
- Min, K. C., Zvyaga, T. A., Cypess, A. M., and Sakmar, T. P. (1993) Characterization of mutant rhodopsins responsible for autosomal dominant retinitis pigmentosa. Mutations on the cytoplasmic surface affect transducin activation. *J. Biol. Chem.* **268**:9400-9404.
- Min, K. C. (1996) Functional reconstitution of recombinant heterotrimeric transducin: mechanism of phosphodiesterase activation. *Doctoral Dissertation, The Rockefeller*

References

- O'Dowd, B. F., Hnatowich, M., Caron, M. G., Lefkowitz, R. J., and Bouvier, M. (1989) Palmitoylation of the human β 2-adrenergic receptor. Mutation of Cys341 in the carboxyl tail leads to an uncoupled nonpalmitoylated form of the receptor. *J. Biol. Chem.* **264**:7564-7569.
- O'Dowd, B. F., Hnatowich, M., Regan, J. W., Leader, W. M., Caron, M. G., and Lefkowitz, R. J. (1988) Site-directed mutagenesis of the cytoplasmic domains of the human β 2-adrenergic receptor. Localization of regions involved in G protein- receptor coupling. *J. Biol. Chem.* **263**:15985-15992.
- Onrust, R., Herzmark, P., Chi, P., Garcia, P. D., Lichtarge, O., Kingsley, C., and Bourne, H. R. (1997) Receptor and β gamma binding sites in the α subunit of the retinal G protein transducin. *Science* **275**:381-384.
- Oprian, D. D., Molday, R. S., Kaufman, R. J., and Khorana, H. G. (1987) Expression of a synthetic bovine rhodopsin gene in monkey kidney cells. *Proc. Natl. Acad. Sci. U. S. A.* **84**:8874-8878.
- Osawa, S. and Weiss, E. R. (1994) The carboxyl terminus of bovine rhodopsin is not required for G protein activation. *Mol. Pharmacol.* **46**:1036-1040.
- Osawa, S. and Weiss, E. R. (1995) The effect of carboxyl-terminal mutagenesis of Gt α on rhodopsin and guanine nucleotide binding. *J. Biol. Chem.* **270**:31052-31058.
- Ovchinnikov, Y. A., Abdulaev, N. G., and Bogachuk, A. S. (1988) Two adjacent cysteine residues in the C-terminal cytoplasmic fragment of bovine rhodopsin are palmitylated. *FEBS Lett.* **230**:1-5.
- Palczewski, K., Kumasaka, T., Hori, T., Behnke, C. A., Motoshima, H., Fox, B. A., Le Trong, I., Teller, D. C., Okada, T., Stenkamp, R. E., Yamamoto, M., and Miyano, M. (2000) Crystal structure of rhodopsin: A G protein-coupled receptor. *Science* **289**:739-745.
- Phillips, W. J. and Cerione, R. A. (1992) Rhodopsin/transducin interaction. I. Characterization of the binding of the transducin- $\beta\gamma$ subunit complex to rhodopsin using fluorescence spectroscopy. *J. Biol. Chem.* **267**:17032-17039.
- Phillips, W. J., Wong, S. C., and Cerione, R. A. (1992) Rhodopsin/transducin interactions. II. Influence of the transducin- $\beta\gamma$ subunit complex on the coupling of the transducin- α subunit to rhodopsin. *J. Biol. Chem.* **267**:17040-17046.
- Posner, B. A., Mixon, M. B., Wall, M. A., Sprang, S. R., and Gilman, A. G. (1998) The A326S mutant of G α 1 as an approximation of the receptor-bound state. *J. Biol. Chem.* **273**:21752-21758.
- Quilliam, L. A., Zhong, S., Rabun, K. M., Carpenter, J. W., South, T. L., Der, C. J., and Campbell-Burk, S. (1995) Biological and structural characterization of a Ras

References

- transforming mutation at the phenylalanine-156 residue, which is conserved in all members of the Ras superfamily. *Proc. Natl. Acad. Sci. U. S. A.* **92**:1272-1276.
- Ramdas, L., Disher, R. M., and Wensel, T. G. (1991) Nucleotide exchange and cGMP phosphodiesterase activation by pertussis toxin inactivated transducin. *Biochemistry* **30**:11637-11645.
- Remmers, A. E., Engel, C., Liu, M., and Neubig, R. R. (1999) Interdomain interactions regulate GDP release from heterotrimeric G proteins. *Biochemistry* **38**:13795-13800.
- Resek, J. F., Farahbakhsh, Z. T., Hubbell, W. L., and Khorana, H. G. (1993) Formation of the meta II photointermediate is accompanied by conformational changes in the cytoplasmic surface of rhodopsin. *Biochemistry* **32**:12025-12032.
- Ross, E. M. and Gilman, A. G. (1980) Biochemical properties of hormone-sensitive adenylate cyclase. *Annu. Rev. Biochem.* **49**:533-64.
- Sakmar, T. P. (1998) Rhodopsin: a prototypical G protein-coupled receptor. *Prog. Nucleic Acid Res. Mol. Biol.* **59**:1-34.
- Sakmar, T. P. (2001) Color vision. In *Adler's Physiology of the Eye*. in press.
- Sakmar, T. P., Franke, R. R., and Khorana, H. G. (1989) Glutamic acid 113 serves as the retinylidene schiff base counterion in bovine rhodopsin. *Proc. Natl. Acad. Sci. U. S. A.* **86**:8309-8313.
- Sakmar, T. P. and Khorana, H. G. (1988) Total synthesis and expression of a gene for the α -subunit of bovine rod outer segment guanine nucleotide-binding protein (transducin). *Nucleic Acids Res.* **16**:6361-6372.
- Scheer, A. and Gierschik, P. (1995) S-prenylated cysteine analogues inhibit receptor-mediated G protein activation in native human granulocyte and reconstituted bovine retinal rod outer segment membranes. *Biochemistry* **34**:4952-61.
- Schoenlein, R. W., Peteanu, L. A., Mathies, R. A., and Shank, C. V. (1991) The first step in vision: femtosecond isomerization of rhodopsin. *Science* **254** :412-5.
- Sheikh, S. P., Zvyaga, T. A., Lichtarge, O., Sakmar, T. P., and Bourne, H. R. (1996) Rhodopsin activation blocked by metal-ion-binding sites linking transmembrane helices C and F. *Nature* **383**:347-350.
- Shichi, H., Yamamoto, K., and Somers, R. L. (1984) GTP binding protein: properties and lack of activation by phosphorylated rhodopsin. *Vision Res.* **24** :1523-1531.
- Shieh, T., Han, M., Sakmar, T. P., and Smith, S. O. (1997) The steric trigger in rhodopsin activation. *J. Mol. Biol.* **269**:373-384.
- Skiba, N. P., Bae, H., and Hamm, H. E. (1996) Mapping of effector binding sites of

References

- transducin α -subunit using G α t/G α i1 chimeras. *J. Biol. Chem.* **271**:413-424.
- Slep, K. C., Kercher, M. A., He, W., Cowan, C. W., Wensel, T. G., and Sigler, P. B. (2001) Structural determinants for regulation of phosphodiesterase by a G protein at 2.0 Å. *Nature* **409**:1071-1077.
- Sondek, J., Bohm, A., Lambright, D. G., Hamm, H. E., and Sigler, P. B. (1996) Crystal structure of a G-protein $\beta\gamma$ dimer at 2.1 Å resolution. *Nature* **379**:369-74.
- Sondek, J., Lambright, D. G., Noel, J. P., Hamm, H. E., and Sigler, P. B. (1994) GTPase mechanism of G proteins from the 1.7-Å crystal structure of transducin α -GDP-AIF-4. *Nature* **372**:276-279.
- Sprang, S. R. (1997) G protein mechanisms: insights from structural analysis. *Annu. Rev. Biochem.* **66**:639-678.
- Stryer, L. (1988) Molecular basis of visual excitation. *Cold Spring Harb. Symp. Quant. Biol.* **53 Pt 1**:283-94.
- Takemoto, D. J., Morrison, D., Davis, L. C., and Takemoto, L. J. (1986) C-terminal peptides of rhodopsin. Determination of the optimum sequence for recognition of retinal transducin. *Biochem. J.* **235**:309-312.
- Taylor, J. M., Jacob-Mosier, G. G., Lawton, R. G., VanDort, M., and Neubig, R. R. (1996) Receptor and membrane interaction sites on G β . A receptor-derived peptide binds to the carboxyl terminus. *J. Biol. Chem.* **271**:3336-9.
- Thomas, T. C., Schmidt, C. J., and Neer, E. J. (1993) G-protein α_o subunit: mutation of conserved cysteines identifies a subunit contact surface and alters GDP affinity. *Proc. Natl. Acad. Sci. U. S. A.* **90**:10295-8.
- Valencia, A., Chardin, P., Wittinghofer, A., and Sander, C. (1991) The ras protein family: evolutionary tree and role of conserved amino acids. *Biochemistry* **30**:4637-4648.
- Wald, G. (1968) The molecular basis of visual excitation. *Nature* **219**:800-7.
- Warner, D. R. and Weinstein, L. S. (1999) A mutation in the heterotrimeric stimulatory guanine nucleotide binding protein α -subunit with impaired receptor-mediated activation because of elevated GTPase activity. *Proc. Natl. Acad. Sci. U. S. A.* **96**:4268-4272.
- Warner, D. R., Weng, G., Yu, S., Matalon, R., and Weinstein, L. S. (1998) A novel mutation in the switch 3 region of Gs α in a patient with Albright hereditary osteodystrophy impairs GDP binding and receptor activation. *J. Biol. Chem.* **273**:23976-23983.
- Wedegaertner, P. B., Wilson, P. T., and Bourne, H. R. (1995) Lipid modifications of trimeric G proteins. *J. Biol. Chem.* **270**:503-6.

References

- Weiss, E. R., Osawa, S., Shi, W., and Dickerson, C. D. (1994) Effects of carboxyl-terminal truncation on the stability and G protein-coupling activity of bovine rhodopsin. *Biochemistry* **33**:7587-7593.
- Wess, J. (1997) G-protein-coupled receptors: molecular mechanisms involved in receptor activation and selectivity of G-protein recognition. *FASEB J.* **11**:346-354.
- Wheeler, G. L. and Bitensky, M. W. (1977) A light-activated GTPase in vertebrate photoreceptors: regulation of light-activated cyclic GMP phosphodiesterase. *Proc. Natl. Acad. Sci. U. S. A.* **74**:4238-42.
- Wilden, U., Hall, S. W., and Kühn, H. (1986) Phosphodiesterase activation by photoexcited rhodopsin is quenched when rhodopsin is phosphorylated and binds the intrinsic 48-kDa protein of rod outer segments. *Proc. Natl. Acad. Sci. U. S. A.* **83**:1174-8.
- Woolfson, D. N. and Williams, D. H. (1990) The influence of proline residues on α -helical structure. *FEBS Lett.* **277**:185-188.
- Yang, K., Farrens, D. L., Altenbach, C., Farahbakhsh, Z. T., Hubbell, W. L., and Khorana, H. G. (1996) Structure and function in rhodopsin. Cysteines 65 and 316 are in proximity in a rhodopsin mutant as indicated by disulfide formation and interactions between attached spin labels. *Biochemistry* **35**:14040-14046.
- Yau, K. W. (1994) Phototransduction mechanism in retinal rods and cones. The Friedenwald Lecture. *Invest. Ophthalmol. Vis. Sci.* **35**:9-32.
- Yeagle, P. L., Alderfer, J. L., and Albert, A. D. (1996) Structure determination of the fourth cytoplasmic loop and carboxyl terminal domain of bovine rhodopsin. *Mol. Vis.* **2**:12.
- Yee, R. and Liebman, P. A. (1978) Light-activated phosphodiesterase of the rod outer segment. Kinetics and parameters of activation and deactivation. *J. Biol. Chem.* **253**:8902-9.